USF Tampa Graduate Theses and Dissertations

February 2022

Adrenergic Modulation of Precursor Cells of Ovarian Cancer

Sweta Dash
University of South Florida

Adrenergic Modulation of Precursor Cells of Ovarian Cancer

by

Sweta Dash

A dissertation submitted in partial fulfillment
of the requirements for the degree of
Doctor of Philosophy
Department of Cell Biology, Microbiology and Molecular Biology
College of Arts and Sciences
University of South Florida

Major Professor: Alvaro N.A. Monteiro, Ph.D.
Shelley Tworoger, Ph.D.
Florian Karreth, Ph.D.
Jamie Teer, Ph.D.
Eric Lau, PhD
Simon Gayther, Ph.D.

Date of Approval:
February 7, 2022

Keywords: Norepinephrine, *HOXA5*, Stress, HGSOC

DEDICATION

I would like to dedicate this dissertation thesis,

To my parents, Chitta Ranjan and Anita Dash, for your abundant love and support. As an international student from India, the first few months living so far away from home had been difficult, especially with me acclimatizing to a new environment on my own. Thank you for being ever-willing to go an extra mile to take care of me and for always being my source of strength and inspiration. I am extremely grateful that you have always encouraged me to follow my dreams. Thank you! You have sacrificed so much to give me opportunities.

To my wonderful sister, Shruti Dash, who has always been there for me and has supported me through everything. Thank you for always making my day brighter, especially during days I felt stuck due to failed experiments.

To my grandparents, Ajaa, Aee and Bouma, whose blessings have helped me at every stage of my life. And to my aunt, uncle and cousins, Sonia and Sanjay, who have been my source of comfort and joy. Thank you!

ACKNOWLEDGMENTS

TABLE OF CONTENTS

LIST OF TABLES

LIST OF FIGURES

ABSTRACT

Ovarian cancer remains one of the most lethal gynecological cancer and ranks eighth in cancer-related mortality among women. The high mortality rate can be attributed to majority of the cases being diagnosed at advanced stages of the disease when the survival rate and overall prognosis are poor. There is lack of effective screening modalities to detect ovarian cancer at early stages. Hence, a better understanding of the molecular mechanisms leading to ovarian cancer initiation is required.

Epidemiological studies have reported that conditions which cause chronic behavioral stress are associated with a higher risk of developing ovarian cancer. The activation of the sympathetic nervous system during stress leads to rapid release of catecholamines. In the ovary, norepinephrine (NE) has been identified as the most abundant catecholamine. Several studies have shown that high level of NE is associated with poor prognosis and can contribute to tumor progression by promoting survival, growth, migration and invasion of ovarian cancer cells. Although the effect of NE stimulation in ovarian cancer progression is well studied, its role in initiation of ovarian cancer remains mostly unknown.

The purpose of this study is to explore the extent to which NE can influence ovarian cancer initiation. Therefore, we used normal cell lines that are presumed to be the cells of origin for ovarian cancer - fallopian tube surface epithelial cells and ovarian surface

epithelial cells. We conducted a short-term/acute NE stimulation experiment in which cells were treated with NE for 15 mins, 1 h and 4 h. In addition, we also conducted a long-term/chronic NE stimulation experiment in which the cells were continuously exposed to NE for 137 days. In this study, we provide evidence that acute vs chronic NE stimulation have distinct transcriptional profiles. Additionally, we identify transcription factor HoxA5 to be induced by short-term NE treatment and provide evidence for the attenuation of HoxA5 induction in long-term treated NE cells. In summary, this project explores the role of NE in ovarian cancer initiation and highlights the difference between acute vs chronic NE stimulation in the precursor cells of ovarian cancer.

CHAPTER ONE

BACKGROUND

Ovarian Cancer

Subtypes:

Ovarian cancer is the second most common gynecological cancer and is the eighth leading cause of death in women from cancer (1, 2). It also accounts for a higher mortality rate in comparison to other female genital tumors (2, 3). Approximately 90% of ovarian cancers are epithelial in origin and also known as Epithelial Ovarian Carcinoma (EOC). The remaining 10% of ovarian tumors are sub-grouped into germ cell and sex cord-stromal tumors (4). Evidence has shown that EOC is a heterogeneous disease. Based on histopathology and molecular analysis, it can be further divided into five major subtypes: high-grade serous ovarian carcinoma (HGSOC), low-grade serous ovarian carcinoma (LGSOC), ovarian endometrioid carcinoma (EC), clear cell carcinoma (CCC) and mucinous carcinoma (MC). These subtypes represent distinct diseases with differences in pathogenesis, precursor lesions, treatment and prognosis. Among them, HGSOC is the most prevalent and accounts for approximately 70% of total cases, while

LGSOC has lower prevalence, contributing to less than 5% of total cases (3, 5, 6). The incidence of EOC also differs by age, subtype, and ethnicity. In the US, non-Hispanic white women have the highest incidence of EOC, and the Asian/Pacific Islanders have the highest incidence of clear cell and endometroid carcinoma. Additionally, the African-American women have much worse outcome and mortality. Both clear cell and endometroid carcinoma occur at a younger age (~ 50 years) compared with serous subtype which peak at about 60-70 years of age (4).

Pathology and Genetics:

In general, ovarian tumors of epithelial origin can be classified as benign, borderline malignancy, and carcinoma depending on the rate of cell proliferation, degree of atypical nuclei, and presence or absence of stromal invasion. Borderline cancers show greater epithelial proliferation and higher nuclear atypia than that seen in their benign counterparts. However, unlike carcinomas, they do not exhibit stromal invasion (6). To determine the extent of ovarian carcinoma progression in the body, the American Joint Committee on Cancer (AJCC) or International Federation of Gynecology and Obstetrics (FIGO) staging system is used (7). Both these staging systems use the TNM classification, where T refers to the size of the tumor, N refers to local lymph node metastasis and M refers to metastasis to distal organs. Stage I cancers are considered early-stage and confined to the ovaries. Patients with Stage I ovarian cancers have excellent prognosis and 15% of total ovarian cancer patients are diagnosed at this stage. In Stage II ovarian carcinoma, cancer has spread to other areas of the pelvis and it comprises 19% of total cases. In Stage III ovarian carcinoma, cancer has spread to other

areas of the abdominal cavity and/or nearby lymph nodes, but not to distant sites. About

60% of all ovarian cancer cases are diagnosed at this stage. Stage IV ovarian carcinoma

represent cancers that have metastasized to distant organs beyond abdomen. Both Stage

III and IV cancers are considered advanced stages and have poor prognosis with median

5-year survival rate of less than 50% (7).

High-grade serous ovarian carcinoma: HGSOC represent the most common

ovarian carcinoma subtype and the median age of diagnosis is 56 years. Most HGSOC

patients are diagnosed at advanced stages (3, 7) (Table 1.1).

Table 1.1: Pathologic classification of epithelial ovarian carcinomas (EOC)

Subtype	Stage at Diagnosis	Proliferation	Prognosis	Percentage of all ovarian carcinoma
High-grade serous ovarian carcinoma	Advanced (Stage III or IV)	High	Poor	70%
Low-grade serous ovarian carcinoma	Early with few Advanced Stage	Low	Favorable	<5%
Ovarian endometrioid carcinoma	Early with few Advanced Stage	Low	Favorable	10-15%
Clear cell carcinoma	Early with few Advanced Stage	Low	Intermediate	6-10%
Mucinous carcinoma	Early (Stage I or II)	Intermediate	Favorable	3-4%

Adapted from (3)

In 2014, WHO officially recognized the classification of EOC subtypes into two

broad categories: Type I and Type II. The Type I neoplasms are genomically stable and

develop in a step-wise progression from pre-cancerous lesions. Genetically, these tumors

exhibit wild-type p53 and display frequent oncogenic alterations in pathways such as

RAS-MAPK and PI3K-AKT. Clinically, Type I neoplasms and confined to the ovary and have excellent prognosis. In contrast, Type II neoplasms are more aggressive, have poor prognosis and are characterized by high genomic instability and *TP53* alterations. Type II tumors are predominantly HGSOC. These carcinomas have large, hyperchromatic and pleomorphic nuclei along with prominent eosinophilic nucleoli (8, 9).

Numerous studies have identified genetic alterations in the tumor suppressor gene *TP53* to be the most prevalent mutation in HGSOC (approximately 96% of cases). The most common oncogenic alterations of p53 are the hotspot mutations at the codons R175, R273 and R248, comprising 19.7% of all *TP53* alterations in HGSOC (10-12). p53 protein functions as a tetramer and these hotspot mutations inhibit tetramerization even in the presence of wild type p53 protein, by forming dominant-negative mutants. These oncogenic mutant proteins scarcely retain the normal p53 activity and are also far more stable than their wild-type counterparts due to lack of interaction with their negative regulator, mdm2 (11-14). Apart from *TP53*, much lower frequency of alterations in few other genes such as *BRCA1* (12.5% - both germline and somatic), *BRCA2* (11.5% - both germline and somatic), *CSMD3* (6%), *NF1* (4% - somatic), *CDK12* (3% - somatic), *GABRA6* (2% - somatic) and *RB1* (2% - somatic) have been observed in HGSOC samples (9, 15). In contrast, HGSOC is characterized by high genomic instability including increased frequency of copy number alterations, highly abnormal karyotypes and structural variants. The most frequently amplified genes include *CCNE1* (Cyclin E1), *MYC* (c-myc) and *MECOM.* These three genes are amplified in more than 20% of cases (15-20) (Table 1.2).

Table 1.2: Genetic alterations present in epithelial ovarian carcinomas subtypes

Subtypes	Germline variants	Somatic variants (descending order of frequency of genetic alterations)
High-grade serous ovarian carcinoma	*BRCA1, BRCA2, RAD51C, RAD51D*	*TP53, BRCA1, BRCA2, CCNE1, MYC, MECOM, CSMD3, NF1, CDK12, GABRA6, RB1*
Low-grade serous ovarian carcinoma		*KRAS, NRAS, BRAF, USP9X, MACF1, ARID1A, NF2, DOT1L, ASH1L*
Ovarian endometrioid carcinoma	*MLH1, MSH2, MSH6, PSM2*	*CTNNB1, TP53 (only in high grade ovarian EC), PTEN, PIK3CA, AKT, KDR, PPP2R1A, POLE*
Clear cell carcinoma		*ARID1A, PIK3CA, PTEN, TERT*
Mucinous carcinoma		*CDKN2A, KRAS, TP53, HER2*

Adapted from (5, 9, 20-28)

A method integrating copy number alterations, mutational frequency and changes in gene expression revealed defective homologous recombination DNA repair pathway in 51% of the cases, including germline and somatic mutations in *BRCA1* and *BRCA2* in 20% of the cases (15). An additional 11% of the cases had silenced *BRCA1* gene due to promoter hypermethylation (15). In addition, women carrying an allele with germline pathogenic variants in *BRCA1* and *BRCA2* have increased risk of developing HGSOC, and the other allele is frequently lost in tumors (9, 20).

Previously, the tissue of origin for HGSOC was thought to be the ovarian surface epithelium (OSE). At that time, it had been difficult to locate precancerous lesions for HGSOC, and thus, to identify a site of origin (29, 30). Additionally, it was thought that during ovulation, certain parts of OSE could invaginate and get trapped under the surface of the ovary forming cortical inclusion cysts (CICs). CICs were thought to be susceptible to become cancerous due to exposure to various hormones present in the ovary that are

capable of promoting proliferation and differentiation (31). Nevertheless, OSE as the site of origin for HGSOC remained questionable mainly because, histologically, HGSOC resembles Müllerian epithelium (32, 33).

Studies have shown that a majority of the HGSOC arise from epithelium of distal fallopian tube (34). An early observation identifying fallopian tube as the site of origin came from a study wherein high-risk patients with inherited BRCA mutations exhibited dysplastic lesions in the epithelium of their surgically removed fallopian tubes (35). Additionally, the identification of precursor serous tubal intraepithelial carcinoma (STIC), an early noninvasive tumor lesion preferentially formed in the fallopian tube epithelium, changed the traditional view of OSE as the only site of origin for HGSOC (36-38). These precancerous lesions are histologically similar to HGSOC exhibiting enlarged nuclei, coarse chromatin aggregates and hyperchromasia (33). Further studies showed the STIC lesions, similar to HGSOC, also display high proliferative activity, loss of polarity, genomic instability and presence of a 'p53 signature' (39-43). The 'p53 signature' refers to secretory cells in the distal fallopian tube (fimbria) which have a high frequency of alterations in p53 and stain positive for γ-H2AX (marker for DNA damage) but are benign in appearance and have minimal proliferative capacity (39, 44-46). Both features, 'p53 signature' and STIC, have been identified in HGSOC patients (39, 47). A genomic analysis study comparing primary fallopian tube lesions ('p53 signature' and STICs), fallopian tube carcinomas, ovarian cancers, and metastases from the same patients suggested an evolutionary relationship placing 'p53 signature' lesions as the earliest event followed by development of STICs and subsequent progression to HGSOC. Evolutionary analysis also suggested a 7-year window between acquisition of STIC

lesions and initiation of HGSOC (43). Another study, using mathematical models, showed that development of STIC lesions from a p53 alteration take a prolonged time (in decades) followed by a relatively short time-span (6 years) for initiation of HGSOC from STICs (41).

Other potential sites of origin for HGSOC include the ovarian hilum (junction between the ovary and the fallopian tube) and the secondary Müllerian system consisting of endometrium-like tissue outside the uterus (endometriosis), fallopian tube-like epithelium on the peritoneal surface (endosalpingiosis) and the Müllerian epithelium-resembling tubular structures near the ovarian hilum (rete ovarii) (48-51). Studies in mouse models have shown that genetically modified mouse ovarian surface epithelial cells (mOSE) are capable of transforming into carcinoma resembling human HGSOC histopathologically; although, unlike inherently aggressive human HGSOC, they exhibit weak metastatic capability (52, 53). It is crucial to determine the precise cells of origin of HGSOC as it would improve early-detection and prevention rates and also offer insights into developing effective treatment.

Low-grade serous ovarian carcinoma: LGSOC accounts for approximately 3% of all ovarian carcinoma cases and the median age of diagnosis is at 43 years, approximately a decade lower than HGSOC. LGSOC patients are diagnosed at both early and advanced stages (Table 1.1). Diagnosis at early stages is associated with excellent prognosis, while late-stage LGSOC have poor prognosis (3, 21). LGSOC tumors are classified as Type I ovarian carcinoma and are distinct from HGSOC in having mild to moderate nuclear atypia, fewer mitosis and necrosis events, low proliferation index and presence of wild-type p53 (21, 22). Concentric lamellated calcified structures known as

Psammoma bodies are frequently observed in LGSOC. Ascites is rarely present, which is in contrast to HGSOC, where ascites is common (3, 21, 54). Additionally, unlike HGSOC, LGSOC is not associated with germline *BRCA1/2* mutations and lacks chromosomal instability (23).

The most common molecular alterations (Table 1.2) in LGSOC include mutations in key RAS/RAF pathway genes such as *KRAS*, *NRAS*, and *BRAF*. More than half of the cases have alterations in genes linked to the RAS/RAF pathway (23, 55, 56). A recent genomic study identified ubiquitin-specific protease 9X (*USP9X*), an X-linked deubiquitinase, as another frequently altered gene (~27%) (23). *USP9X* plays a major role in tissue homoeostasis and is dysregulated in multiple cancers. Evolutionary analysis suggested that alterations in these genes could be early events in LGSOC pathogenesis (22, 23). Mutations were also observed in other genes including *MACF1* (11%), *ARID1A* (9%), *NF2* (4%), *DOT1L* (6%), and *ASH1L* (4%) (Table 1.2). Apart from RAS/RAF pathway, other top altered pathways included: FGFR signaling (15%), MAPK signaling (15%), ErbB4 signaling (13%), chromatin organization (10%), and ubiquitination (10%). Immunohistochemistry analysis revealed frequent estrogen receptor (ER) and progesterone receptor (PR) positivity (22, 23).

The site of origin for LGSOC is thought to be the cortical inclusion cysts (CICs), which develops from invaginated OSE and transforms into serous borderline tumors and serous cystadenomas/adenofibromas. It is rare for LGSOC to develop into HGSOC and it is associated with longer overall survival and progression-free survival compared with HGSOC (5, 22, 57).

Ovarian endometrioid carcinoma: Ovarian endometrioid carcinoma (ovarian EC) is the second most common ovarian carcinoma histotype accounting for 10-15% of all cases (Table 1.1) and has a median age of diagnosis at 51 years. Most ovarian EC cases are diagnosed at early stages and are frequently associated with endometriosis. About 40% of cases have atypical endometriosis as precursor lesions. Common molecular alterations have been found in both tumor and adjacent endometrial site. Endometrial epithelium is usually considered as the site of origin for ovarian EC (20, 58-60). EC tumors are classified under Type I ovarian carcinoma and are generally low-grade cancers having mostly well differentiated with occasional moderately/poorly differentiated carcinomas. A useful diagnostic feature is squamous differentiation, which is frequently observed in ovarian EC tumors (3, 8). Similar to LGSOC, ovarian EC stain positive for estrogen receptor (ER) and progesterone receptor (PR) and have wild-type p53 expression. In contrast to low grade EC, high grade EC usually show alterations in p53 (3, 22).

The molecular profile of ovarian EC (Table 1.2) is generally similar to its adjacent endometrial tissue. EC are heterogeneous and have been classified into four molecular subtypes: 3% *POLE* ultramutated, 19% microsatellite instability hypermutated, 17% copy-number high (serous-like *TP53* mutated) and 61% copy-number low (endometrioid-like) (3, 24, 61). *POLE*, a gene coding for DNA Polymerase Epsilon Catalytic Subunit A, is a gene involved in DNA replication and studies have shown that mutations in its exonuclease domain led to defective proof-reading during replication of the DNA and ultimately resulted in neoplastic transformation (61, 62).

POLE ultramutated ovarian EC mostly have excellent prognosis (22, 62, 63). Microsatellite instability hypermutated ovarian EC have alterations in mismatch repair proteins (MMR) such as *MLH1*, *PMS2*, *MSH2*, and *MSH6*; the most common alteration being the hypermethylation of *MLH1* promoter. Mutations in genes coding for MMR proteins are usually germline and follow the 'two-hit' hypothesis to become cancerous. On the other hand, epigenetic alterations such as hypermethylation of *MLH1* promoter leads to sporadic development of ovarian EC (64-69). The third ovarian EC molecular subtype, copy number high, is characterized by high *TP53* alterations, higher genomic complexity, diagnosis at advanced stages and have poor prognosis. This subtype closely resembles HGSOC (25). The fourth ovarian EC subtype, copy-number low, is characterized by low genomic complexity, excellent prognosis, diagnosis at early stages and presence of *CTNNB1* (β-catenin) mutations, which are mutually exclusive with *TP53* alterations (70). A recent study comparing endometriosis patients and patients with ovarian EC demonstrated common mutated genes (*PIK3CA*, *AKT*, *KDR* and *PTEN*), signaling pathways (angiogenesis, apoptosis, PI3 kinase, EGF signaling, VEGF and TGF signaling), biological processes and molecular functions in both groups (67).

Ovarian EC has many histological and molecular alterations similar to endometrial endometrioid carcinoma (endometrial EC), mainly because of common endometrial epithelial precursor cell of origin. While endometrial EC is the most frequent subtype of endometrial carcinoma, accounting for 70–80% of endometrial carcinoma cases; ovarian EC make up only 10-15% of ovarian carcinoma cases. Both ovarian EC and endometrial EC have mutations in *PTEN*, *PIK3CA*, *PPP2R1A*, and *CTNNB1* (β-catenin) genes (71, 72). However, the difference between the two is mostly in the frequency of these

alterations, specifically *PTEN* and *CTNNB1*. Approximately 53-60% of ovarian EC have *CTNNB1* mutations compared with 27% of endometrial EC; while *PTEN* mutations are more frequent in endometrial EC (67.0%) compared to ovarian EC (16.6%) (73).

Clear cell carcinoma: Clear cell carcinomas (CCC) are similar to the ovarian EC subtype as they are associated with endometriosis and are most often diagnosed at low-stages (3). CCC is classified under Type I ovarian carcinoma and accounts for 10% of ovarian carcinoma cases (Table 1.1) (8). Early stage CCC have favorable outcome, whereas advanced stage CCC have poor prognosis that is even worse than HGSOC. This could be due to low sensitivity to standard chemotherapy. However, CCC associated with MMR deficiency had better prognosis and long survival even at advanced stages, possibly due to high tumor immunogenicity and PD-1/PD-L1 expression (3, 22, 74).

The molecular profile of ovarian CCC (Table 1.2) is characterized by frequent mutations in *ARID1A* (a gene coding for SWI/SNF chromatin remodeling complex protein) and *PIK3CA*; both of which appear to co-exist in approximately half of the cases (26). Other alterations include loss of *PTEN* by mutations or loss of heterozygosity (LOH) and mutations in promoter of telomerase reverse transcriptase (*TERT*) gene. A study in 2014 showed that mutations in *TERT* promoter were found in ~16% of the ovarian CCC cases, while other gynecological cancers had wild-type *TERT*. Additionally, *TERT* mutations appeared to be mutually exclusive with *ARID1A* and *PIK3CA* mutations in ovarian CCC (68). Finally, less than 10% of ovarian CCC have alterations in MMR proteins (75).

Mucinous carcinoma: Mucinous carcinoma (MC) is rare, accounting for only 3-4% of total ovarian carcinoma cases (Table 1.1) and the site of origin for these tumors is unknown. Although a subgroup of MC may derive from ovarian teratomas; in most cases, no teratoma have been observed (3, 22, 27). Morphologically, MC is heterogeneous and displays a mixture of benign, borderline carcinomatous and carcinoma components. Immunohistochemistry profile of MCs show high positivity for cytokeratin 7 (CK7) in more than 80% cases and are weakly positive for CK20. In contrast, teratoma-derived MCs are frequently CK7 negative/CK20 positive (3, 22). At the molecular level (Table 1.2), the most common alteration in MC is the loss of *CDKN2A* gene in 76% of the cases. This is followed by alterations in *KRAS* (64%), *TP53* (64%) and *HER2* (26%) genes (28, 76). A recent genomic analysis study showed that both *KRAS* and *CDKN2A* were early events that led to initiation of benign mucinous tumors (BMT). The development of mucinous borderline tumors (MBT) from BMT likely had additional copy number alterations. Finally, progression from MBT to MC appeared to be associated with more copy number alterations and *TP53* alterations. *TP53* alterations were also strongly associated with genomic instability (28). Another study showed that *TP53* alterations were higher in MC (~60%) compared to MBT (~11%) suggesting that p53 modifications occur later in MC development (76). This is in contrast to HGSOC where *TP53* alterations are the earliest genetic changes (41, 43).

Signs and Symptoms:

Over the years, ovarian cancer has been considered to be a 'silent killer' as the symptoms associated with the early stages of ovarian cancer are not specific to the

disease. Although more than 80% of patients have symptoms during the early stages, most of these symptoms are similar to other common illnesses such as many gastrointestinal and genitourinary pathologies, and are hence disregarded by the patients. Consequently, early diagnosis of ovarian cancer has remained difficult (77, 78). The common symptoms of early-stage ovarian cancer include abdominal bloating or swelling, frequent urination, discomfort in the pelvis area and early satiety. Over the past decade, evidence has shown that when these symptoms are of recent onset and occur more than 12 times in a month, then ovarian cancer could be a possibility and should be included in diagnosis (79, 80). As the disease progresses, the symptoms become more apparent and severe such as increased pain, diarrhea, weight loss, fatigue and obstruction of the urinary tract/intestines. Unfortunately, diagnosis at advanced stages is associated with poor prognosis (77, 79, 80).

Diagnosis:

More than 75% of ovarian carcinoma cases are diagnosed at advanced stages (Stage III and IV), mostly because of non-specificity of symptoms during early-stages of the disease. Additionally, approximately 60% of patients have metastasis at the time of diagnosis (77, 81). Different methods such as physical examination, imaging and laboratory testing are used to detect ovarian cancer. Physical examination includes a rectovaginal examination with empty bladder to evaluate for abdominal and pelvic masses. This technique has limited accuracy as a mass could easily be missed or, if detected, could be caused by other conditions (81, 82). Imaging using transvaginal ultrasonography is another method used for detecting ovarian cancer. This technique is

beneficial as it can assess ovarian architecture and vascularity, differentiate between cystic and solid masses, as well as detect ascites (81, 83, 84). A third method used to detect ovarian cancer is testing for serum cancer antigen 125 (CA125). While CA125 is upregulated in 80% of epithelial ovarian cancer cases overall, less than 50% of early-stage ovarian carcinomas have elevated CA125. Additionally, benign conditions such as endometriosis and fibroids also have higher CA125 levels (85, 86). Another serum biomarker used for detection is human epididymis protein 4 (HE4). This glycoprotein is expressed in ovarian cancers lacking CA125 expression. HE4 is mainly used to assess disease progression and recurrence (86).

The current conventional diagnostic tools used for detection of epithelial ovarian carcinoma – transvaginal ultrasonography, CA125 and HE4 – are not sensitive and specific enough to diagnose the disease in early stages (86-88). Additionally, these techniques also have a high rate of false-positive results leading to unnecessary surgery in cancer-free women and they are not recommended in the general population (87-91). Hence, there is a need for developing new diagnostic and screening methods, and identifying new biomarkers.

A promising new noninvasive method is liquid biopsy and research focused on identifying new molecular biomarkers in circulating tumor cells, circulating cell-free DNA and small noncoding RNAs is ongoing (92). In addition, it is also important to be able to successfully classify diagnosed patients into the different epithelial ovarian carcinoma subtypes: HGSOC, LGSOC, ovarian EC, CCC and MC. This is because these subtypes have distinct clinicopathological features and their prognosis, histopathology and treatments. While the *TP53* alteration status can be considered a reliable marker for a

diagnosis of HGSOC cases, which comprise majority of the ovarian carcinoma cases and have poor prognosis, there are few important caveats: 1) 2-4% of HGSOC cases have wild-type *TP53* and 2) approximately 20% of high-grade ovarian ECs have *TP53* alterations. Additional criteria such as association with STIC and mutation of *CCNE1*, *BRCA1/2*, and *MDM2* amplification can support a diagnosis of HGSOC (3, 22, 93).

Treatment:

Treatment for ovarian carcinoma depends on the stage at which the disease is diagnosed. Patients with Stage I ovarian cancer are generally treated with surgery and their 5-year disease free survival rate is over 90% (94). Depending on the extent of spread, surgery can be the removal of 1) both ovaries and fallopian tubes, 2) the uterus, 3) the omentum (fatty tissue covering the intestine) and 4) nearby lymph nodes. Treatment after surgery depends on the sub-stage and it usually involves 3 cycles of chemotherapy such as paclitaxel or carboplatin (94). Alternatively, cisplatin can be used instead of carboplatin, and paclitaxel can be replaced with docetaxel. Stage II ovarian cancer is first treated with surgery followed by adjuvant chemotherapy for 3-6 cycles and results in a five-year survival rate of 80% (94). Unfortunately, only around 25% of the patients are diagnosed at early stages and have good prognosis. The remaining 75% of the diagnosed cases have usually advanced to Stage III or IV. The treatment regimen for Stage III and IV ovarian cancer patients is similar to Stage II. First, a cytoreductive surgery is performed and is followed by at least 6 cycles of combination chemotherapy of paclitaxel and carboplatin (or cisplatin) (77, 95, 96). Additionally, targeted therapy such as angiogenesis inhibitor bevacizumab, can also be co-administered with chemotherapy.

Another option is neoadjuvant therapy where first chemotherapy is administered, then surgery is performed followed by additional chemotherapy (94, 97). Neoadjuvant chemotherapy is used in cases of bulky unresectable tumors to decrease tumor load (98). While randomized clinical trials have shown that neoadjuvant chemotherapy lead to improved quality of life of patients, there are still some problems associated with this treatment strategy (99, 100). These include loss of opportunity for debulking surgery for patients with significant side effects due to chemotherapy and lack of certainty of visual assessment of tumor dissemination following neoadjuvant chemotherapy (98-100).

The prognosis of Stage III and IV patients depends on the extent of residual disease remaining after debulking surgery. The long-term overall survival rate for optimally debulked patients (residual tumor < 1cm) is 25%. Patients with sub-optimally debulked disease have worse prognosis (77). Several studies have shown that chemotherapy increases survival in women with optimally or sub-optimally debulked advanced stage ovarian carcinoma and thus, it has remained the standard treatment to date (77, 95, 96, 101-103). Unfortunately, despite advances in chemotherapy and surgery, recurrence occurs in 90% of women diagnosed with advanced stage ovarian carcinoma, leading to high mortality rate. Recurrence can be either platinum-sensitive or platinum-resistant. A common observation for platinum-sensitive recurrence is increased response to retreatment with platinum-based chemotherapy (cisplatin or carboplatin), thus making it the standard of care. Most patients with recurrent ovarian carcinoma, including platinum-sensitive recurrence, eventually become platinum-resistant (77).

Targeted therapies have been the major focus clinical trials for the treatment of recurrent ovarian cancer in the past decade. Some successes include the use of agents

targeting the vascular endothelial growth factor (VEGF) pathway such as bevacizumab, pazopanib, nintedanib and cediranib (97). Bevacizumab, a humanized anti-VEGF antibody, is the first targeted therapy to be approved in the US in 2014 for treating platinum-resistant ovarian carcinoma based on a positive randomized clinical trial. Additionally, in Europe the drug has also been approved for 'frontline plus maintenance' therapy as well as treating platinum-sensitive ovarian carcinoma (104-107). Unfortunately, bevacizumab is associated with toxicity and adverse effects such as bowel perforation, renal dysfunction, and hypertension (104, 105). Additionally, only a subset of patients was shown to benefit from this drug (97, 108). Other agents targeting VEGF pathway include receptor Tyrosine Kinase inhibitors (TKIs) such as pazopanib, nintedanib and cediranib. Targets of these TKIs include vascular endothelial growth factor receptor (VEGFR), fibroblast growth factor receptor (FGFR) and platelet-derived growth factor receptor (PDGFR). Although appealing since they have multiple target engagement, these TKIs are also associated with increased toxicity compared to bevacizumab (97).

PARP inhibitors: Poly-(ADP)-ribose polymerase (PARP) inhibitors are a class of oral anticancer drugs, which are used as a targeted therapy to mostly arrest growth in cancer cells harboring *BRCA1* or *BRCA2* inactivating mutations (109). PARPs are polymerases that belong to a family of related enzymes which have the ability to transfer ADP-ribose to target proteins. These proteins play an important role in many cellular functions such as transcription, replication and recombination (110). Of particular interest is the role of PARPs in DNA repair, wherein certain cancers with homologous recombination deficiency (HRD) rely on PARP-mediated DNA repair for survival and

become sensitive to its inhibition resulting in 'synthetic lethality' (110). The most common causes of HRD are somatic and germline pathogenic variants in *BRCA1* and *BRCA2* genes, both of which function in homologous recombination (HR) DNA repair process that uses the undamaged sister chromatid to carry out error-free repair of DNA double-strand breaks (DSBs) (110). Additionally, mutations in other genes involved in HR repair pathway can also cause HRD (111). In HRD cancer cells, PARPs play an essential role in repairing damaged DNA through alternate processes such as base excision repair (BER) and nucleotide excision repair (NER), thus preventing accumulation of excessive DNA damage and apoptosis (112). Additionally, PARP proteins, specifically PARP1, have also been shown to regulate classical non-homologous end-joining (cNHEJ), alternative non-homologous end joining (aNHEJ) and maintain replication fork stability (113-115).

PARP inhibitors (PARPis) are small molecule NAD+ mimetics that inhibit PARylation by binding to the NAD+ site in the catalytic domain of PARP. This results in 'PARP-trapping' as PARPs are required to self-PARylate in order to release themselves from DNA. Trapped PARP-DNA complexes were found to be more cytotoxic than unrepaired damaged DNA caused by PARP inactivation, thus stimulating intense research in developing PARPis as targeted therapy in various cancers (116, 117). Olaparib was the first PARPi to be approved in 2014 for use as monotherapy in advanced ovarian cancer patients having germline BRCA1/2 pathogenic variants (118). This was followed by approval of PARPis niraparib and rucaparib for maintenance treatment of *BRCA1/2*-mutated ovarian cancer (119).

Recently, several clinical trials have focused on the use of PARPis at various stages of treatment of newly diagnosed advanced stage ovarian cancer patients and

irrespective of *BRCA1/2* status (118, 120-123). In the PAOLA-1 trial, it was shown that in patients receiving chemotherapy with bevacizumab as first-line standard therapy, the addition of bevacizumab with olaparib as maintenance therapy provided a progression-free survival rate of 22.1 months in olaparib treated patients compared with 16.2 months progression-free survival of the placebo group. While patients with *BRCA1/2* inactivating mutations had the greatest survival benefit from olaparib with median progression free survival of 37.2 months, those with *BRCA1/2* wild-type and some measure of HRD had a better survival benefit (28.1 months) than the overall group (22.1 months). Conversely, HR proficient *BRCA1/2* wild-type had the least survival benefit of 16.6 months (120). The ENGOT-OV16/NOVA trial showed that irrespective of the *BRCA1/2* or HRD status, patients with platinum-sensitive recurrent ovarian carcinoma had longer progression free survival with niraparib (21 months) compared to placebo (5.5 months) (121). Other clinical trials have also shown that the maximum benefit of PARPi therapy is seen in patients with *BRCA1/2* inactivating variants, followed by patients with *BRCA1/2* wild-type and some measure of HRD and finally, in patients with platinum-sensitive recurrent ovarian carcinoma (122, 123). This currently active field of investigation focuses on exploring various combinations of ovarian carcinoma treatment approaches (chemotherapy, bevacizumab and PARP inhibition) as well as understanding the mechanisms by which de novo or acquired resistance to PARPis develop (118, 120-123).

Risk and Protective Factors:

Increased risk for ovarian cancer incidence has been associated with factors such as early menarche, late menopause and nulliparity; all of which increase the number of

lifetime ovulations (124). Additionally, various studies have demonstrated, though not consistently, the association of diabetes mellitus, high body mass index (BMI), stress, alcohol and tobacco use with increased risk for specific subtypes of ovarian cancer (125-130). Apart from aforementioned lifestyle risk factors, several studies have identified a range of genetic susceptibility alleles for ovarian carcinoma (131). Familial studies identified *BRCA1* and *BRCA2* as highly penetrant genes responsible for increased familial risk for ovarian carcinoma (132). Germline pathogenic variants in several other genes coding for proteins involved in the HR pathway such as *RAD51C, RAD51D, BRIP1* and *PALB2* have recently been shown to be associated with a moderate increase (Relative Risk ~ 7) in ovarian carcinoma risk (133-135). Germline pathogenic variants in mismatch repair genes such as *MLH1, MSH2, MSH6* and *PSM2* were also associated with a moderate increase (Cumulative Absolute Risk = 10%-13%) in ovarian carcinoma risk (136). Different ovarian carcinoma subtypes have varying frequencies of pathogenic variants in these genes. For instance, increased risk for HGSOC is frequently associated with germline pathogenic variants in genes involved in HR pathway (Table 1.2) (9, 15, 19, 136). On the other hand, frequent association of pathogenic variants in mismatch repair genes with increased ovarian EC risk has been demonstrated (Table 1.2) (25, 66, 136).

Several factors have also been associated with reduced risk for ovarian cancer and have been hypothesized to confer a protective effect by reducing the number of lifetime ovulations. These factors include parity, lactation, use of oral contraceptives, and certain surgeries such removal of the ovaries and fallopian tubes. Several studies have shown that use of oral contraceptives is associated with a 40-50% lower risk of developing ovarian cancer and that a greater benefit is observed with prolonged use, which can last

for about 15 years even after discontinuation (137, 138). A recent study showed that even in *BRCA1* heterozygotes, a greater reduction in ovarian cancer risk is associated with longer usage of oral contraceptives compared to shorter duration (139). In addition, no significant difference was observed in risk reduction between different ovarian carcinoma subtypes, suggesting that the protective effect of oral contraceptive is uniform across different subtypes (58, 140, 141). Tubal ligations have also been associated with a 34% overall risk reduction of ovarian carcinoma in women at average risk for ovarian cancer (142). In women at high risk for ovarian carcinoma, such as those carrying *BRCA1/2* germline pathogenic variants, bilateral tubal ligation leads to a risk reduction of 57% (143).

Summary:

In conclusion, ovarian carcinoma, specifically the most common subtype HGSOC, remains one of the most lethal gynecological cancer and several factors contribute to it: 1) diagnosis at advanced stages, 2) poor prognosis, 3) lack of effective screening modalities to detect cancer at early stages and 4) resistance to current standard of care. Hence, a better understanding of the disease is critical, especially for developing strategies for early detection and prevention. Unravelling mechanisms leading to initiation of HGSOC would help identify novel biomarkers that can aid early diagnosis.

Stress and Cancer

Human Nervous System:

The human nervous system is a complex system that transmits signals to different parts of the body and is required for response to external stimuli and maintenance of internal homeostasis (144, 145). Structurally, it can be divided into two components: the central nervous system (CNS) and the peripheral nervous system (PNS). The CNS comprises of the brain and spinal cord, and is responsible for receiving, processing, and responding to sensory information. While most of these functions are responsibilities of the brain, the spinal cord acts as a messenger that relays information from the sensory organs to the brain and then sends motor commands from the brain to the peripheral body to bring about an adequate response (Figure 1.1) (144, 145).
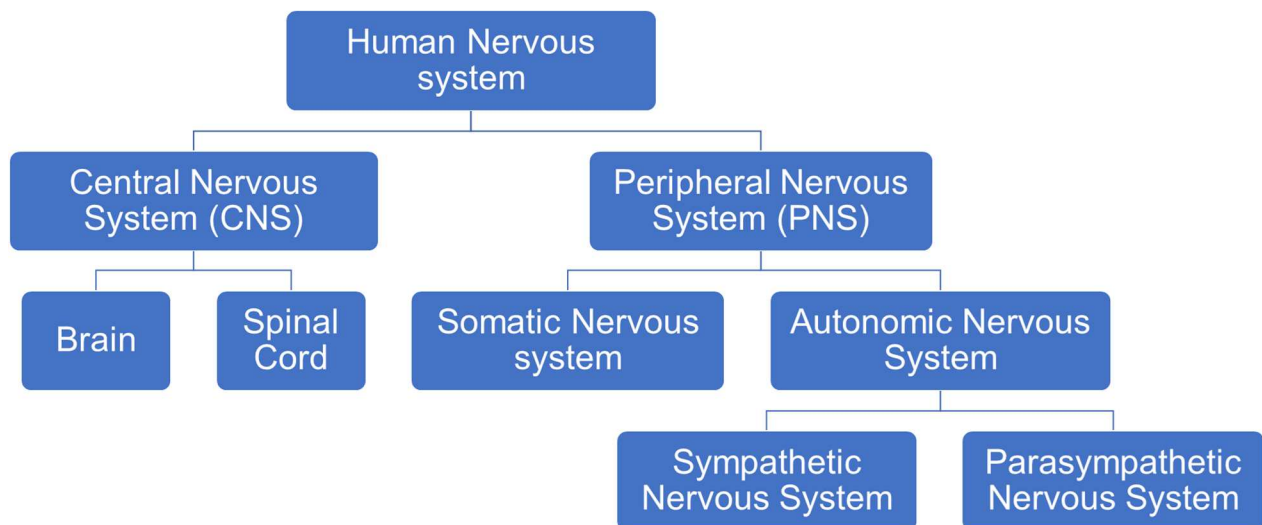
Figure 1.1. Subdivisions of the human nervous system. Adapted from (144-146)

The PNS refers to parts of the nervous system outside the brain and spinal cord and comprises of cranial nerves, spinal nerves, peripheral nerves, and neuromuscular junctions. The main function of the PNS is to transmit signals to and from the central nervous system and can be divided into somatic nervous system and autonomic nervous system (Figure 1.1). While the somatic arm of the PNS is responsible for the voluntary control of the body movements, the autonomic arm regulates involuntary physiologic processes such as respiration, digestion, heart rate and blood pressure (145, 146). Autonomic nervous system has two anatomically distinct divisions: sympathetic and parasympathetic (Figure 1.1) (145). Activation of the sympathetic nervous system (SNS) is triggered by perceived stress and leads to the "fight or flight" response, which is a state of overall elevated activity. In this state, there is an increase in blood pressure and heart rate, induction of glycogenolysis and cessation of gastrointestinal peristalsis. The SNS innervates almost every tissue in the body. Conversely, the parasympathetic nervous system (PSNS) maintains body homeostasis and promotes the "rest and digest" processes. PSNS only innervates the head, viscera, and external genitalia; making it a significantly smaller system than the SNS (147, 148).

Catecholamines:

Activation of SNS by an external stimulus that triggers stress response leads to release of neurotransmitter acetylcholine (Ach) from the preganglionic sympathetic splanchnic nerves, which binds to nicotinic receptors present on chromaffin cell membranes in the adrenal medulla (149). The chromaffin cells make up the parenchyma of the adrenal medulla and are modified postganglionic sympathetic neurons. After

activation by Ach, these cells produce and secrete chemicals called 'catecholamines' into the blood stream (150). The released catecholamines act at sites distant from the site of secretion and prepares the body for 'fight or flight' (149, 150). In addition to activating adrenal medulla, the postganglionic nerves of SNS can themselves produce catecholamines and release them directly to the target tissues via synaptic cleft and trigger 'fight or flight' stress response (149).

Catecholamines are physiologically active organic compounds that have a benzene ring with two hydroxyl side groups next to each other, known as catechol, and a side chain amine. These compounds can either act as neurotransmitters when they are released by the synaptic cleft of SNS postganglionic nerves, or they can act as hormones when released into the bloodstream by the adrenal medulla. Dopamine, norepinephrine and epinephrine make up the catecholamine family (149).

Dopamine: Dopamine is the predominant neurotransmitter found in the brain and is involved in many neurological and psychiatric disorders such as aromatic l-amino acid decarboxylase (AADC) deficiency and Parkinson's disease. It modulates the output of neurons in regions of the brain involved in voluntary motor movements (151). The majority of dopamine production in the body occurs in the anterior pituitary gland at the base of the brain and is a major part of CNS and its synthesis is independent of SNS activation (152, 153).

On the other hand, while the stress-induced activation of SNS leads to some synthesis and release of dopamine in the adrenal medulla and the postganglionic

sympathetic nerve endings, most of it acts as precursors for norepinephrine and epinephrine. Hydroxylation of amino acid tyrosine results in the production of DOPA, which then undergoes decarboxylation to form dopamine. Dopamine then undergoes further hydroxylation to form norepinephrine. Methylation of norepinephrine results in the production of epinephrine (149). The molecular structure of all three catecholamines in shown in Figure 1.2.
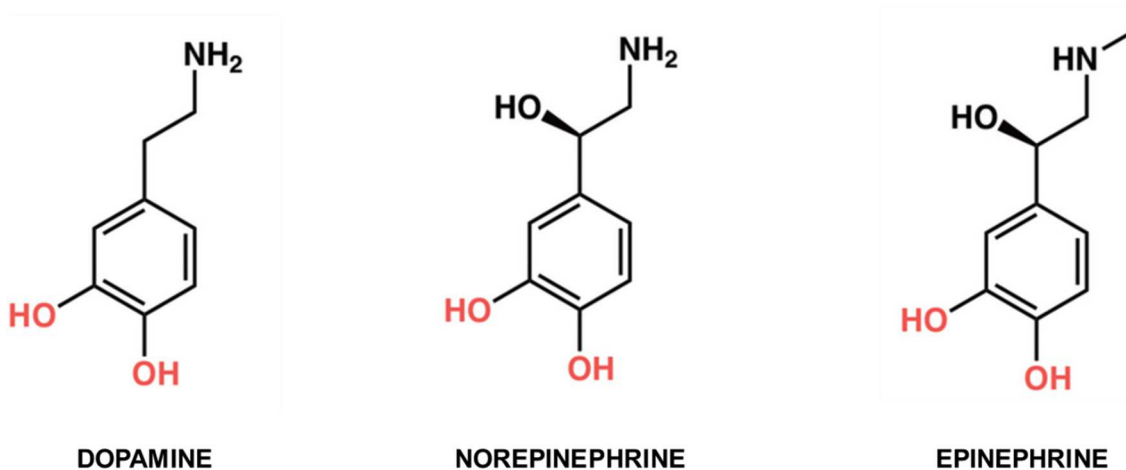
Figure 1.2. Structure of catecholamines (Adapted from (154))

Norepinephrine: The release of noradrenaline or norepinephrine (NE) via sympathetic arm of the nervous system leads to the following effects: increased heart rate, increased constriction of the arterial blood vessels, increased production of glucose by liver, increased lipolysis in adipose tissue and multiple effects on the immune system (155-159). The majority of NE molecules present in the body is primarily synthesized in and released by SNS postganglionic nerve endings directly to the target tissue, with only some amount being synthesized released into the blood circulation by adrenal medulla.

Norepinephrine acts on adrenergic receptors to bring about its effects (149, 150). Adrenergic receptors are transmembrane receptors belonging to the G protein–coupled receptor (GPCR) superfamily that activate heterotrimeric G proteins. These receptors were originally divided into α- and β-adrenergic receptors and then subdivided into three α1- adrenergic receptors (α1A, α1B, and α1D), three α2- adrenergic receptors (α2A, α2B, and α2C), and three β- adrenergic receptors (β1, β2, and β3) (149, 160).

α1 adrenergic receptors are expressed mainly in non-striated smooth muscles, which are found in the walls of blood vessels, lymph vessels and hollow organs such as stomach, intestines, bladder and uterus (147, 148, 161). Activated α1 adrenergic receptors signal through G protein induction of phospholipase C leading to activation of calcium flux and protein kinase C (PKC). α2 adrenergic receptors are expressed on smooth muscles and platelets, as well as on presynaptic neurons where they inhibit NE release by negative feedback loop by coupling to inhibitory G proteins. Other actions include decreased insulin and increased glucagon release from pancreas, increased platelet aggregation and contraction of sphincters of gastrointestinal tract (160, 161).

β1 adrenergic receptors (ADRB1) signal through G protein-mediated activation of cyclic 3′-5′ adenosine monophosphate (cAMP), which stimulates the serine-threonine protein kinase A (PKA) and mitogen-activated protein kinases (MAPK). These receptors are predominantly found in the smooth muscles of heart and kidney, and in fat cells (160, 162). Like ADRB1, β2 adrenergic receptors (ADRB2) also signal through activation of cAMP and corresponding stimulation of PKA and MAPK signaling. ADRB2 receptors are expressed on a plethora of different cell types such as epithelial cells, mast cells, airway smooth muscle cells, vascular endothelial cells, eosinophils, lymphocytes and skeletal

muscle cells (160, 163). β3 adrenergic receptors (ADRB3) are predominately expressed in adipose tissue, and like ADRB1 and ADRB2, signal through G protein/cAMP stimulation of PKA and MAPK (160).

Epinephrine: Unlike NE, which is primarily synthesized in the postganglionic nerves of SNS and released at target site, adrenaline or epinephrine (Epi) is mostly synthesized in the chromaffin cells of the adrenal medulla and then released into to blood circulation to be distributed to distant sites (160, 164). Like NE, Epi also acts on different adrenergic receptors to bring about its effects. In small doses, it has greater affinity for beta receptors; while in large doses, it selectively binds to α receptors. Through its action on α1 adrenergic receptors, Epi induces increased vascular smooth muscle contraction and intestinal sphincter muscle contraction. It also increases heart rate and myocardial contractility by acting on ADRB1. Action of Epi on ADRB2 produces bronchodilation (165).

Acute and Chronic SNS activation:

The perception of acute threat mediated by CNS can activate SNS in two ways: 1) activation of the sympathetic splanchnic nerves, which release acetylcholine to stimulate the nicotinic receptors on chromaffin cells of the adrenal medulla, and 2) activation of the postganglionic sympathetic nerve fibers directly innervating most of the body's organ systems. Adrenal medulla rapidly releases Epi (with lesser amount of NE) into blood circulation to be distributed to distant sites, causing Epi levels in the plasma to spike more than 10-fold, which then typically returns to baseline levels within 20–60 minutes after

abatement of perceived threat (160, 166). On the other hand, activation of the postganglionic sympathetic nerve fibers directly regulates organ function by µ-molar concentrations of NE released from nerve terminals. NE can also in enter the blood circulation by spilling over from sympathetic innervation of smooth muscles that surrounds blood vessels. The rapid release of Epi and NE brings about physiological alterations associated with 'fight or flight' response such as increased heart rate, increased respiratory rate and mobilization of energy by activation of ADRB2 and ADRB3 receptors in adipose tissue and liver (160, 166).

Chronic or repetitive SNS activation upregulates NE levels more strongly than Epi levels and is commonly observed in people suffering from post-traumatic stress disorder (PTSD) or who have been exposed to adverse social environments for a prolonged period (160, 167). Studies in animal models have also shown that chronic social stress can also lead to neo-innervation, which is an increase the growth and branching of sympathetic nerve fibers in target tissues, thereby upregulating basal activity of adrenergic receptors (168, 169). Chronic SNS activation has also been found to play a major part in modulating constitutive gene expression in a wide range of target tissues. For example, within the bone marrow, chronic SNS signaling transcriptionally stimulates the development of myeloid lineage immune cells such as monocytes and granulocytes at the expense of erythroid and lymphoid lineages, resulting in a pro-inflammatory shift in the circulating leukocyte pool (170, 171). Chronic SNS signaling has also been shown to act on innate immune cells such as macrophages, monocytes and natural killer (NK) cells to upregulate transcription of pro-inflammatory cytokines, chemokines and prostaglandin synthesis enzymes (170, 172-174). Although SNS-mediated transcriptional activation is required to

adequately respond to threatening environments and might have been an evolutionarily adaptive process, it has also enabled chronic stimulation of biological and molecular processes that can enable the development and progression of cancer (160, 175).

SNS Regulation of Cancer:

Analyses of SNS effects in animal models have shown that behavioral stress can accelerate the progression of different cancers such as neuroblastomas, leukaemia, pancreatic, prostate, breast and ovarian carcinomas; and these biological effects could be efficiently blocked using β-adrenergic antagonists (176-183). Various cellular and molecular processes mediating the effects of SNS activation by chronic stress include DNA damage and repair, angiogenesis, oncogene activation, survival and apoptosis and inflammation and immune response (160).

Several studies in animal models have shown that chronic stress can induce DNA damage and inhibit DNA repair, which can in turn promote tumorigenesis (160, 184, 185). Molecular pathways implicated in inhibition of DNA damage repair by catecholamines include stimulation of β-arrestin-induced AKT pathway and ataxia-telangiectasia and Rad3-related (ATR) pathway by activated ADRB2 receptors, which in turn stimulate degradation of p53 protein via murine double minute 2 (MDM2). This inhibits p53-mediated DNA damage response such as apoptosis and cell cycle arrest and leads to accumulation of damaged DNA (184-186).

Several oncogenic pathways were also shown to be stimulated by SNS-induced adrenergic signaling. For example, Src protein was shown to be phosphorylated at

residue Y419 by protein kinase A (PKA), a downstream component of adrenergic signaling. This resulted in activation of a complex signaling network that aid tumor growth, migration and invasion in animal models (187). Catecholamines were also shown to prominently stimulate *Her2* promoter activity and mRNA expression via activation of STAT3, leading to increased aggressiveness of breast cancer cells (188, 189).

Chronic stress can also regulate a wide variety of growth and survival processes such as protection of tumor cells from anoikis (programmed cell death induced by cells detaching from the neighboring cells and extracellular matrix) through activation of focal adhesion kinase (FAK), and protection of tumor cells from apoptosis by inactivating proapoptotic protein BAD (190, 191).

In addition to acting on tumor cells directly, catecholamines can also act on other cells of the tumor microenvironment such as stromal cells and immune cells (160). For example, activation of SNS-induced adrenergic signaling has been shown to increase proliferation of cancer associated fibroblast, recruit circulating stromal cells precursors to tumor sites and play a role in differentiating these precursor cells into different lineages favoring inflammation and malignancy (192, 193). Emerging data also suggests that chronic stress can modulate pro-metastatic processes by promoting the expression of mesenchymal gene expression programs through activation of SNAIL transcription factor family, thereby leading to epithelial-mesenchymal transition (EMT) (160, 194, 195). SNS-induced adrenergic signaling has also been shown to catalyze the development of blood vessels by upregulating the expression of angiogenic growth factors such as VEGF and IL-6; and increase tumor invasiveness by stimulating the expression of matrix metalloproteinase (MMP)-2, and MMP-9 (196-198).

Several studies in mouse models have shown that SNS activation can stimulate inflammatory signaling to enhance tumor progression and metastasis. SNS-induced adrenergic signaling has been shown to stimulate production of chemotactic factors such as CSF1 and MPC1 in tumor cells and enhance macrophage recruitment to tumor site. Activated adrenergic signaling in macrophages can also stimulate expression of genes that promote tumor progression, such as TGFβ, VEGF, MMP9 and IL6 (177, 199). Additionally, adrenergic signaling can also inhibit the transcription of the Type I and Type II interferons and suppress the cytotoxic function of T lymphocytes and NK cells, thereby attenuating cell-mediated immune responses against cancers and increasing cancer cell dissemination during surgery (177, 200-203).

While all these studies show how SNS-induced adrenergic signaling can aid tumor growth, survival and progression, it is yet to be determined if effects of SNS signaling are sufficient to induce tumor initiation.

Tumor innervation: Over the years, there has been intense research on how SNS catecholamines access tumor sites. One possible channel is via the vasculature that infiltrates into tumors. However, it is still unclear if circulating NE or Epi can readily penetrate the solid tumor parenchyma (160). Another possible channel is direct innervation of solid tumors by SNS. The most common innervation pattern involves entry of sympathetic nerve fibers into tumor parenchyma in association with blood vessels or from surrounding healthy tissue (164, 204, 205). Tumor cells can also express neurotrophic factors such as nerve growth factor (NGF), brain-derived neurotrophic factor (BDNF) and netrins actively promote neurogenesis and growth and branching of nerve

fibers (164, 204, 206). Tumor innervation by SNS seems to be the main channel through which most of catecholamines reach tumor site because catecholamine levels within tumor parenchyma are generally higher than the catecholamine levels in blood circulation (207).

Norepinephrine and Ovary:

Catecholamines present in the mammalian ovary and are involved in regulation of various functions such as steroidogenesis and initial follicular development (208). In rat ovaries, these functions were found to be predominantly regulated by NE by acting on ADRB2 receptors present in granulosa cells and stimulating the production of progesterone and androgens (208-210). Additionally, NE was found to be the most abundant catecholamine in the ovary and 90% of its synthesis and release was by sympathetic nerve endings (209, 211, 212). Experiments in monkeys showed that NE could also be synthesized by oocytes, which have membrane dopamine transporters that take up dopamine and hydroxylate it to form NE via dopamine β-hydroxylase (213). Studies in rats showed that ovarian nonneuronal granulosa cells can store NE and release them in a regulated way, thus acting as intraovarian NE-storing compartment (210). In aging rats, progressively reduced ovulatory capacity was associated with an increase in ovarian NE concentration. Additionally, acute denervation lead to an increase in healthy follicles (214). Experiments in mice also demonstrated a spontaneous increase in SNS activity in aging mice, which lead to increased NE levels and development of a polycystic condition (215).

SNS activation was also observed in polycystic ovary syndrome (PCOS), a common hormonal disorder that leads to formation of numerous cysts in the ovary of women of reproductive age as well as excess production of male hormone androgen (216). A study demonstrated that women with PCOS had increased sympathetic drive, which was measured using multi-unit muscle SNS activity (MSNA) (217). In rodents, PCOS models have shown elevated levels of NGF, a sympathetic neurotrophin, accompanying increased ovarian sympathetic outflow along with a range of metabolic abnormalities associated with increased SNS activity such as insulin resistance and impaired lipid metabolism (218-220). The NE levels were also found to be higher in PCOS animal models compared to control, suggesting a role for NE in maintaining this condition (216, 218). Recently, it has been hypothesized that increased SNS activity and NE levels may interconnect PCOS and ovarian cancer because: 1) women with PCOS have SNS hyperactivity and have higher cancer incidence and 2) SNS activation has a stimulatory effect on tumor growth and progression (221).

Norepinephrine and Ovarian Cancer Progression:

Several epidemiological studies have reported that PTSD, depression, and social isolation, conditions which cause chronic SNS activation, are associated with a higher risk of developing ovarian cancer (129, 130, 222-224). Additionally, higher tumor NE and ascites NE levels were observed in ovarian carcinoma patients lacking social support and living in isolation (207). Tumor NE levels also varied depending on the stage of the disease with high-grade advanced stage tumors having higher NE levels compared to early-stage low grade tumors (207). Population-based studies demonstrated a strong

33

association of psychosocial factors, such as anxiety and depression, with ADRB2-positive ovarian tumors (224). In contrast, increased eudaimonic well-being, where well-being is seen as the realization and promoting growth of full human potential, was associated with lower levels of tumor NE in ovarian cancer patients (225, 226). These studies suggest that in presence of chronic stress, levels of tumor NE gradually increases, which in turn acts on ADRB2 receptors to regulate different cellular processes leading to ovarian cancer progression.

The monthly process of ovulation has also been hypothesized to be a physical stressor mediating effects similar to chronic SNS responses. This is because during ovulation, plasma NE levels were found to be significantly elevated (227, 228). In addition, ovaries and surrounding tissues are exposed to high NE concentrations during ovulation through direct sympathetic neural innervation of the ovary (207, 229). This correlates with data demonstrating that processes involved in reducing the number of lifetime ovulation cycles, such as parity and use of oral contraceptives, are associated with reduced risk for ovarian cancer (137, 138).

Elevated NE levels can increase ovarian cancer cell growth, survival, metastasis and angiogenesis by acting on ADRB2 receptors present on the ovarian cancer cells as well as on surrounding stromal cells (160). Abnormal activation of the Src protein by elevated NE in ovarian carcinoma cells leads to enhanced proliferation and migration (187, 197). Abnormal activation of STAT3 by NE leads to increased MMP2 and MMP9 production that leads invasive potential of ovarian cancer cell lies (230). Additionally, NE can impair the responsiveness of ovarian carcinoma cells to paclitaxel chemotherapy by inducing the expression of DUSP1 (231, 232). Norepinephrine can also increase the

metastatic capability of ovarian carcinoma cells through prostaglandin E2 (PGE2) synthesis by upregulating prostaglandin E synthase gene (*PTGES*) via the ADRB2-Nf-kB axis (233). NE was also shown to induce DNA double-strand breaks, which could be abrogated by treatment with ADRB2 blocker propranolol. Interestingly, NE reduced cisplatin-induced DNA damage in receptor independent manner, suggesting that NE can modulate cisplatin resistance and affect DNA integrity in ovarian carcinoma cells (234). Other mechanisms induced by NE to promote ovarian carcinoma progression includes 1) evasion of anoikis through phosphorylation of FAK, 2) increased angiogenesis driven by elevated expression of VEGF, IL-6 and IL-8, and 3) increased EMT through upregulation of transcription factors Slug, Snai1 and Snai2 (176, 191, 235-237). A recent study showed that elevated NE levels can also lead to increased innervation of tumor tissue by acting on ADRB3 receptor instead of ADRB2 and inducing neurotrophic factor BDNF. This initiates a feed-forward loop wherein SNS activation leads to increased NE levels, which then increases innervation causing more SNS activity (238).

Norepinephrine and Ovarian Cancer Initiation:

As described in previous sections, the majority of research has focused on testing the association of chronic stress with ovarian cancer progression and on identifying various molecular mechanisms through which NE promotes tumor growth, survival and metastasis. In contrast, molecular mechanisms through which stress might affect ovarian cancer initiation remains largely unknown. Only in cancers with viral etiology, such as cervical carcinoma, a more prominent role of chronic stress in cancer initiation has been demonstrated (239). Early work showed that presence of glucocorticoid stress hormone

dexamethasone was required for oncogenic transformation of primary cervical cells containing viral glucocorticoid-responsive element in HPV-16 DNA and Ras oncogene (240). Steroid hormones upregulated E6 and E7 HPV 16 oncogenes, which degraded p53 by binding to the protein, resulting in apoptotic failure and cancer initiation (241).

Although there is no experimental evidence yet, most of the mechanisms disrupted by NE to promote cancer progression can also potentially cause tumor initiation. For example, dysregulation of DNA damage repair pathways and oncogene activation are key processes involved in cancer initiation (242). This raises the possibility that chronic SNS activation might lead to tumor initiation.

CHAPTER TWO

EFFECTS OF SHORT-TERM NOREPINEPHRINE TREATMENT

Note to reader:

Portions of this chapter have been previously published in Sci Rep. 2018 May 29;8(1):8291. doi: 10.1038/s41598-018-26670-4 and Sci Rep. 2021 Jul 12;11(1):14334. doi: 10.1038/s41598-021-93506-z; and have been reproduced with permission.

Introduction

Since the mechanisms through which stress affects ovarian cancer initiation remains mostly unknown, the main objective of this study is to determine the role of stress in normal cells likely to give rise to ovarian cancer in order to understand how stress regulates tumor initiation. As mentioned previously, NE is the most abundant stress hormone present in the ovary and elevated NE levels are associated with development of PCOS and increased risk of ovarian cancer (207, 210, 214-217, 222-224). Therefore, we chose NE as our stress hormone of interest.

Since HGSOC is the most common ovarian carcinoma subtype and recent evidences have shown that they mainly arise from fallopian tube cells (29, 38, 40, 41, 43), we chose normal *TERT*-immortalized fallopian tube secretory epithelial cells, iFTSEC283, as our model for precursor cells for ovarian cancer in addition to normal *TERT*-immortalized ovarian surface epithelial cells, iOSE11 (243-246). Because *TP53* alterations are highly prevalent and happen early in the development of HGSOC (11-13, 15), we also evaluated exposure to NE in fallopian tube and ovarian epithelial isogenic cell derivatives expressing a dominant-negative TP53 mutant p.(R175H).

Materials and Methods

Cell lines:

We used immortalized fallopian tube secretory epithelial cell lines, iFTSEC283, iFTSEC282^{p53R175H} and immortalized ovarian surface epithelial cells, iOSE11 (provided by Simon Gayther; Cedars Sinai, CA). These cells have been extensively characterized and are considered cell line models of precursor cells of HGSOC (243-246). We also used iFTSEC283^{p53R175H} and iOSE11^{p53R175H} derivative cell lines, which overexpress mutant p53, generated in the laboratory (see below).

NOSE-CM medium consisting of MCDB105 and Medium 199 (Sigma-Aldrich) (1:1) supplemented with 15% fetal bovine serum (Sigma-Aldrich), 0.5 mg/ml hydrocortisone (Sigma-Aldrich), 10 ng/ml epidermal growth factor (Thermo Fisher Scientific), 5 mg/ml insulin (Sigma-Aldrich), and 34 mg protein/ml bovine pituitary extract (Thermo Fisher

Scientific) was used to culture iFTSEC283, iFTSEC282^{p53R175H}, iFTSEC283^{p53R175H}, iOSE11 and iOSE11^{p53R175H} cells. Ovarian cancer cell line, OVCAR8, was cultured in DMEM (Thermo Fisher Scientific) supplemented with 10% fetal bovine serum (Sigma-Aldrich). Another ovarian cancer cell line SKOV3 was cultured in McCoy's 5A (ATCC) supplemented with 10% fetal bovine serum (Sigma-Aldrich). Cell lines were periodically tested for mycoplasma. iFTSEC283, iFTSEC283^{p53R175H}, iOSE11 and iOSE11^{p53R175H} cells were authenticated using short tandem repeat (STR) analysis.

Lentivirus transduction for p53R175H overexpression:

A V5 tagged pLenti6/V5-p53_R175H (Addgene plasmid 22,936, Junk Lab) plasmid was used to overexpress the dominant-negative mutant TP53 p.(R175H) in iFTSEC283 and iOSE11 cells. The p53R175H mutation in the plasmid was confirmed by Sanger sequencing. pLP1, pLP2, and pLP/VSVG ViraPower (Thermo Fisher) viral packaging vectors were used along with pLenti6/V5-p53_R175H to make virus particles in HEK293FT cells. Virus particles were used to transduce iFTSEC283 and iOSE11 cells, followed by blasticidin (2.5 μg/ml) selection. Single cells were then plated in 96 well plates to obtain single-cell clones. Expression of the TP53 p.(R175H) mutant was confirmed by western blot using V5-tag Rabbit antibody (D3H8Q; Cell Signaling).

RNA isolation:

iFTSEC283 and iOSE11 cells were plated on 100 mm plates and cultured for 24 h after plating to reach 80% confluency. Cells were then briefly washed with PBS (Thermo Fisher Scientific) and fresh medium containing 10 μM norepinephrine (Sigma-Aldrich) or vehicle (H_2O) and incubated for 15 min, 1h and 4h (Figure. 2.1A). Cells were harvested

immediately after treatment and processed for total RNA extraction using the RNeasy Mini Kit (Qiagen, Hilde, Germany) following manufacturer's protocol, including the optional "on-column DNase digestion" step using freshly prepared DNase. Quality and purity of the RNA samples was tested by Nanodrop (ratio of absorbance at 260/230 was ≥2). Reverse transcription was performed using the QuantiTect Reverse Transcription kit (Qiagen). RNA samples were used for sequencing and for verification of gene expression by qPCR.

A

B
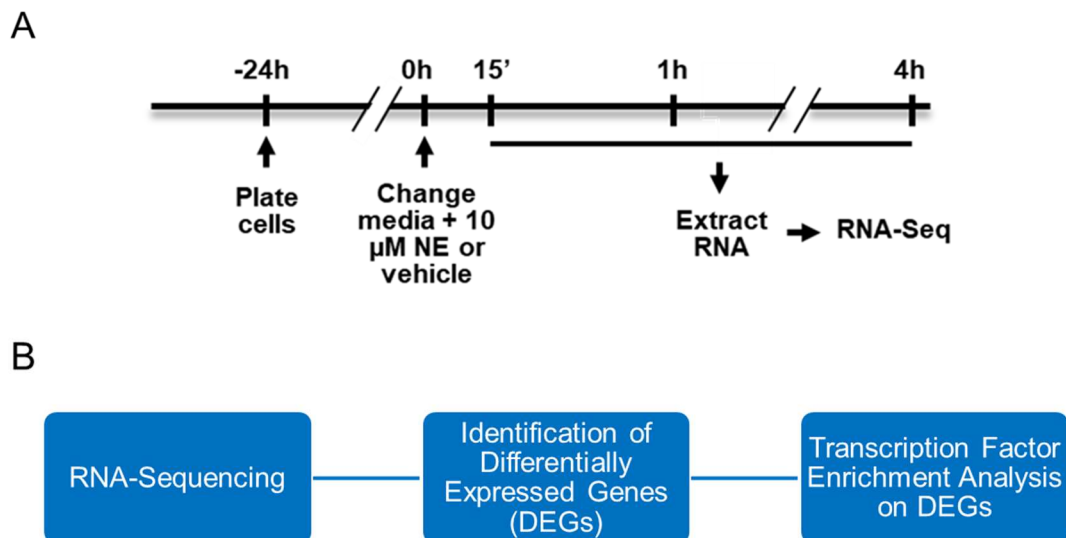
Figure 2.1. Early transcriptional response to norepinephrine (NE). (A) Experimental timeline (**B**) Schematic of analysis performed after RNA-sequencing

Library preparation and RNA sequencing:

Total RNA was collected for each cell line and each treatment condition in three independent replicates. 100 ng of total RNA was used for library preparation using Ovation Human FFPERNA-seq multiplex system (NuGEN Technologies, San Carlos,

CA). Sequencing was performed on an Illumina NextSeq500 instrument with 75 bp paired end reads. On average, 23 million pairs of reads were generated for each sample. The average alignment rate was 92.5% with Q30 ≥ 94%. (*Library Preparation and RNA-sequencing was performed by the Molecular Genomics Core at Moffitt Cancer Center*).

RNA-Seq analysis:

Following initial quality assessment and adaptor trimming, sequencing reads were aligned with Tophat v2.0.13 against human reference genome hs37d5 (247). Quantification of read counts aligned to the region associated with each gene was performed using HTSeq v0.6.1 based on National Center for Biotechnology information (NCBI) RefSeq gene model (248). Read counts of all samples were normalized using the median-of-ratios method implemented in R/Bioconductor package DESeq2 v1.6.3 (249). Differential expression analysis between the two groups was performed by serial dispersion estimation and statistical model fitting procedures implemented in DESeq2. Genes with a p-value (adjusted for multiple testing with the Benjamini-Hochberg correction) of less than 0.1 (and/or a fold change of 2 and above) were determined to be significantly differentially expressed (Figure 2.1B). (*RNA-sequencing data analysis was performed by Dr. Ling Cen from the Department of Biostatistics and Bioinformatics at Moffitt Cancer Center*).

Over-representation analysis of regulatory motif:

oPOSSUM (250) single site analysis was applied with the following options: 0.40 conservation cutoff, 85% matrix match threshold, sequences of −5,000 to 5,000 bp from the transcription start site, and all genes in the oPOSSUM database. Shared common

genes with a p-value < 0.1 from the differential analysis in the iOSE11 and iFTSEC283 cell lines were used as an input to be searched against the Jaspar database. Enriched of transcription factor binding sites (TFBSs) were identified through computing two complementary statistical measures, Fisher exact test and Z-score. Fisher scores which are based on a one-tailed Fisher exact probability assess the number of genes with the TFBS motifs in the foreground set vs. the background set. Z-scores are based on normal approximation to the binomial distribution that measures the change in the relative number of TFBS motifs in the foreground gene set compared with the background set.

qPCR:

cDNA was synthesized from isolated RNA using Qiagen QuantiTect Reverse Transcription Kit with genomic DNA removal. PowerUp™ SYBR™ Green Master Mix (Thermo Fisher Scientific) was used for performing gene expression analysis of the following genes: *ADRB2* and *HOXA5* with *ACTB* (β-actin) as an internal control. Analysis was performed on two independent replicates and each had three technical replicates (total n = 6). Expression for each gene of interest was calculated as a relative expression ratio normalized to *ACTB* expression levels. The Δ-Δct method was used for calculating the relative expression of genes compared to mock-treated cells.

Western blotting:

NE and mock-treated cells were cultured up to 80% confluence in 100 mm plates. Cells were harvested by scraping followed by extraction of the cytoplasmic fraction by incubation for 2 min on ice in lysis buffer A [20 mM Tris pH 7.4, 10% glycerol, 10 mM KCL, 0.2% NP-40, 1 mM EDTA, 0.6 mM β-mercaptoethanol] supplemented with

1 × protease inhibitor cocktail (Roche, Basel, Switzerland) and 1 mM PMSF. Following centrifugation (12,000 rpm) at 4 °C, the supernatant containing the cytoplasmic fraction was collected and the pellets were re-suspended in nuclear extract buffer B [20 mM Tris (pH 7.4), 20% glycerol, 10 mM KCL, 0.4 M NaCl, 1 mM EDTA, 0.6 mM β-mercaptoethanol, 1 mM PMSF and 1 × protease inhibitor cocktail]. Resuspended cells were incubated for 30 min on ice. Bradford Assay (Bio-Rad Laboratories, Hercules, California) was used to determine protein concentration. Whole cell lysates containing 50 µg of both cytoplasmic and nuclear fractions were resolved in 10% polyacrylamide gels and transferred to methanol-activated PVDF using the TransBlot Turbo system (Bio-Rad Laboratories, Hercules, California). Antibodies: V5-tag Rabbit antibody (D3H8Q; Cell Signaling) and HoxA5 (Santa Cruz).

HOXA5 induction time course study (qPCR):

iFTSEC283, iFTSEC283^{p53R175H}, iFTSEC282^{p53R175H}, iOSE11, iOSE11^{p53R175H}, SKOV3 and OVCAR8 cells having 80% confluency were treated with vehicle control (H$_2$O) or NE for 15 min, 45 min, 1h, 1.5h, 2h, 3h and 4h. Cells were harvested immediately after treatment and processed for total RNA extraction using the RNeasy Mini Kit (Qiagen, Hilde, Germany) followed by cDNA synthesis from isolated RNA using QuantiTect Reverse Transcription Kit (Qiagen, Hilde, Germany) and qPCR using PowerUp™ SYBR™ Green Master Mix (Thermo Fisher Scientific) and Δ-Δct method.

HOXA5 luciferase reporter assay:

Three experimentally validated promoters for HOXA5 were identified using Eukaryotic Promoter Database (EPD) (251) (Figure 2.2). An approximately 2500 bp

region including these promoters as well as a part of *HOXA5* coding region was cloned into pGL3 enhancer vector (Promega) (Figure 2.2). 8000 iFTSEC283 and 10000 iOSE11 cells each were plated in 96 well plates in 8 technical replicates. After overnight incubation, they were transfected with pGL3 vector containing the *HOXA5* promoter (50 ng per well) (Promega) and pRL *Renilla* luciferase vector (20 ng per well) (Promega), which was used as internal control. pGL3 control vector (50 ng per well) (Promega) was used as positive control for the assay. Cells with the transfection medium containing Opti-MEM (Gibco), FuGENE HD (Promega) and the vectors were centrifuged for 30 min at 1000 rpm before incubating for 48 h. Following incubation, the cells were treated with 10 µM norepinephrine (Sigma-Aldrich) or vehicle (H_2O) control containing fresh medium and incubated for 15 min, 45 min, 1 h, 1.5 h, 2 h, 3 h or 4 h. After treatment, Dual-Glo® Luciferase Assay System (Promega) was used to measure luciferase activity following manufacturer's protocol. SpectraMax L microplate reader was used for reading the output and luciferase/renilla ratio was calculated.
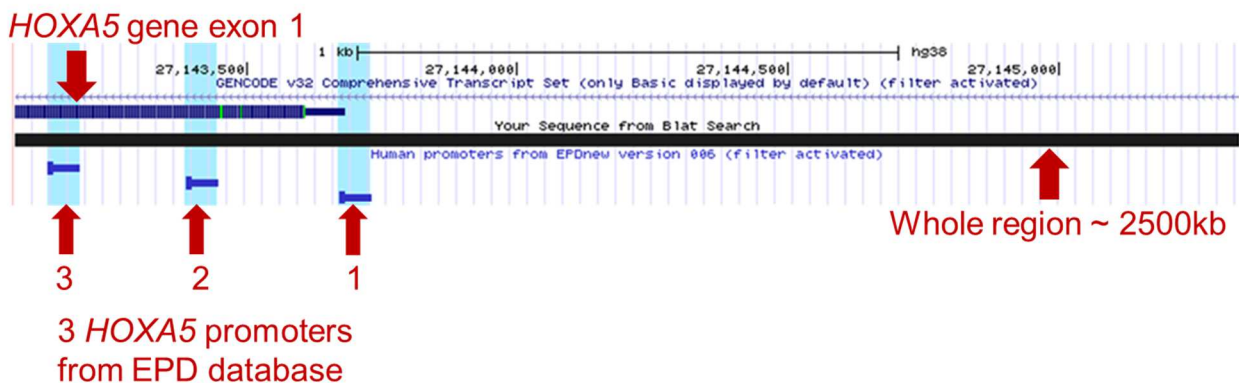
Figure 2.2. Luciferase reporter assay. *HOXA5* promoter region construct design. This construct was cloned into pGL3 enhancer vector (Promega)

HoxA5 ChIP-Seq:

iFTSEC283 cells were plated on 150 mm plates and cultured for 48 h until they reached 80% confluency. They were then briefly washed with PBS (Thermo Fisher Scientific) and treated with 10 µM NE (Sigma-Aldrich) or vehicle (H_2O) containing fresh medium and incubated for 15 mins, 1 h or 4 h. After treatment, the cells were immediately fixed with formaldehyde (Sigma-Aldrich) for 15 min. Cells were scraped and suspended in Shearing Buffer (Active Motif) and chromatin was sheared to 200-700 bp using M220 Focused-ultrasonicator (Covaris). Chromatin immunoprecipitation was performed using the ChIP-IT High Sensitivity Kit (Active Motif) following manufacturer's protocol with validated HoxA5 antibody (Santa Cruz). HoxA5 antibody was validated using mass spectrometry (Figure 2.3). In addition, the HoxA5 antibody was also validated by western blotting following silencing of the *HOXA5* gene using siRNA (Figure 2.11D). Three independent replicates for each condition were used for sequencing with input DNA for each condition as control. Library preparation was performed using TruSeq ChIP Library Preparation Kits (Illumina) followed by sequencing on an Illumina NextSeq500 instrument with 75 bp paired end reads. (*Library Preparation and ChIP-sequencing was performed by the Molecular Genomics Core at Moffitt Cancer Center*).

Cluster of Homeobox protein Hox-A5 OS=Homo sapiens OX=9606 GN=HOXA5 PE=1 SV=2 (HXA5_HUMAN)

Index	Peptide	Prob	Exclusive To	Valid	HXA5_HUMAN	H0B5_HUMAN	HXC5_HUMAN	HXC9_HUMAN	HXA6_HUMAN (+2)	H0B6_HUMAN (+5)
1	KLHISHDNIGGPEGK	16%	Homeobox protein Hox-A5 OS=Homo sapiens OX=9606 GN=HOXA5 PE=1 SV=2	✓	1.00					
2	LHISHDNIGGPEGK	100%	Homeobox protein Hox-A5 OS=Homo sapiens OX=9606 GN=HOXA5 PE=1 SV=2	✓	1.00					
3	NSLSNSSGASADAGSTHISSR	100%	Homeobox protein Hox-A5 OS=Homo sapiens OX=9606 GN=HOXA5 PE=1 SV=2	✓	1.00					
4	RADCGPGEGR	18%	Homeobox protein Hox-C9 OS=Homo sapiens OX=9606 GN=HOXC9 PE=1 SV=3	✓				1.00		
5	RIEIAHALCLSER	100%	Homeobox protein Hox-A5 OS=Homo sapiens OX=9606 GN=HOXA5 PE=1 SV=2	✓	1.00	0.00				
6	SMSMAAAGGAFRP	100%	Homeobox protein Hox-A5 OS=Homo sapiens OX=9606 GN=HOXA5 PE=1 SV=2	✓	1.00					
7	SYAASASAAPAEPR	100%	Homeobox protein Hox-A5 OS=Homo sapiens OX=9606 GN=HOXA5 PE=1 SV=2	✓	1.00					
8	TWLEPLSGAVSFPSFPAGGR	7%	Homeobox protein Hox-C9 OS=Homo sapiens OX=9606 GN=HOXC9 PE=1 SV=3	✓				1.00		
9	YGYGYNGMDLSVGR	100%	Homeobox protein Hox-A5 OS=Homo sapiens OX=9606 GN=HOXA5 PE=1 SV=2	✓	1.00					
10	YPNGPDYQLHNYGDHSSVSE…	100%	Homeobox protein Hox-A5 OS=Homo sapiens OX=9606 GN=HOXA5 PE=1 SV=2	✓	1.00					
11	YQTLELEK	100%		✓	0.96	0.00	0.00	0.03	—	—
12	YQTLELEKEFHFNR	100%		✓	0.99	0.00	0.00		—	
13	YSQPATSTHSPQPDPLPCSAV…	100%	Homeobox protein Hox-A5 OS=Homo sapiens OX=9606 GN=HOXA5 PE=1 SV=2	✓	1.00					

Figure 2.3. Antibody validation. HoxA5 Cluster: Probability of peptide from each protein of HoxA5 cluster

HoxA5 ChIP-Seq analysis:

Galaxy tool, MACS2 call peak (252), was used to identify peaks using input as control and a q-value of less than 0.05. The HoxA5 ChIP-seq peaks were correlated with RNA-seq genes. Those genes which had HoxA5 ChIP-seq peaks and were differentially expressed in RNA-seq were subjected to MEME and FIMO analysis to look for HoxA5 binding motif.

HoxA5 siRNA silencing:

50000 iFTSEC283 cells were seeded in 6 well plate. The next day these cells were transfected with 12 µl of 10 µM siControl (Dharmacon) and 12µl of 10 µM siHoxA5 (Dharmacon) in 6.6 µl of Lipofectamine™ RNAiMAX Transfection Reagent (Thermo Fisher Scientific) in Opti-MEM media (Gibco) following manufacturer's protocol. After transfection, the plate was centrifuged for 30 min at 1000 rpm. After 72 h, cells were collected for confirmation of silencing by qPCR and western blots. In addition, after 72 h following first round of transfection, a second round of transfection was performed using

the same protocol and cells were incubated for additional 24, 48 and 72 h following the first round of transfection with 72 h incubation.

Results

Differentially expressed genes identified by RNA-Seq:

To explore the effect of NE on cells postulated to be the precursors of epithelial ovarian cancer, we compared the transcriptome of immortalized ovarian surface epithelial and fallopian tube secretory epithelial cells (iOSE11 and iFTSEC283) mock-treated or treated with 10 µM NE for 15 min, 1 h and 4 h (Figure 2.4A and B). At 15 min time point, we did not find any significant differentially regulated genes in response to NE treatment. In contrast, we identified a total of 53 and 234 differentially (False Discovery Rate < 0.1) expressed genes in iOSE11 and iFTSEC283 cells, respectively, upon 10 µM NE treatment for 1 h (Tables 2.1 and 2.2). Forty-five of these genes were significantly (FDR < 0.1) differentially expressed and in the same direction (34 up and 11 down-regulated) in both cell lines (Figure 2.4A).

Figure 2.4. Early transcriptional response to NE. Venn diagram showing genes differentially expressed in response to norepinephrine (NE) treatment in iOSE11 and iFTSEC283 cells at (**A**) 1 h time point (adapted from (253)) and (**B**) 4 h time point. Upregulated and downregulated genes are depicted in blue and red fonts, respectively. Underlined genes are common to both cell lines at both time points.

Table 2.1: Differentially expressed genes in iOSE11 cells (1 h - mock versus 10 µM NE treated)

Gene	log2FoldChange	p-value	p-value adjusted
SIK1	1.21220746	3.64E-42	3.75E-38
PDE4B	0.98328472	1.03E-29	5.31E-26
PTGS2	0.76471814	9.81E-20	2.02E-16
RASD1	0.76312992	2.90E-21	7.47E-18
NR4A3	0.75591465	1.98E-21	6.82E-18
NFIL3	0.74311316	1.10E-17	1.61E-14
DUSP5	0.70052814	1.93E-18	3.32E-15
CEBPB	0.63514461	1.93E-13	1.66E-10
ARRDC3	0.63275582	9.00E-13	6.63E-10
DMBT1	0.62296336	1.47E-12	1.01E-09
CHMP1B	0.61857907	1.01E-14	1.30E-11
ZNF331	0.61629145	2.81E-12	1.70E-09
NR4A2	0.58192864	5.08E-14	5.24E-11
DUSP1	0.55979815	1.48E-13	1.39E-10

Table 2.1 (continued)

Gene	log2FoldChange	p-value	p-value adjusted
RGS2	0.55536132	3.72E-13	2.95E-10
DUSP10	0.53391708	1.90E-09	9.30E-07
PDE4D	0.51800154	2.63E-09	1.18E-06
ID3	0.51733626	3.17E-10	1.72E-07
AVPI1	0.50439297	6.33E-09	2.72E-06
TBX3	0.50200657	9.01E-09	3.57E-06
CEBPD	0.47494877	5.38E-08	1.98E-05
ITPRIP	0.46696773	2.43E-08	9.27E-06
THBD	0.45848117	1.84E-07	6.55E-05
HOXA5	0.45317918	3.66E-07	0.0001256
MAFB	0.44105817	7.62E-09	3.14E-06
TGIF1	0.43583761	1.00E-06	0.0003226
RHOB	0.42324558	1.97E-06	0.0005975
SNAI2	0.40161762	4.42E-07	0.0001468
HOXA3	0.3929196	8.58E-06	0.0023902
SGK1	0.39039705	3.54E-06	0.001042
PPP1R3B	0.38687999	1.41E-05	0.0036327
KLF9	0.37242948	8.32E-06	0.0023815
DUSP4	0.36223074	1.14E-05	0.003014
ETS2	0.35657672	5.19E-05	0.0127424
SOWAHC	0.35153508	7.34E-05	0.0175872
PER1	0.32992079	0.00011843	0.0271204
VEGFA	0.31631637	4.22E-05	0.0105958
FAM46A	0.31198635	0.00046009	0.0911782
BCL3	0.30996563	0.00041405	0.0867902
BTG1	0.29711909	0.00034977	0.0766889
HAS1	0.28535756	7.54E-05	0.0176649
DDIT4	0.25704244	0.00043554	0.0880045
IER3	-0.2766351	0.0002268	0.0508077
CTGF	-0.2850368	0.00042111	0.0867902
ZNF93	-0.2947416	0.0004863	0.0945534
PCF11	-0.3125827	0.00039771	0.085384
PLK2	-0.3597374	1.08E-05	0.0029218
ZNF281	-0.3913146	1.58E-06	0.0004927

Table 2.1 (continued)

Gene	log2FoldChange	p-value	p-value adjusted
JUN	-0.479222	1.99E-09	9.30E-07
FILIP1L	-0.5342485	7.89E-10	4.07E-07
CYR61	-0.5346815	3.55E-14	4.07E-11
GADD45A	-0.5833515	2.41E-12	1.55E-09
DUSP6	-0.5950225	1.58E-11	9.03E-09

Table 2.2: Differentially expressed genes in iFTSEC283 cells (1 h - mock versus 10 µM NE treated)

Gene	log2FoldChange	p-value	p-value adjusted
HAS1	2.900319	4.19E-177	5.29E-173
SIK1	2.6854741	2.72E-164	1.72E-160
NR4A2	2.6465167	2.21E-111	7.00E-108
DMBT1	2.2506773	6.16E-91	1.30E-87
CHMP1B	2.0716141	3.38E-139	1.42E-135
RGS2	1.9957328	1.08E-62	1.25E-59
DDIT4	1.8981113	1.99E-82	3.15E-79
CEBPB	1.6675739	1.65E-74	2.32E-71
AVPI1	1.6245957	2.12E-47	1.92E-44
IL11	1.5178151	4.27E-42	3.37E-39
DUSP5	1.4110911	1.93E-89	3.49E-86
NFIL3	1.3890883	6.37E-48	6.19E-45
RHOB	1.3237344	1.23E-43	1.04E-40
TSC22D3	1.3041029	2.75E-36	1.93E-33
LINC00473	1.2809875	2.51E-29	1.38E-26
DUSP1	1.2593277	2.59E-67	3.28E-64
PPAP2B	1.1851065	1.21E-30	6.96E-28
TGIF1	1.1525237	7.78E-26	3.64E-23
TBX3	1.1043658	1.85E-48	1.95E-45
PPP1R3B	1.0963492	3.14E-24	1.32E-21
PRDM1	1.0919267	2.41E-22	9.51E-20
HEXIM1	1.0575094	1.22E-31	7.37E-29

Table 2.2 (continued)

Gene	log2FoldChange	p-value	p-value adjusted
DUSP10	1.0494288	3.08E-33	1.95E-30
IER5L	1.0395233	5.95E-35	3.96E-32
ID2	1.0103278	7.17E-21	2.67E-18
PER1	0.9831064	2.11E-26	1.07E-23
ID3	0.9830162	3.00E-29	1.58E-26
MAFK	0.9815906	1.24E-19	4.25E-17
ID1	0.9601098	2.24E-22	9.15E-20
ARRDC3	0.9591987	9.22E-17	2.84E-14
PDE4D	0.9539821	1.86E-15	5.22E-13
SNAI1	0.9396428	2.32E-16	6.97E-14
SGK1	0.8580679	2.06E-21	7.89E-19
TNS4	0.8203659	9.45E-13	2.34E-10
SH2D2A	0.7970015	4.39E-13	1.11E-10
REL	0.7883187	3.97E-11	8.36E-09
ITPRIP	0.7779744	8.32E-21	2.92E-18
METRNL	0.7760654	8.32E-17	2.63E-14
CD200	0.7715012	9.07E-11	1.76E-08
PTGS2	0.7382926	5.88E-10	1.09E-07
CRISPLD2	0.7091045	1.32E-11	2.92E-09
SIM2	0.7046947	1.05E-15	3.09E-13
CPEB4	0.7029461	3.84E-15	1.06E-12
CLK1	0.6948822	7.84E-11	1.55E-08
C1orf63	0.6911563	7.11E-10	1.28E-07
ATOH8	0.6833275	2.59E-09	4.25E-07
CEBPD	0.6789227	6.17E-09	9.51E-07
GZF1	0.6704045	4.14E-11	8.58E-09
SNAI2	0.6643754	1.40E-18	4.53E-16
BDNF	0.6594385	2.18E-11	4.67E-09
ARID3B	0.6572524	5.00E-09	7.80E-07
VAMP1	0.6492821	6.25E-08	8.32E-06
FAM167A	0.6443373	1.84E-14	4.85E-12
C12orf44	0.6400114	2.21E-10	4.18E-08
KLF9	0.637445	4.99E-15	1.34E-12
CTH	0.6216777	1.99E-07	2.47E-05

Table 2.2 (continued)

Gene	log2FoldChange	p-value	p-value adjusted
SMOC1	0.6157067	2.34E-07	2.84E-05
IRAK2	0.6156758	8.54E-08	1.13E-05
CD55	0.6148516	7.02E-10	1.28E-07
KLF4	0.6127613	2.64E-07	3.18E-05
HOXA3	0.6106769	1.29E-07	1.65E-05
AKAP12	0.606582	1.04E-12	2.54E-10
GAS1	0.6010344	1.20E-07	1.54E-05
AREG	0.6006386	2.61E-08	3.76E-06
GPCPD1	0.5905623	5.32E-07	6.05E-05
FOXO1	0.5902658	4.28E-08	5.88E-06
MIRLET7BHG	0.5901622	2.16E-07	2.65E-05
TOB1	0.5838902	1.32E-08	1.95E-06
TCF21	0.5830134	3.46E-09	5.53E-07
GATA2	0.5767454	3.45E-09	5.53E-07
EDN1	0.5631947	1.17E-07	1.52E-05
FOXF1	0.5543941	2.52E-06	0.00027022
TM4SF1	0.5541799	1.95E-10	3.73E-08
PDE4B	0.5521835	4.23E-06	0.00043464
ZFP36	0.547249	5.62E-08	7.55E-06
IRS2	0.5470725	1.00E-09	1.76E-07
CAMKK1	0.545766	5.10E-06	0.00051573
C13orf33	0.5423618	8.35E-09	1.27E-06
ETS2	0.5416942	9.67E-09	1.46E-06
ARRDC2	0.5391679	7.06E-06	0.00068658
FST	0.5384358	5.87E-06	0.00058406
WDR91	0.5297365	5.19E-06	0.00052073
INSIG1	0.5282283	2.70E-08	3.84E-06
BHLHE40	0.5275175	1.58E-08	2.29E-06
MN1	0.5264201	6.62E-06	0.00065418
NEAT1	0.5153852	7.81E-06	0.00074832
TUBB2A	0.5149091	1.28E-09	2.16E-07
NUAK2	0.5115665	3.21E-07	3.76E-05
IRF2BP2	0.5091569	1.16E-09	1.98E-07
GADD45B	0.4985766	3.46E-07	4.01E-05

Table 2.2 (continued)

Gene	log2FoldChange	p-value	p-value adjusted
KLF15	0.4914478	2.88E-06	0.00030332
GEM	0.4903549	3.93E-05	0.00344987
SLC19A2	0.4898012	1.50E-05	0.00140205
BCL3	0.4891517	7.05E-06	0.00068658
PLAT	0.4875634	4.10E-08	5.69E-06
STC1	0.4787462	6.48E-05	0.00535622
TSPYL2	0.4692723	5.05E-06	0.00051452
SSTR1	0.4690885	3.34E-05	0.00299209
RAB3A	0.4657725	5.98E-05	0.00497473
OSGIN1	0.4642161	9.70E-05	0.00771317
FOSL2	0.4642081	1.36E-09	2.26E-07
TNFRSF1B	0.4565888	7.78E-06	0.00074832
FLVCR2	0.4537692	4.77E-05	0.00410053
LINC00085	0.4496213	8.29E-05	0.00680717
BCOR	0.4434309	1.57E-07	1.99E-05
JOSD1	0.4421268	5.21E-08	7.08E-06
NPTX1	0.4383807	3.81E-05	0.0033689
INHBA	0.4369085	2.96E-08	4.15E-06
ADAMTS4	0.4337598	0.00015592	0.01159321
PCDH9	0.4323805	0.00019724	0.01432822
CLCN2	0.4279573	0.00027191	0.01930874
RASD1	0.4261694	3.10E-07	3.66E-05
HOXA5	0.4233995	0.00013317	0.01007964
ZC3H12C	0.4178567	3.79E-05	0.0033689
TRAF4	0.4168094	0.00029694	0.02073641
SNHG12	0.4157281	0.00033937	0.02344084
VEGFA	0.4102453	4.31E-09	6.81E-07
C19orf26	0.4093799	0.00055373	0.03552834
DLX2	0.4080821	0.00052594	0.0340919
MAP3K8	0.4067646	0.00050329	0.03283599
SYTL2	0.4055885	0.00072377	0.04419538
LOC642852	0.403033	0.00014096	0.01054285
CBX8	0.401747	0.00073437	0.04462705
ARL4D	0.401364	0.00082694	0.04964231

Table 2.2 (continued)

Gene	log2FoldChange	p-value	p-value adjusted
FOSB	0.4009077	0.00083198	0.04964231
SAT1	0.3998881	0.00027543	0.01944904
GABARAPL1	0.3997573	0.00068591	0.04229203
BAG1	0.3950007	0.0006334	0.03945246
SLC7A5	0.3924564	4.39E-07	5.04E-05
GRAMD1B	0.3918603	0.00083261	0.04964231
PTPRN	0.3918461	0.00027071	0.01930874
SIK2	0.3844193	4.46E-05	0.00388593
PPP1R3C	0.3830166	0.00137452	0.07826101
IL24	0.3815462	0.00070697	0.04337885
MIR614	0.374167	0.00010159	0.0079758
SOCS3	0.3719633	0.00012656	0.00969533
JUND	0.3644705	0.00045124	0.03017842
GTF2IRD1	0.3548459	0.00178437	0.09759002
MEF2D	0.3506495	0.00012101	0.00932621
SOCS5	0.3489442	0.00029114	0.02044414
ARC	0.3478326	0.00010995	0.00857889
CPEB2	0.3439302	0.00040647	0.02747477
CYP1B1	0.338931	0.00088843	0.05247534
CXCL2	0.3378742	0.00180665	0.09759002
SHC4	0.3324083	0.00063361	0.03945246
SNHG1	0.3316155	0.00043636	0.02933788
C11orf96	0.3299062	2.34E-05	0.00213157
UGCG	0.3286272	4.93E-05	0.00417941
CDK17	0.3206274	0.00158276	0.0885227
RRAD	0.3203394	8.73E-05	0.00707102
ZFP36L2	0.3172371	0.00016266	0.01202312
RBM39	0.315007	8.41E-05	0.00685618
USP36	0.3053598	0.00017526	0.01287933
PTP4A1	0.3039009	0.00011521	0.00893383
HERPUD1	0.3026682	0.00124311	0.07174855
TOB2	0.2968797	0.00060909	0.03830309
HYMAI	0.2928214	0.0014124	0.07969996
SYNPO	0.2917082	0.00180478	0.09759002

Table 2.2 (continued)

Gene	log2FoldChange	p-value	p-value adjusted
ARID5B	0.2723919	0.00033238	0.02308397
B4GALT1	0.2674636	0.0005957	0.03764795
KLF6	0.2548192	0.00048292	0.03185903
CSNK1E	0.2348346	0.00169421	0.09399276
OXTR	-0.226869	0.00139918	0.07930783
PRR15	-0.23747	0.00109262	0.06393852
PPP1R18	-0.278695	0.0005644	0.03603027
ARSJ	-0.282168	0.0018059	0.09759002
TRIM8	-0.28571	0.00125679	0.07189549
THBS1	-0.28595	0.00066033	0.0409143
XIRP1	-0.297075	0.00048394	0.03185903
ZNF24	-0.298966	0.0005898	0.03746269
ADM	-0.29915	0.00019888	0.01436479
FOSL1	-0.300289	2.49E-05	0.00224878
C5orf30	-0.309251	0.00148815	0.08360095
PLIN2	-0.310542	0.00036489	0.0250665
RIN2	-0.321483	0.00019692	0.01432822
ETS1	-0.322689	0.00013797	0.01038076
CHAMP1	-0.32447	5.66E-05	0.00473553
FBXO30	-0.327388	0.00050397	0.03283599
GLIS2	-0.328569	0.00084559	0.05017961
BIRC3	-0.330591	0.00172252	0.09507723
PHF23	-0.34754	0.00176938	0.09723903
AMIGO2	-0.34892	0.00125703	0.07189549
FOXL1	-0.349088	0.00023162	0.01663462
IER5	-0.352689	0.00053067	0.03422282
RG9MTD1	-0.357794	0.00037753	0.02579464
CDC42EP3	-0.363692	1.80E-07	2.26E-05
CYR61	-0.364016	5.67E-07	6.37E-05
RGMB	-0.364334	1.37E-05	0.0012925
KLF7	-0.365837	9.15E-05	0.00736812
PHF13	-0.369555	0.00169544	0.09399276
TXNIP	-0.375506	0.0003904	0.02653068
PPP1R15A	-0.381222	1.51E-05	0.00140441

Table 2.2 (continued)

Gene	log2FoldChange	p-value	p-value adjusted
SPOCD1	-0.381756	5.04E-05	0.00424855
ST3GAL1	-0.386105	1.15E-05	0.00109184
MIR221	-0.387096	0.00117102	0.06802344
HYLS1	-0.387808	0.00097782	0.05748674
MARS2	-0.389304	0.00117319	0.06802344
CSF3	-0.395721	0.00082187	0.04964231
SIX4	-0.400409	4.84E-05	0.0041332
FOXD1	-0.40587	9.37E-07	0.00010384
HJURP	-0.408481	3.58E-06	0.00037125
TNFAIP3	-0.415641	9.66E-05	0.00771317
TRIB2	-0.419599	0.00045864	0.03051171
EIF1AD	-0.421747	1.87E-05	0.00172388
PLK2	-0.429033	1.15E-06	0.00012489
CCDC71L	-0.431548	9.93E-05	0.00784316
SNX18	-0.444565	2.15E-06	0.000232
HOXD8	-0.459236	4.68E-05	0.00404771
F3	-0.460388	2.95E-07	3.51E-05
FGF5	-0.469252	1.12E-09	1.94E-07
RGS3	-0.479204	2.19E-05	0.00200226
IER2	-0.482954	5.70E-07	6.37E-05
FILIP1L	-0.491787	1.05E-08	1.57E-06
PCF11	-0.508379	2.78E-06	0.00029537
ZNF93	-0.52265	3.32E-06	0.0003472
KRTAP2-1	-0.568911	9.97E-07	0.00010958
ENC1	-0.579784	8.60E-10	1.53E-07
ZNF281	-0.606005	9.81E-12	2.21E-09
ZNF217	-0.609253	1.72E-11	3.75E-09
ZNF175	-0.666675	4.82E-11	9.67E-09
ANGPTL4	-0.673017	1.61E-12	3.78E-10
CTGF	-0.678708	1.47E-15	4.21E-13
SPRY2	-0.679476	9.59E-12	2.20E-09
ANKRD1	-0.6813	8.21E-21	2.92E-18
IER3	-0.68395	2.92E-14	7.54E-12
JUN	-0.688935	1.52E-12	3.63E-10

Table 2.2 (continued)

Gene	log2FoldChange	p-value	p-value adjusted
EGR3	-0.700971	4.36E-11	8.89E-09
SPRY4	-0.744724	1.45E-25	6.55E-23
RGS4	-0.793161	4.76E-19	1.58E-16
TRIB1	-1.133809	5.36E-25	2.34E-22
GADD45A	-1.191898	8.02E-42	5.96E-39
EGR1	-1.265036	4.07E-26	1.98E-23
DUSP6	-2.279744	9.42E-93	2.38E-89

After 4 h of 10 µM NE treatment, we identified a total of 34 and 313 differentially (False Discovery Rate < 0.1) expressed genes in iOSE11 and iFTSEC283 cells, respectively (Tables 2.3 and 2.4). Twenty-two of these genes were significantly (FDR < 0.1) differentially expressed and in the same direction (13 up and 9 down-regulated) in both cell lines (Figure 2.4B). Four genes – *HAS1, CHMP1B, PDE4D* and *DMBT1* – were upregulated in both iOSE11 and iFTSEC283 cell lines at both 1 h and 4 h time point (Figure 2.4A and B). In iFTSEC283 cells, a total of seventy-one genes overlapped between 1 h and 4 h time points; while in iOSE11 cells, only four genes overlapped between the two time points.

Table 2.3: Differentially expressed genes in iOSE11 cells (4 h - mock versus 10 µM NE treated)

Gene	log2FoldChange	p-value	p-value adjusted
FGF5	-0.4644153	4.50E-14	2.43E-10
GRAMD1B	0.52369169	4.92E-14	2.43E-10
HDAC9	-0.4349691	1.17E-09	2.88E-06
IL11	0.4110791	1.03E-09	2.88E-06
HAS1	0.41871266	3.85E-09	7.59E-06

Table 2.3 (continued)

Gene	log2FoldChange	p-value	p-value adjusted
CHMP1B	0.38167512	7.01E-09	1.15E-05
VEGFC	-0.3134824	3.31E-08	4.66E-05
GPRC5A	0.36634679	4.81E-08	5.93E-05
PID1	0.35263466	2.57E-07	0.000282
NAV3	-0.285688	5.99E-07	0.000537
DMBT1	0.3519153	5.58E-07	0.000537
LOC730755	-0.3246544	1.11E-06	0.000913
HTR1F	-0.3317504	3.18E-06	0.002302
RGS4	-0.3078421	3.27E-06	0.002302
PDE4D	0.3213635	3.92E-06	0.002417
CSGALNACT1	0.3308013	3.78E-06	0.002417
TANC2	0.28240556	8.13E-06	0.004717
FAM167A	0.28763709	9.64E-06	0.00506
MAML3	0.31162106	9.75E-06	0.00506
HBEGF	-0.2893537	1.38E-05	0.006828
RGMB	-0.27074	1.88E-05	0.008818
SH3RF2	-0.2809901	2.25E-05	0.009634
CDC42EP3	-0.2151988	2.24E-05	0.009634
ATP8B1	-0.2644104	2.54E-05	0.010421
ADAMTS1	-0.2651088	4.23E-05	0.016677
GLI2	0.2260765	4.54E-05	0.017227
SMOC1	0.27299091	5.26E-05	0.019227
MTRNR2L8	-0.2873377	5.50E-05	0.019376
FRMD6	-0.2405342	7.24E-05	0.024613
PPP1R10	0.23498592	0.000105	0.034508
OSBP2	0.27267933	0.000119	0.037978
SMOX	0.26942628	0.000134	0.041368
C5orf30	-0.2594622	0.000148	0.043016
CD55	0.26514027	0.000144	0.043016

Table 2.4: Differentially expressed genes in iFTSEC283 cells (4 h - mock versus 10 μM NE treated)

Gene	log2FoldChange	p-value	p-value adjusted
NPTX1	1.62239815	5.66E-47	7.51E-43
PPAP2B	1.03250566	3.86E-24	2.56E-20
CD55	1.0402481	1.99E-23	8.81E-20
NHS	1.09327047	3.99E-21	1.32E-17
TANC2	0.75044353	1.20E-16	3.19E-13
DMBT1	0.93778809	2.95E-16	6.53E-13
PDE4D	0.67694424	3.98E-16	7.55E-13
STAMBPL1	0.81803811	2.52E-15	4.18E-12
MAML3	0.88039798	8.05E-15	1.19E-11
SH2B3	-0.5486988	9.21E-15	1.22E-11
MN1	0.71894431	1.11E-14	1.34E-11
C5orf30	-0.7445767	6.50E-14	7.19E-11
MICALCL	-0.8077031	8.35E-14	8.52E-11
SIK2	0.54272395	1.07E-13	1.02E-10
TBX2	-0.629735	1.85E-12	1.60E-09
XIRP1	-0.8110571	1.93E-12	1.60E-09
GRAMD1B	0.69236509	2.12E-12	1.66E-09
FGF5	-0.666655	3.27E-12	2.41E-09
MIR614	0.75629265	5.45E-12	3.80E-09
FGF7	0.78469861	7.20E-12	4.77E-09
POU2F2	-0.7738673	8.19E-12	5.17E-09
ENC1	-0.5490963	1.05E-11	6.31E-09
IRX3	-0.6175892	3.02E-11	1.74E-08
PDE7B	0.76251988	5.13E-11	2.84E-08
FRMD4A	-0.3963176	7.40E-11	3.92E-08
FAM167A	0.55408378	1.05E-10	5.38E-08
HMGA2	-0.4788033	1.31E-10	6.45E-08
SYTL2	0.6804168	2.92E-10	1.38E-07
MAFK	0.55973334	3.96E-10	1.81E-07
AKAP12	0.50867954	6.00E-10	2.65E-07
FHOD3	0.60047986	6.73E-10	2.88E-07
GALNTL2	0.71435881	7.74E-10	3.19E-07
HIC1	-0.4743062	7.93E-10	3.19E-07

Table 2.4 (continued)

Gene	log2FoldChange	p-value	p-value adjusted
PID1	0.63460767	9.33E-10	3.54E-07
TSC22D1	-0.457691	9.28E-10	3.54E-07
TM4SF1	0.59833447	1.23E-09	4.53E-07
OSBP2	0.70320616	1.33E-09	4.78E-07
NAV3	-0.5771783	1.70E-09	5.92E-07
KRT80	0.69226211	2.32E-09	7.90E-07
ATOH8	0.64366996	3.78E-09	1.25E-06
EIF2AK3	0.58226759	4.59E-09	1.48E-06
B4GALT1	0.4264213	5.98E-09	1.89E-06
C1orf198	-0.5032774	6.15E-09	1.90E-06
EBF3	0.5256697	6.47E-09	1.95E-06
FGF2	0.541923	7.57E-09	2.22E-06
MAP2K3	-0.3857653	7.70E-09	2.22E-06
GPCPD1	0.5657901	9.36E-09	2.64E-06
CD274	-0.5395482	1.32E-08	3.64E-06
TNFSF4	-0.5452859	1.50E-08	4.05E-06
PRR5L	0.48317321	1.74E-08	4.61E-06
MBNL2	0.4686396	1.92E-08	4.98E-06
KRTAP1-5	-0.6307166	3.70E-08	9.45E-06
FHL3	-0.4195283	3.95E-08	9.70E-06
TMEM120B	0.4482191	3.90E-08	9.70E-06
TSHZ3	-0.4815422	4.22E-08	1.02E-05
PODXL	-0.5550582	5.02E-08	1.18E-05
PRICKLE1	-0.6336487	5.06E-08	1.18E-05
PGM2L1	0.61834441	5.31E-08	1.19E-05
SLC20A1	-0.5177062	5.27E-08	1.19E-05
NR2F2	-0.5173823	6.38E-08	1.41E-05
LZTS1	-0.5738258	8.03E-08	1.75E-05
DOT1L	-0.3481552	8.43E-08	1.80E-05
SHC4	0.58604095	8.86E-08	1.87E-05
IL1R1	0.41876307	9.20E-08	1.91E-05
VEGFC	-0.4277081	9.34E-08	1.91E-05
SCUBE3	-0.3697239	9.73E-08	1.96E-05
HAS1	0.55238694	1.38E-07	2.73E-05

Table 2.4 (continued)

Gene	log2FoldChange	p-value	p-value adjusted
RGMB	-0.6112987	1.42E-07	2.78E-05
NAB2	-0.4717975	1.70E-07	3.26E-05
CTH	0.5859115	2.07E-07	3.93E-05
SERPINB2	-0.548347	2.64E-07	4.93E-05
DUSP7	-0.3812494	2.72E-07	5.01E-05
KLF16	-0.4232716	3.08E-07	5.59E-05
BAZ1A	-0.3912654	3.25E-07	5.82E-05
IGF1R	0.3809721	3.39E-07	5.99E-05
PLAT	0.40855245	3.68E-07	6.42E-05
FLI1	-0.375126	3.91E-07	6.74E-05
ANTXR2	-0.319485	4.48E-07	7.62E-05
MGEA5	0.37965342	5.53E-07	9.28E-05
ADAM19	-0.3841368	5.86E-07	9.71E-05
GLIS1	0.46039911	6.36E-07	0.000104
LRRC8A	-0.3497898	6.94E-07	0.000112
FAM59A	0.56029897	7.19E-07	0.000115
NOG	0.57168209	8.29E-07	0.000131
SPRY4	-0.3521154	9.25E-07	0.000144
HSD17B2	0.5476851	1.01E-06	0.000156
ANKRD34A	-0.4966771	1.06E-06	0.000162
BACH1	-0.4342828	1.16E-06	0.000175
ITGA2	-0.4607764	1.23E-06	0.000184
TNS4	0.53230927	1.32E-06	0.000195
ELK3	-0.3436763	1.35E-06	0.000197
SIK3	0.37254173	1.37E-06	0.000197
KLF6	-0.4748284	1.42E-06	0.000202
LOC730755	-0.5196404	1.52E-06	0.000213
SMAGP	-0.3725772	1.53E-06	0.000213
HDAC4	0.48590265	1.58E-06	0.000218
KLF5	-0.3895797	1.65E-06	0.000225
NR4A1	0.55236245	1.68E-06	0.000227
CRISPLD2	0.55248858	2.02E-06	0.000271
ERRFI1	-0.3006087	2.13E-06	0.000282
KRTAP2-1	-0.4975587	2.30E-06	0.000302

Table 2.4 (continued)

Gene	log2FoldChange	p-value	p-value adjusted
IRS1	0.32094524	2.45E-06	0.000315
KRTAP4-12	-0.4572275	2.43E-06	0.000315
PLAUR	-0.350461	2.56E-06	0.000327
ANGPTL4	-0.470669	4.15E-06	0.000524
AVPI1	0.47520514	4.33E-06	0.000542
HTR1F	-0.4623344	4.48E-06	0.000545
JAG1	-0.4904631	4.44E-06	0.000545
PITPNC1	0.52654519	4.47E-06	0.000545
ETS2	0.48017746	4.55E-06	0.000548
BCAR3	-0.3978457	4.62E-06	0.000551
CHMP1B	0.45139205	4.65E-06	0.000551
SEC14L1	-0.2957906	4.90E-06	0.000575
CXXC5	-0.4986749	5.10E-06	0.000593
GABARAPL1	0.50403801	5.28E-06	0.000604
NAGS	-0.46971	5.25E-06	0.000604
FHOD1	-0.3453909	5.42E-06	0.000615
USP36	-0.3380956	5.94E-06	0.000668
FOXL1	-0.4280046	6.16E-06	0.000687
PTGES	0.41150329	6.83E-06	0.000755
DIXDC1	0.41878131	7.24E-06	0.000794
INHBA	0.4042113	7.90E-06	0.000858
NFKB1	-0.3970743	7.95E-06	0.000858
PRKCD	-0.348804	8.87E-06	0.000949
DNMBP	0.35118824	9.56E-06	0.001008
PRKCE	0.48498498	9.57E-06	0.001008
DOCK4	0.50315405	9.70E-06	0.001014
NPR3	0.46021386	1.01E-05	0.001049
MTSS1	-0.4802015	1.05E-05	0.001076
TET3	-0.4540875	1.05E-05	0.001076
C14orf49	-0.4844307	1.12E-05	0.001131
NR2F1	-0.310907	1.13E-05	0.001131
FRMD6	-0.3621208	1.20E-05	0.001197
ARNTL	0.44046924	1.45E-05	0.001433
ARHGAP24	-0.434175	1.49E-05	0.001464

Table 2.4 (continued)

Gene	log2FoldChange	p-value	p-value adjusted
BNC2	0.38797149	1.59E-05	0.001549
GPR77	0.45281876	1.61E-05	0.001559
TUFT1	0.49942602	1.62E-05	0.001559
IKZF2	-0.4653355	1.93E-05	0.001842
SIM2	0.37827456	1.95E-05	0.001849
CUX1	0.27422497	2.01E-05	0.001875
FLNC	-0.2735009	2.00E-05	0.001875
RNF103	0.41601387	2.04E-05	0.001889
FAT1	0.28244147	2.08E-05	0.00192
IGFBP3	-0.3272477	2.17E-05	0.001982
GPRC5A	0.372408	2.19E-05	0.001994
MOK	-0.3339878	2.21E-05	0.001995
ARHGAP29	-0.3851793	2.29E-05	0.002057
PLEKHA2	0.28108714	2.61E-05	0.002305
RAP2B	-0.4007045	2.59E-05	0.002305
EPHA2	-0.3264114	2.71E-05	0.002369
TOP2A	0.27156269	2.70E-05	0.002369
ARHGAP22	-0.4163651	2.84E-05	0.002452
TLR4	-0.4196193	2.85E-05	0.002452
JOSD1	0.32742764	2.92E-05	0.002499
ITGA3	-0.2460382	3.07E-05	0.002612
PTGER4	-0.4614309	3.13E-05	0.002646
IL1RL1	0.39345806	3.26E-05	0.002741
ADAMTS4	0.44840579	3.29E-05	0.002746
CYP1B1	0.4316373	3.39E-05	0.002813
SMURF2	-0.3729809	3.45E-05	0.00284
MAST4	-0.3960836	3.61E-05	0.002956
SH3BP5L	-0.37563	3.73E-05	0.003039
PNRC1	0.37792841	3.76E-05	0.003044
GCLC	-0.3726937	3.85E-05	0.003096
HSF2BP	0.4274597	3.97E-05	0.003171
ADAMTS1	-0.4248581	4.21E-05	0.003338
GK	0.47540648	4.23E-05	0.003338
TRIM8	-0.288048	4.25E-05	0.003339

Table 2.4 (continued)

Gene	log2FoldChange	p-value	p-value adjusted
STX6	-0.3678656	4.35E-05	0.003398
FLRT3	0.442069	4.49E-05	0.003467
TOB2	-0.2770987	4.48E-05	0.003467
S1PR3	-0.3174857	4.85E-05	0.003721
FAM196B	-0.3887288	4.91E-05	0.003747
PPARGC1B	-0.4612627	5.01E-05	0.003795
CPEB4	0.27959461	5.16E-05	0.00389
SPSB1	-0.3917078	5.31E-05	0.003979
FGF18	0.36456185	5.50E-05	0.0041
FOXC2	-0.2915055	5.61E-05	0.00416
TPPP	0.35885706	5.71E-05	0.004205
C12orf44	0.36383049	5.94E-05	0.004332
SERTAD2	-0.3120754	5.92E-05	0.004332
BAIAP2	-0.3456873	5.99E-05	0.004342
FARP1	0.33486663	6.60E-05	0.004758
ETS1	-0.2855806	6.76E-05	0.004847
LIMD1	-0.3405677	6.80E-05	0.00485
PGRMC2	0.27470007	6.91E-05	0.004901
BHLHE40	-0.3652746	7.06E-05	0.004979
FAM176A	-0.3733257	7.30E-05	0.005125
GCC2	0.32227961	7.44E-05	0.005168
TSC22D3	0.39488843	7.42E-05	0.005168
RASA3	-0.2850973	7.54E-05	0.00521
ZEB2	0.29197966	7.70E-05	0.005296
FLVCR2	0.40045534	7.89E-05	0.005395
CMIP	0.32992088	8.01E-05	0.005452
MEIS1	0.30568854	8.10E-05	0.005485
AKAP9	0.29999155	8.16E-05	0.005492
ZBTB16	0.44296332	8.38E-05	0.005617
CHD2	0.2743459	8.67E-05	0.005783
LZTS2	-0.3220394	8.77E-05	0.005817
HDAC9	-0.415717	9.25E-05	0.006109
FMN2	-0.4046531	9.46E-05	0.006212
LINC00341	-0.4082508	9.92E-05	0.006482

Table 2.4 (continued)

Gene	log2FoldChange	p-value	p-value adjusted
MYOCD	0.30903524	0.000103	0.006701
PAPPA	0.44894857	0.000108	0.00697
MEG3	0.31913673	0.000108	0.006974
TNRC6B	0.25478787	0.00011	0.007029
C3orf52	-0.4369337	0.000111	0.007068
PDLIM4	-0.2560523	0.000118	0.007486
SACS	-0.3060968	0.00012	0.007567
C5AR1	0.41176328	0.000125	0.007845
PRRX2	0.29297766	0.000129	0.008055
LOC375295	-0.3238658	0.000141	0.008787
BDNF	0.33407885	0.000145	0.008967
TET1	0.42793947	0.000145	0.008967
GPR68	-0.4397626	0.000155	0.009536
ARHGAP21	0.23925116	0.000157	0.009563
NUMA1	0.25157272	0.000157	0.009563
CLCN5	-0.3697495	0.000162	0.009841
SH2D5	-0.4368537	0.000169	0.010188
CD200	0.39160846	0.000181	0.010843
GTF2IRD1	0.34916485	0.000186	0.011117
OTUD7B	0.29072557	0.00019	0.01128
SEMA7A	-0.3536705	0.000192	0.011324
ZFHX2	-0.4337047	0.000192	0.011324
IFFO2	-0.3349197	0.000198	0.011608
ARHGAP23	-0.2193544	0.000204	0.01194
APBA1	-0.400359	0.000212	0.012354
ATP8B4	0.29379233	0.000221	0.01279
LOC284023	-0.4015877	0.000225	0.01295
OXTR	-0.3740313	0.000225	0.01295
LOC100507632	0.41721149	0.000234	0.013386
EPAS1	0.2761902	0.000248	0.014134
PHF20	0.28583396	0.000249	0.014134
IPO5	0.25038922	0.000256	0.014446
HIVEP3	0.32565238	0.000261	0.014681
SPOCD1	-0.2815809	0.000263	0.014724

Table 2.4 (continued)

Gene	log2FoldChange	p-value	p-value adjusted
AIM1	-0.3347613	0.000268	0.014946
LINC00473	0.24506609	0.000283	0.015724
FOXD1	-0.2655639	0.000287	0.015846
AGPAT4	0.40292645	0.000295	0.016261
HEXIM1	0.31128408	0.000304	0.016659
DDIT4	0.33567364	0.000311	0.016994
GLIS2	-0.2967988	0.000318	0.017228
SLC20A2	-0.3161669	0.000318	0.017228
CDC42EP1	-0.3208319	0.000339	0.018206
ERF	-0.2859279	0.000338	0.018206
GAS1	0.41552481	0.000344	0.018392
TRIM35	-0.3138832	0.00035	0.01863
PXN	-0.2421989	0.00036	0.019023
RAPH1	-0.3186407	0.000359	0.019023
SLC4A7	-0.3555214	0.000369	0.019408
TAOK3	-0.2640564	0.000402	0.021073
SOX12	-0.3113236	0.000415	0.021657
KIAA1217	0.40529993	0.000426	0.022158
ZNF93	0.36858026	0.000475	0.02461
LOC100505696	0.33588938	0.000491	0.025345
PXDC1	-0.296511	0.0005	0.025717
CSK	-0.2679691	0.000508	0.02601
SH2D2A	0.25663026	0.000512	0.02601
TTLL11	-0.329531	0.000512	0.02601
TRNP1	-0.2567182	0.000515	0.026081
BAZ2B	0.31917705	0.000556	0.028064
LOXL3	0.23721177	0.000579	0.029052
REST	-0.2327967	0.00058	0.029052
ZEB1	-0.3034892	0.000596	0.029714
MAGI1	-0.3295738	0.000634	0.031486
SLA	0.26166377	0.000638	0.031602
RAPGEF2	0.25004105	0.000642	0.031662
SGK223	-0.3711329	0.00065	0.031943
C9orf167	-0.2487283	0.000655	0.032072

Table 2.4 (continued)

Gene	log2FoldChange	p-value	p-value adjusted
NEURL1B	0.39282302	0.000659	0.032141
ARHGAP18	-0.3200747	0.000664	0.032292
AUTS2	-0.3447091	0.000721	0.034776
KIF18A	0.31872369	0.00072	0.034776
RASA1	-0.243031	0.000737	0.035428
GABPB1	0.31764707	0.000771	0.036945
GATA6	-0.3874285	0.000802	0.038253
CCNE2	-0.3604853	0.00082	0.038558
GGNBP2	0.24579604	0.000812	0.038558
KRTAP4-8	-0.2874816	0.000815	0.038558
MET	-0.2554524	0.000818	0.038558
NAV2	-0.1986012	0.00083	0.038908
KCNQ1OT1	0.30985258	0.000844	0.039442
EPC2	0.3109656	0.000852	0.039656
CHAMP1	-0.2349291	0.000865	0.040006
GJC1	-0.2582621	0.000868	0.040006
METRNL	0.27177021	0.000868	0.040006
FZD1	0.29322386	0.000891	0.040908
INHBB	0.373923	0.000895	0.040935
PAK1IP1	-0.287679	0.000912	0.041587
C17orf70	-0.2648624	0.000916	0.041626
GK5	0.2565482	0.000949	0.04297
LOC100129550	0.36322846	0.000964	0.043197
SPRED1	-0.2152534	0.000958	0.043197
ZNF175	0.30210649	0.000962	0.043197
C15orf39	-0.2919551	0.00098	0.043778
ARNT	0.24317271	0.000984	0.043786
CNR1	0.35213512	0.001031	0.04575
SGK1	-0.2818265	0.001049	0.046394
SLC37A2	-0.2615421	0.001053	0.046409
AREG	0.37446021	0.00106	0.046559
P4HA3	0.37341612	0.001073	0.046971
PPP1R15A	-0.2748914	0.001098	0.047901
BEND3	-0.3755968	0.001109	0.048099

Table 2.4 (continued)

Gene	log2FoldChange	p-value	p-value adjusted
SATB2	-0.2403532	0.001113	0.048099
ZNF850	0.33383449	0.001112	0.048099
ZNF331	0.33680528	0.001121	0.048286
CHIC2	-0.3244244	0.001132	0.048605
MBD4	0.28664695	0.001142	0.048873
CAPRIN2	-0.2672566	0.001161	0.049512
HEG1	0.23758603	0.001172	0.049833
KLF11	-0.3762246	0.001177	0.049902

Transcription Factor Enrichment Analysis

To infer common gene regulatory mechanisms induced by NE, we explored enrichment of transcription factor binding sites (TFBSs) in the 5 kb sequence up and downstream of transcription start sites of the differentially expressed genes identified in response to 10 µM NE treatment in both cell lines at 1 h and 4 h time points from the RNA-Seq data. In this analysis, we aimed to identify putative transcription factors that might play a central and early role in the transcriptional response to NE. This was done using oPOSSUM, a pre-computed JASPAR database of conserved TFBSs (250). When potential transcription factor binding sites were ranked by Z-scores, transcription factor HoxA5 was found to have a Z-score higher than 2 standard deviations above the mean in iOSE cells treated with NE for both 1 h and 4 h (Figure 2.5A and B). On the other hand, only iFTSEC283 cells treated with NE for 4 h had enriched HoxA5 TFBS with z-score higher than 2 standard deviations above the mean (Figure 2.5A and B). Although the z-score for HoxA5 was lower than 2 standard deviations above the mean for iFTSEC283

cells treated with NE for 1 h, it was still the 6th most enriched transcription factor (Figure 2.5A).
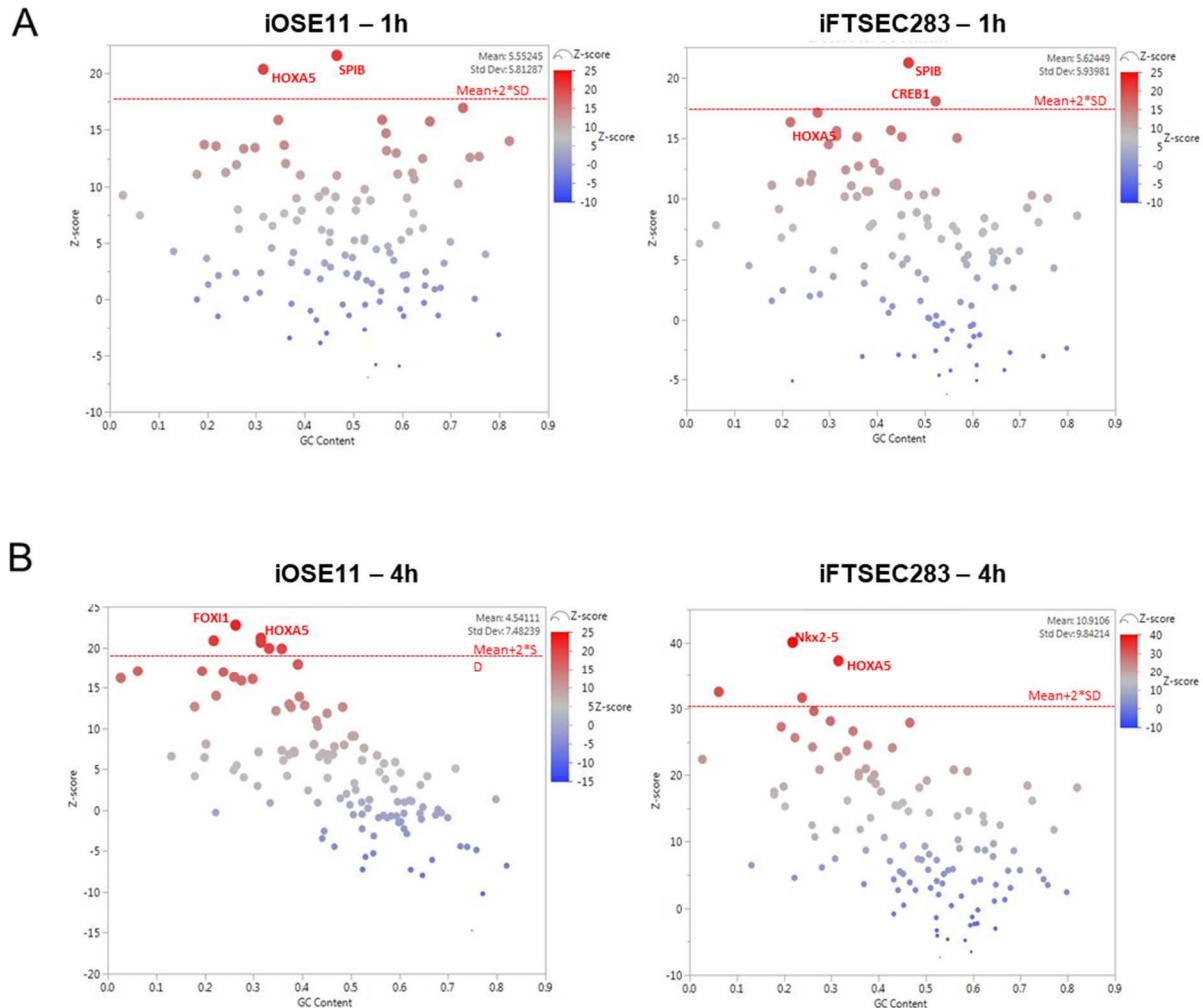
Figure 2.5. Identification of enriched transcription factors using oPOSSUM. Significantly enriched transcription factors identified using Z-score in iOSE11 and iFTSEC283 cells at (**A**) 1 h time point and (**B**) 4 h time point.

HOXA5 induction by NE in normal immortalized cell lines:

Since HoxA5 transcription factor was shown to be significantly enriched in both iOSE11 and iFTSEC283 at both time points in 'transcription factor enrichment analysis'

(Figure 2.5), and *HOXA5* mRNA was upregulated at the 1 h time point in both cell lines in the RNA Seq dataset (Table 2.1 and 2.2) (Figure 2.4), we performed a time course study to assess *HOXA5* induction curve upon treatment with NE. iFTSEC283 and iOSE11 cells were treated with vehicle control (H_2O) or 10µM NE for 15 mins, 45 mins, 1.5 h, 2 h, 3 h and 4 h, following which the cells were harvested for qPCR. The induction of *HOXA5* transcript by NE started around 1 h and peaked at 3 h time point before returning to base-line levels in both cell lines (Figure 2.6A).

Next, to confirm that *HOXA5* was induced by NE, we cloned an ~2.5kb region containing three experimentally validated *HOXA5* promoters obtained from EPD database (Figure 2.2) into pGL3-enhancer vector containing firefly luciferase and constitutively active SV40 promoter (Figure 2.6B) and transfected the construct into iFTSEC283 and iOSE11 cell lines. Relative light unit (RLU) was used to measure *HOXA5* induction levels by NE at different time points (Figure 2.6C).

Similar to the *HOXA5* mRNA time course, luciferase fused to *HOXA5* promoter showed increased activity with NE treatment in both cell lines. For iFTSEC283 cells, the luciferase activity started to significantly increase at 2 h time point, while for iOSE11 cells, the started to significantly increase at 3 h time point (Figure 2.6C). These assays indicate that *HOXA5* induction by NE is modulated via *HOXA5* promoter.
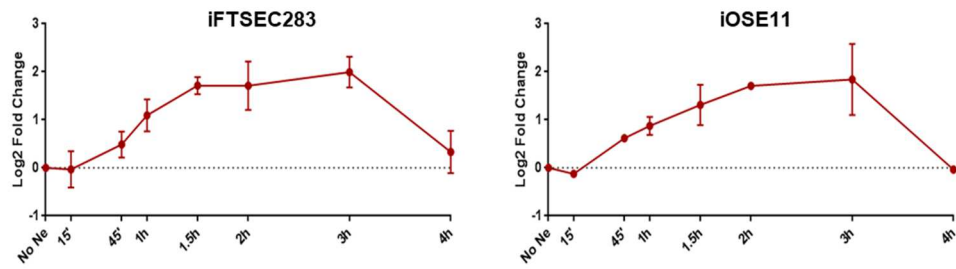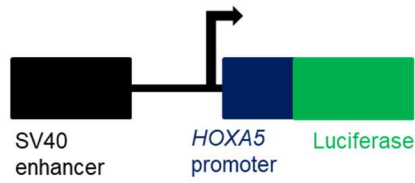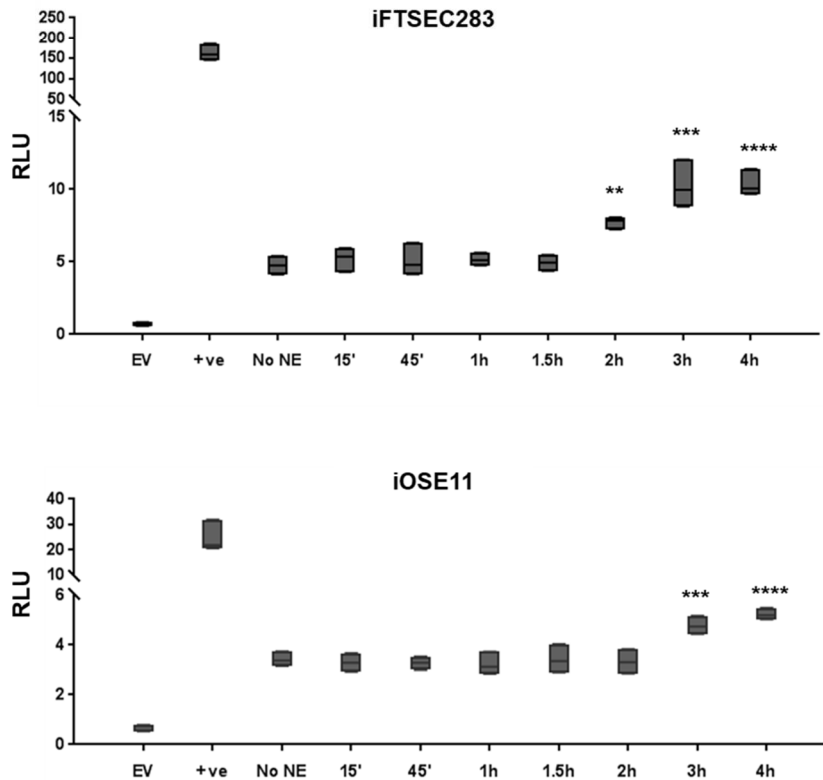
Figure 2.6. *HOXA5* induction by NE. (**A**) *HOXA5* induction time course by NE in iOSE11 and iFTSEC283 cells at transcript level (**B**) schematic of pGL3 enhancer vector with HOXA5 promoter region construct (**C**) iOSE11 and iFTSEC283 containing pGL3 enhancer vector

HOXA5 induction by NE in partially transformed and cancer cell lines:

Next, we performed a similar time course study on partially transformed cell lines and ovarian cancer cell line to assess *HOXA5* induction curve upon treatment with NE. To obtain partially transformed cell lines, we generated iFTSEC283 and iOSE11 cells that overexpressed a dominant-negative *TP53* mutant (p.R175H), because p53 alterations are the earliest and most prevalent in HGSOC. Cells were transduced with a V5-tagged p53R175H cDNA, and single-cell clones were selected. Expression of mutant p53 was confirmed by western blotting (Figure 2.7).
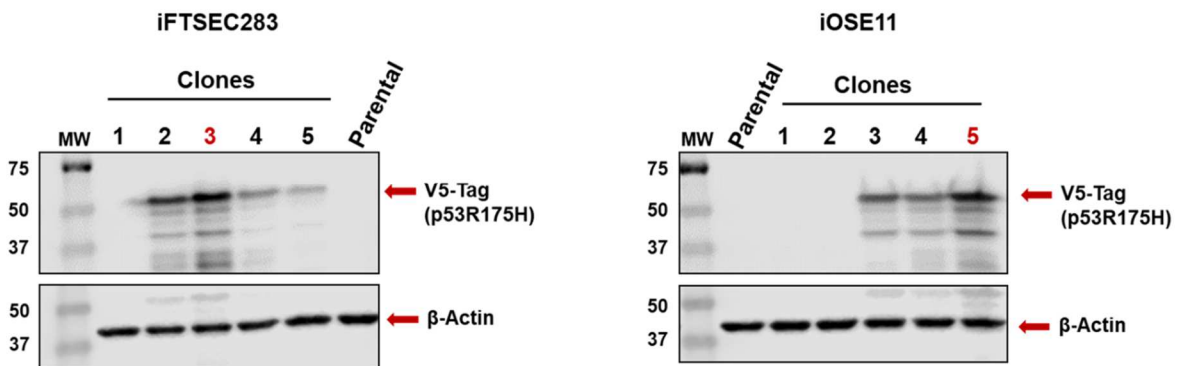
Figure 2.7. Generation of partially transformed cells. Selection of iFTSEC283 and iOSE11 clones stably expressing V5-tagged p53 (p.R175H). Clones used for subsequent experiments are denoted by red font. (Adapted from (254))

Similar to the *HOXA5* mRNA time course curve in the normal immortalized cells, partially transformed iFTSEC283[p53R175H], iFTSEC282 [p53R175H] and iOSE11 [p53R175H] cells also showed increased *HOXA5* induction by NE (Figure 2.8A). In contrast, in the ovarian cancer cell lines, OVCAR8 and SKOV3, the induction of *HOXA5* transcript by NE was abrogated (Figure 2.8B). Next, in order to verify if the loss of *HOXA5* induction in the

cancer cells was due to reduced ADRB2 receptor levels, we performed western blots with anti-ADRB2 antibody and found that the receptor levels in ovarian cancer cell lines were similar to normal and partially transformed cell lines (Figure 2.8C). This suggests a difference in NE signaling in the cancer cells when compared with normal or partially transformed cell lines.
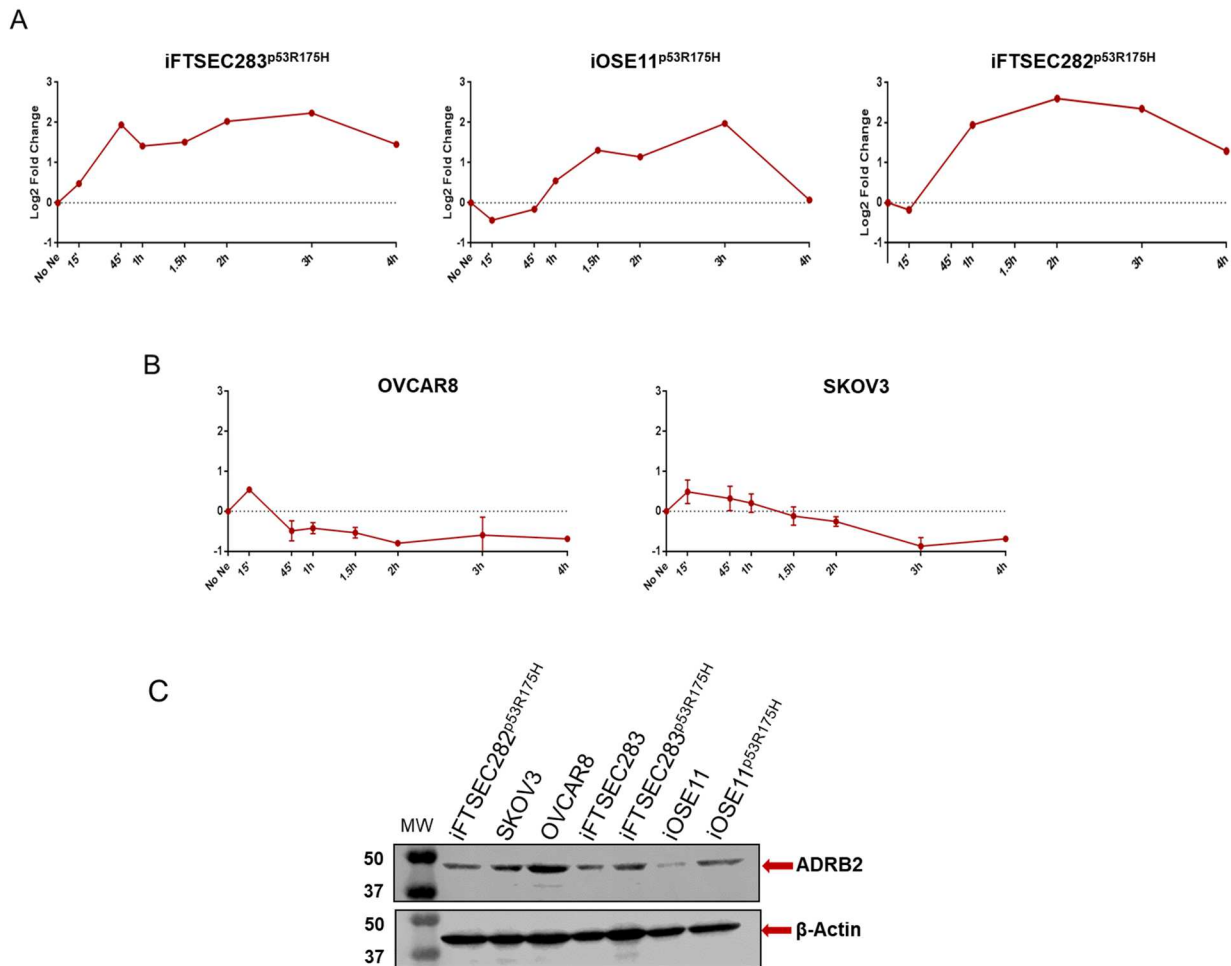
Figure 2.8. *HOXA5* induction. *HOXA5* induction time course by NE in iOSE11 and iFTSEC283 cells at transcript level in (**A**) p53 (p.R175H) overexpressing partially transformed cell lines and (**B**) ovarian cancer cell lines. (**C**) ADRB2 receptor protein levels in normal, partially transformed and ovarian cancer cell lines

HoxA5 target genes identification:

Since *HOXA5* induction by NE was confirmed in the normal immortalized cell lines at transcript level through qPCR (Figure 2.6A) and promoter level through luciferase reporter assays (Figure 2.6B), we decided to identify the HoxA5 target genes in order to dissect its role in short-term response to NE treatment. Because recent evidence has shown fallopian tube to be the main site of origin for HGSOC (32, 33, 36, 38, 40, 41, 43) and our RNA-Seq data showed that iFTSEC283 cells had more differentially regulated genes, we chose this cell line for further experiments. First, we performed an in-silico analysis using oPOSSUM database on differentially regulated RNA-Seq genes to identify targets containing putative HoxA5 binding sites. Approximately 85% of the differentially regulated genes at 1 h and 4 h time points had putative HoxA5 binding sites (Figure 2.9). Fifty-nine genes having putative HoxA5 binding sites were common to both time points.
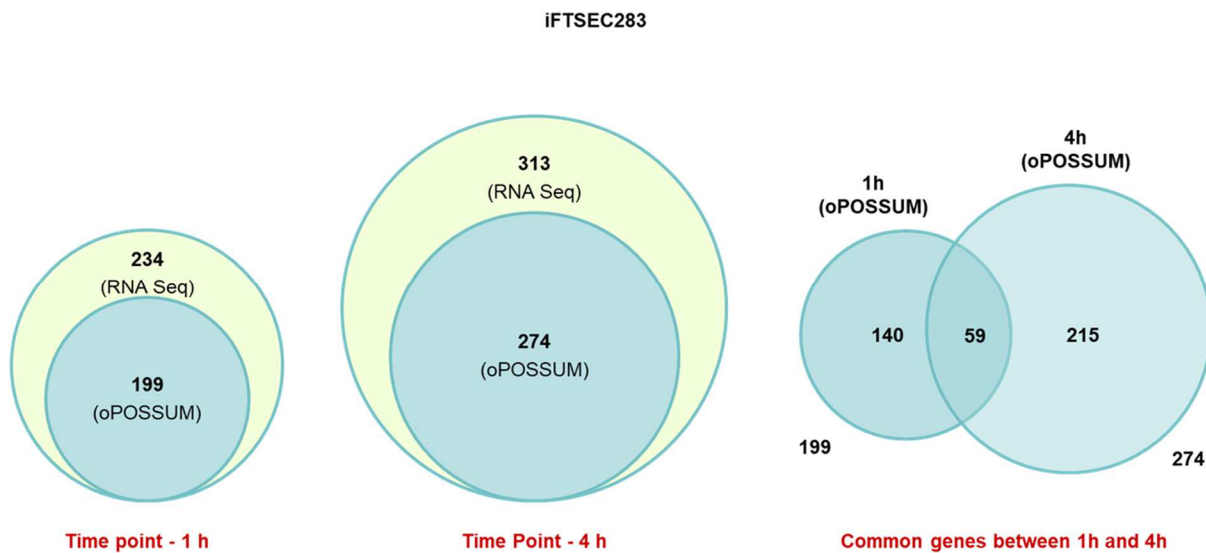
Figure 2.9 oPOSSUM analysis of HoxA5 binding sites. Venn diagrams of the genes containing putative HoxA5 binding sites that were differentially regulated in iFTSEC283 cells at 1 h and 4 h time points and those common to both time points.

Next, we performed ChIP-Seq to identify genomic sites that bind differentially to HoxA5 in response to NE. To identify target genes differentially regulated by HoxA5 in response to NE, we combined the data from RNA-Seq, oPPOSSUM analysis and ChIP seq at 1 h and 4 h time points. Nine genes had ChIP-seq peaks with fold enrichment > 4 and FDR < 0.05 (Table 2.5). These genes were also differentially regulated in the RNA-Seq analysis and contained putative HoxA5 TFBSs in oPPOSSUM analysis (Table 2.5).

Table 2.5: Differentially expressed genes in iFTSEC283 cells (4 h - mock versus 10 µM NE treated)

Genes with ChIP-seq peaks	RNA Seq	oPPOSSUM
PPAP2B	1h and 4h	1h and 4h
FRMD4A	4h	4h
CSF3	1h	1h
PRKCE	4h	4h
FHOD3	4h	4h
MAML3	4h	4h
DMBT1	1h and 4h	1h and 4h
NAV3	4h	4h
TSC22D3	1h and 4h	1h and 4h

HoxA5 belongs to Hox family of genes which have conserved DNA binding domains (255). Although the core binding sequence for Hox proteins is 'TAAT', different Hox proteins display modest differences in DNA binding specificities in the nucleotides flanking the core TAAT motif (Figure 2.10 A) (255). Hence, we used MEME tool to check if the HoxA5 binding motif was present in the sequences of ChIP-seq peaks of the nine genes. MEME is a tool that discovers novel un-gapped motifs in the input sequences (256). The most significantly enriched motif identified through MEME contained the CTAATT sequence (Figure 2.10B) that had the core 'TAAT' sequence along with flanking C and T nucleotides preferred by HoxA5 (Figure 2.10A). Next, we performed Find

Individual Motif Occurrences (FIMO) analysis and identified that six out of the nine genes

contained the 'CTAATT' motif in the ChIP-Seq peak sequence (Figure 2.10C).

A

Protein	Nucleotides preferred 5′		Core	Nucleotides preferred 3′	
HoxA5	A > G, C > T	C > G, T > A	TAAT	T > G > A, C	G, A > T, C
HoxB4	A, G > C, T	C > G, T > A	TAAT	T, G > A > C	G, A > T, C
HoxA7	A, G > C, T	C, G > T, A	TAAT	T > G, A > C	G > A > T, C
HoxC8	A > G > C, T	C, G > T, A	TAAT	T > A, G > C	G, A > T, C
HoxB1	A > G > C, T	C > G > T, A	TAAT	T > A, G > C	G, A > T, C

B
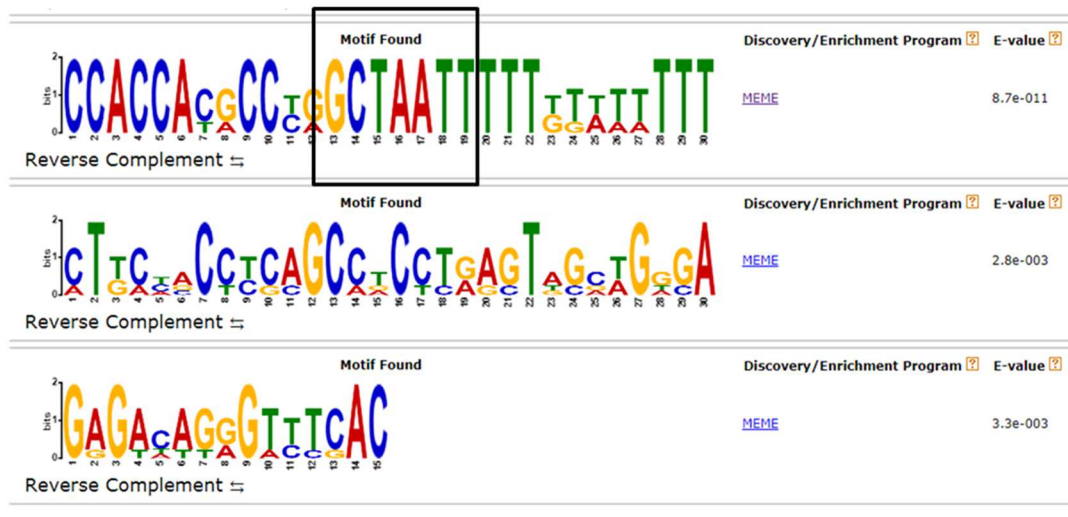
C

Motif ID	Alt ID	Sequence Name	Strand	Start	End	p-value	q-value	Matched Sequence
CCACCACGCCYGGCTAATTTTTKTWTTTTT	MEME-1	TSC22D3	-	122	151	5.79e-18	3.94e-14	CCACCACGCCCGGCTAATTTTTGTATTTTT
CCACCACGCCYGGCTAATTTTTKTWTTTTT	MEME-1	FRMD4A	-	45	74	2.06e-17	7.01e-14	CCACCATGCCTGGCTAATTTTTGTATTTTT
CCACCACGCCYGGCTAATTTTTKTWTTTTT	MEME-1	CSF3	-	220	249	5.9e-17	1.34e-13	CCACCATGCCTGGCTAATTTTTTTTTATTT
CCACCACGCCYGGCTAATTTTTKTWTTTTT	MEME-1	PPAP2B	+	161	190	8.5e-17	1.45e-13	CCACCACACCCAGCTAATTTTTGTATTTTT
CCACCACGCCYGGCTAATTTTTKTWTTTTT	MEME-1	PRKCE	-	154	183	1.08e-16	1.47e-13	CCACCACGCCTGGCTAATTTTTTGTATTTT
CCACCACGCCYGGCTAATTTTTKTWTTTTT	MEME-1	MAML3	+	259	288	1.34e-15	1.52e-12	CCACCATGTCTGGCTAATTTTTTTTTTTTT

Figure 2.10. HoxA5 targets. (**A**) Comparison of preferences for flanking nucleotides (Adapted from (255)) (**B**) MEME analysis and (**C**) FIMO analysis of the nine ChIP-seq peak sequences.

HoxA5 silencing and ChIP-seq targets validation:

In order to understand the role of HoxA5 in short-term NE response in normal cells, we knocked down HoxA5 using siRNA pool. We performed a single transfection with siHoxA5 followed by 72 h incubation and collected the iFTSEC283 cells to check the knockdown efficiency at mRNA and protein levels by qPCR and western blotting respectively (Figure 2.11A). While the *HOXA5* mRNA level showed a significant reduction of ~85% compared with control (Figure 2.11C); there was no significant reduction at the protein level (Figure 2.11D). Therefore, we performed two rounds of transfection and incubated the cells for a total of 96, 120 and 144 h (Figure 2.11B).

Figure 2.11. *HOXA5* Silencing in iFTSEC283 cells. Experimental timeline for (**A**) single round transient transfection and (**B**) double round transient transfection with siScramble and si*HOXA5*. (**C**) Transcript levels of *HOXA5* and (**D**) protein levels of HoxA5 after knockdown.

After double transfection and a total of 96, 120 and 144 h incubation, greater than 90% downregulation of *HOXA5* mRNA transcripts were observed at all 3 time points (Figure 2.11C). However, at the protein level, maximum reduction of HoxA5 was observed at 120 and 144 h (Figure 2.11D). Therefore, we chose 120 h time-point for *HOXA5* silencing and further experiments such as validation of the genes identified through ChIP-seq. These experiments are currently ongoing.

Summary

In this chapter, we focused on early transcriptional changes induced in normal and ovarian and fallopian tube surface epithelial cells by stress hormones. We compared the transcriptome of cells derived from ovarian (iOSE11) and fallopian tube surface epithelium (iFTSEC283), mock-treated and treated with 10 µM NE for 1 and 4 h. We identified that homeotic transcription factor HoxA5 was induced in normal ovarian and fallopian tube epithelial cells in response to short-term NE treatment. Additionally, six genes – *TSC22D3, CSF3, FRMD4A, MAML3, PPAP2B* and *PRKCE* – were identified to be regulated by HoxA5 in response to NE through combination of ChIP-seq, RNA-Seq, oPOSSUM, MEME and FIMO analysis.

In the partially transformed iFTSEC283^{p53R175H}, iFTSEC282^{p53R175H} and iOSE11^{p53R175H} cells, similar *HOXA5* mRNA induction curve was observed in response to short-term NE treatment. In contrast, the ovarian cancer cell lines - OVCAR8 and SKOV3 - showed attenuation of *HOXA5* induction by NE, in spite of similar ADRB2 receptor

levels, suggesting that in cancer cells NE may trigger different signaling pathways compared to normal or partially transformed cells.

CHAPTER THREE

EFFECTS OF LONG-TERM NOREPINEPHRINE TREATMENT

Note to reader:

Portions of this chapter have been previously published in Sci Rep. 2021 Jul 12;11(1):14334. doi: 10.1038/s41598-021-93506-z and have been reproduced with permission.

Introduction

The next step focused on understanding the effects of long-term NE treatment on precursor cells of ovarian cancer. To determine the extent to which stress hormones influence ovarian cancer initiation, we conducted a long-term (> 3 months; > 40 population doublings) experiment in which normal immortalized fallopian tube secretory and ovarian surface epithelial cell lines in tissue culture were continuously exposed to NE. Additionally, because *TP53* alterations are highly prevalent and happen early in the development of HGSOC (10-13, 17) we also evaluated exposure to continuous NE in fallopian tube and ovarian epithelial isogenic cell derivatives expressing a dominant-

negative TP53 mutant (p.R175H). Following long-term NE treatment, these cells were evaluated for changes in morphology, proliferation, colony-forming ability, number of chromosomes, transcriptomics and expression of *HOXA5*.

Materials and Methods

Long-term treatment with NE:

Cell lines iFTSEC283, iFTSEC283[p53R175H], iFTSEC282[p53R175H], iOSE11 and iOSE11[p53R175H] were plated in 12-well plates at density of 10,000 cells per well. Each cell line had four treatment conditions: 100 nM, 1 µM, 10 µM of NE (Sigma-Aldrich), and vehicle (H_2O) control. Each cell line had three independent replicates with different passage numbers and plated on different days. Cells were treated for 137 consecutive days (4 ½ months). iFTSEC283, iFTSEC283[p53R175H], iFTSEC282[p53R175H] were re-seeded at the ratio of 1:6 every seven days and, at the end of treatment, achieved a cumulative population doubling level (PDL) of 49. iOSE11 and iOSE11[p53R175H] were re-seeded in the ratio of 1:5 every seven days and, at the end of treatment, achieved a cumulative PDL of 44. After this treatment, cells were referred to as long-term NE-treated cells (LTNE) or mock-treated cells (Figure 3.1).
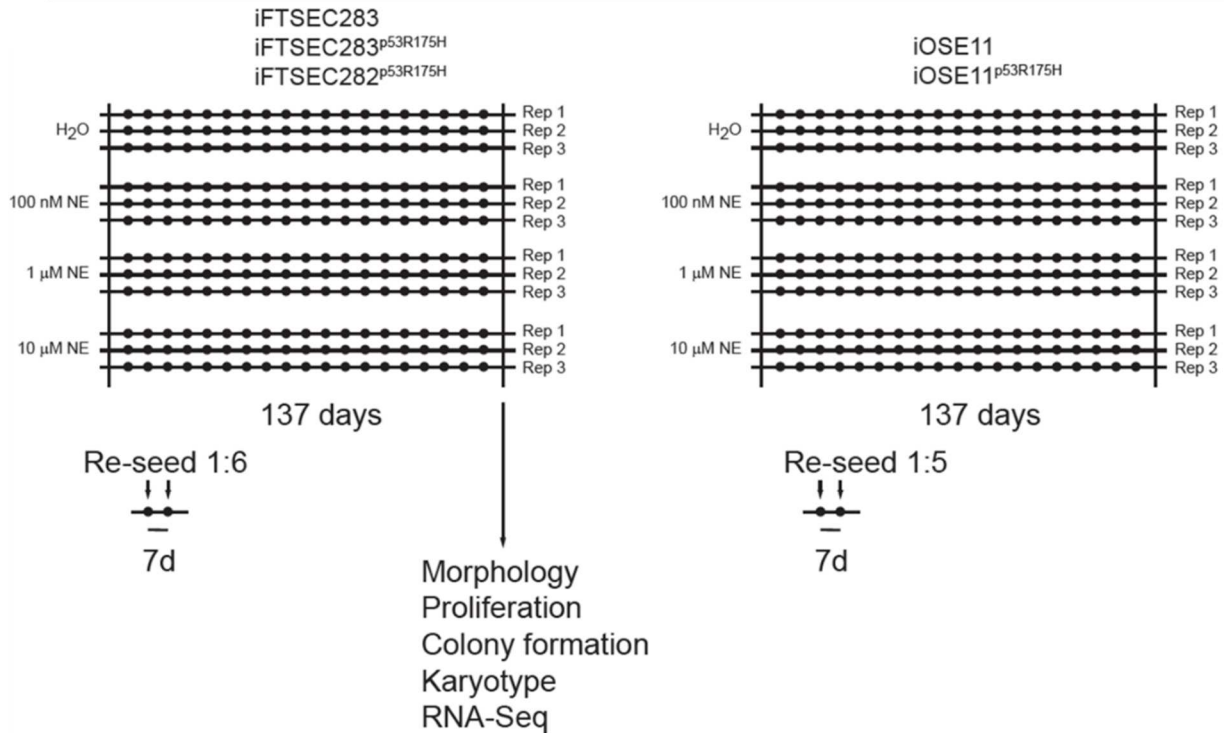
Figure 3.1. Experimental design of long-term treatment. Diagram of the experimental design representing each independent replicate and different treatments. Black dots represent subculturing by trypsinization and re-seeding. (Adapted from (254))

Proliferation assay:

Three independent replicates of LTNE and mock-treated cells were seeded in 6-well plates at a density of 500 cells per well. Each replicate was seeded on a different day over a three-day period; therefore, each condition had three biological replicates. For each independent biological replicate, there were two technical replicates (total n = 6). They were then treated with the same concentration of NE they had been treated during the long-term treatment (100 nM, 1 µM, or 10 µM NE or vehicle control [H_2O]) every alternate day until one of the wells became 90% confluent. Cells were then trypsinized and counted using Trypan blue and hemocytometer.

Colony forming assay:

Three independent replicates of LTNE and mock-treated cells were seeded in 6-well plates at a density of 200 cells per well. For each independent biological replicate, there were two technical replicates (total n = 6). Each replicate was seeded on a different day over a three-day period. They were then treated with 100 nM, 1 µM, and 10 µM NE or vehicle control (H_2O) every alternate day for 11 days. Colonies of cells were fixed in methanol for 20 min. After removing methanol, 0.5% crystal violet solution made in 20% methanol was added to the plates and incubated for 30 min. Plates were then rinsed with dd H_2O until the color no longer came off during rinsing and dried overnight.

Karyotyping:

LTNE (10 µM) iFTSEC283 and iFTSEC283^{p53R175H} cells and their respective mock-treated cells were split at a 1:10 ratio two days prior to karyotyping. Colchicine (0.02 µg/ml; Sigma-Aldrich) was added to the cells and incubated at 37 °C for 3 h. Cells were scraped and washed with PBS, followed by gentle addition of hypotonic solution (0.075 M KCl in H_2O). After 15 min of incubation at 37 °C, cells were centrifuged (1200 rpm), and the pellet was re-suspended in fixative (3:1 methanol:glacial acetic acid). This step was repeated three times. Next, cells were placed onto clean slides and air-dried in a humidifying chamber to enable optimal spreading. The metaphase spreads were imaged at 900 × magnification in an inverted microscope, and chromosomes in each spread were manually counted.

RNA isolation:

LTNE (10 µM) iFTSEC283 and iFTSEC283^{p53R175H} cells and their respective mock-treated control cells were grown to reach 80% confluence on a 100 mm plate. Cells were harvested and processed for total RNA extraction using the RNeasy Plus Mini Kit (Qiagen, Hilde, Germany) following the manufacturer's protocol, which includes removal of genomic DNA by gDNA Eliminator columns. The samples' ratio of absorbance at both 260/280 and 260/230 was ≥ 2 as measured by Nanodrop. The isolated RNA samples were used for sequencing.

Library preparation and sequencing:

Total RNA (100 ng) was isolated from three independent replicates for each condition: LTNE (10 µM) iFTSEC283 and iFTSEC283p53R175H cells and their respective mock-treated control cells. Twelve libraries were prepared using the Nugen Universal RNA Seq Kit (NuGEN Technologies, San Carlos, CA). Illumina NextSeq500 instrument was used for sequencing with 75 bp paired-end reads. Approximately 28 million pairs of reads for each sample were generated on average, and the average alignment rate was ≥ 94.2% (Table 3.1). (*Library Preparation and RNA-sequencing was performed by the Molecular Genomics Core at Moffitt Cancer Center*).

Table 3.1: Total number of reads and alignment rate per RNA-Seq library

Sample Number	Sample Name (FASTQ file)	Total number of reads (RNA-Seq)	Alignment rate (%)
1	283_s1_10uM	35,439,694	95.42
2	283_s2_10uM	30,212,959	94.21
3	283_s3_10uM	42,520,26	97.04
4	283_s1_UT	21,303,36	96.73
5	283_s2_UT	34,278,75	97.29
6	283_s3_UT	38,732,244	97.11
7	283_p53_s1_10uM	46,855,034	97.02
8	283_p53_s2_10uM	35,025,454	97.1
9	283_p53_s3_10uM	22,064,244	96.59
10	283_p53_s1_UT	23,599,444	96.92
11	283_p53_s2_UT	28,033,555	97.22
12	283_p53_s3_UT	35,205,768	97.08

RNA-sequencing analysis:

Sequencing reads were aligned against human reference genome hs37d5 using TopHat2. HTSeq with Gencode v19 was used to determine gene-level quantification by summation of raw counts of reads aligned to the region associated with each gene. DESeq2 was used for library size normalization and differential expression analysis. Sequencing depth, gene length, and RNA composition were considered for normalization and differential expression analysis. iFTSEC283 and iFTSEC283^{p53R175H} cells were normalized separately, and differential expression analysis was performed on NE-treated vs. mock-treated cells for the two cell lines. Significantly differentially expressed genes were determined using padj (p-value adjusted for multiple testing with the Benjamini–Hochberg correction) of less than 0.1. Data for the RNA-Seq experiments described here are available through NCBI Gene Expression Omnibus (GSE168097). (*RNA-sequencing data analysis was performed by Ling Cen from the Department of Biostatistics and Bioinformatics at Moffitt Cancer Center*).

Regulatory motif enrichment analysis:

oPOSSUM single-site analysis was applied to identify transcription factor binding sites enriched in our input gene set: differentially expressed genes (FDR < 0.1) obtained from RNA sequencing analysis in iFTSEC283 and iFTSEC283^{p53R175H} cell lines. We used 'Single Site Analysis' to identify transcription factor binding sites (TFBS) enriched in 5 kb sequence upstream and downstream of the transcription start site. We ranked the enriched TFBS using two complementary statistical models: Fisher test, a one-tailed probability test comparing the proportion of the target gene set containing a TFBS to background (http://opossum.cisreg.ca/oPOSSUM3/help.html#fisher), and Z-score, a two-tailed analysis that uses the normal approximation to the binomial distribution to compare the rate of occurrence of a TFBS in the target gene set to the expected rate estimated from the background set (http://opossum.cisreg.ca/oPOSSUM3/help.html#zscore). The following options were used for oPOSSUM analysis: 85% matrix match threshold, sequences of − 5,000 to + 5,000 bp from the transcription start site, 0.40 conservation cutoff, and all genes in the oPOSSUM database.

Gene ontology and pathway analysis:

Gene Ontology (GO) enrichment analysis was performed using PANTHER (Version 15.0 released 2020-02-14) Statistical Overrepresentation Test. Binomial test type and False Discovery Rate correction (FDR < 0.05) were applied.

Western blotting:

LTNE and mock-treated cells were cultured up to 80% confluence in 100 mm plates. Cells were harvested by scraping followed by extraction of the cytoplasmic fraction

by incubation for 2 min on ice in lysis buffer A [20 mM Tris pH 7.4, 10% glycerol, 10 mM KCL, 0.2% NP-40, 1 mM EDTA, 0.6 mM β-mercaptoethanol] supplemented with 1 × protease inhibitor cocktail (Roche, Basel, Switzerland) and 1 mM PMSF. Following centrifugation (12,000 rpm) at 4 °C, the supernatant containing the cytoplasmic fraction was collected and the pellets were re-suspended in nuclear extract buffer B [20 mM Tris (pH 7.4), 20% glycerol, 10 mM KCL, 0.4 M NaCl, 1 mM EDTA, 0.6 mM β-mercaptoethanol, 1 mM PMSF and 1 × protease inhibitor cocktail]. Resuspended cells were incubated for 30 min on ice. Bradford Assay (Bio-Rad Laboratories, Hercules, California) was used to determine protein concentration. Whole cell lysates containing 50 µg of both cytoplasmic and nuclear fractions were resolved in 10% polyacrylamide gels and transferred to methanol-activated PVDF using the TransBlot Turbo system (Bio-Rad Laboratories, Hercules, California). Antibodies: Anti-ADRB2 (Thermo Fisher Scientific; dilution 1:1000).

qPCR:

cDNA was synthesized from isolated RNA using Qiagen QuantiTect Reverse Transcription Kit with genomic DNA removal. PowerUp™ SYBR™ Green Master Mix (Thermo Fisher Scientific) was used for performing gene expression analysis of the following genes: *ADRB2, CDKNA1, PUMA, APOBEC3C, TP53I3, NPTX1, SCD, PTGES, MCAM, PLAU, PLAC8, DSP, ABI3BP, POSTN, BGN, MAPK13, LRRC17*, *RCAN2* and *HOXA5* with β-actin as an internal control. Analysis was done on two independent replicates and each had three technical replicates (total n = 6). Expression for each gene of interest was calculated as a relative expression ratio normalized to ACTB (β-actin)

expression levels. The Δ-Δct method was used for calculating the relative expression of genes compared to mock-treated cells.

Results

Long-term treatment with norepinephrine:

Five cell lines (iFTSEC283, iFTSEC283[p53R175H], iFTSEC282[p53R175H], iOSE11 and iOSE11[p53R175H]) were continuously cultured with either vehicle control (H_2O) or three concentrations of NE (100 nM, 1 µM or 10 µM) for 137 days (Figure 3.1). NE represents the largest fraction of ovarian catecholamines and concentrations increase markedly in pre-ovulatory follicles (257). NE can reach local levels up to 45 ng/ml in the vesicular fraction in the ovaries of experimental models (258). Additionally, tumor NE levels were observed to reach µM concentrations in ovarian carcinoma patients (207). We thus assessed the effects of NE at three concentrations representing the higher end of concentrations (i.e. 100 nM, 1 µM, 10 µM) that ovarian cells might be exposed.

To our knowledge, there is no available information about the stability of NE in tissue culture. Studies of stability of epinephrine and NE solution in storage conditions suggest that NE is stable (defined as 90% of the drug) for 28 days at room temperature when protected from light; and approximately 90% of the initial concentration remains after seven days at 26.6 °C (259). We therefore chose to replace medium with fresh media containing either vehicle control or the three concentrations of NE were added to the cells (after removing old media) every two days. After 137 days, there was no significant

difference in the Beta-2 Adrenergic (ADRB2) receptor at mRNA transcript and protein levels (Figure 3.2A and B). Additionally, no change in cell morphology was observed in any cell lines, even at the highest concentration of NE (Figure 3.3).

A
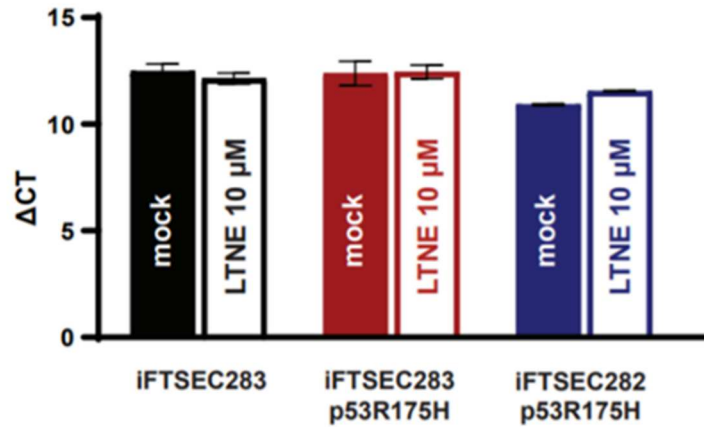
B
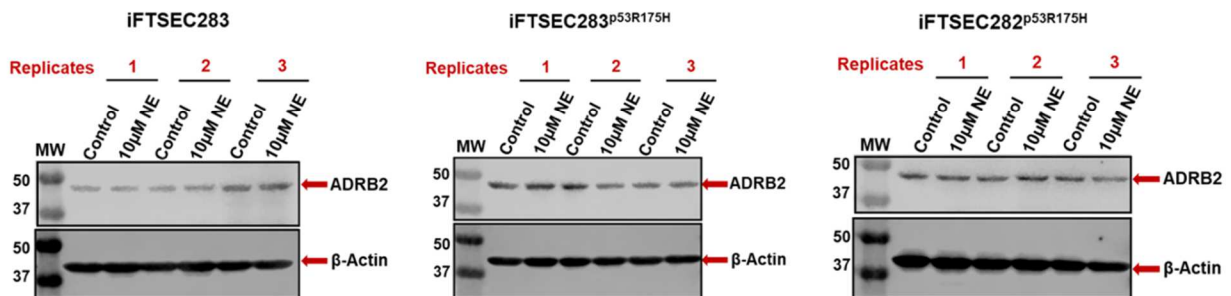
Figure 3.2. Receptor levels. Expression levels for Adrenergic beta-2 receptor (**A**) transcripts (*ADRB2*) (Adapted from (254)) and (**B**) protein (ADRB2) in mock and long-term norepinephrine exposure treated cells.
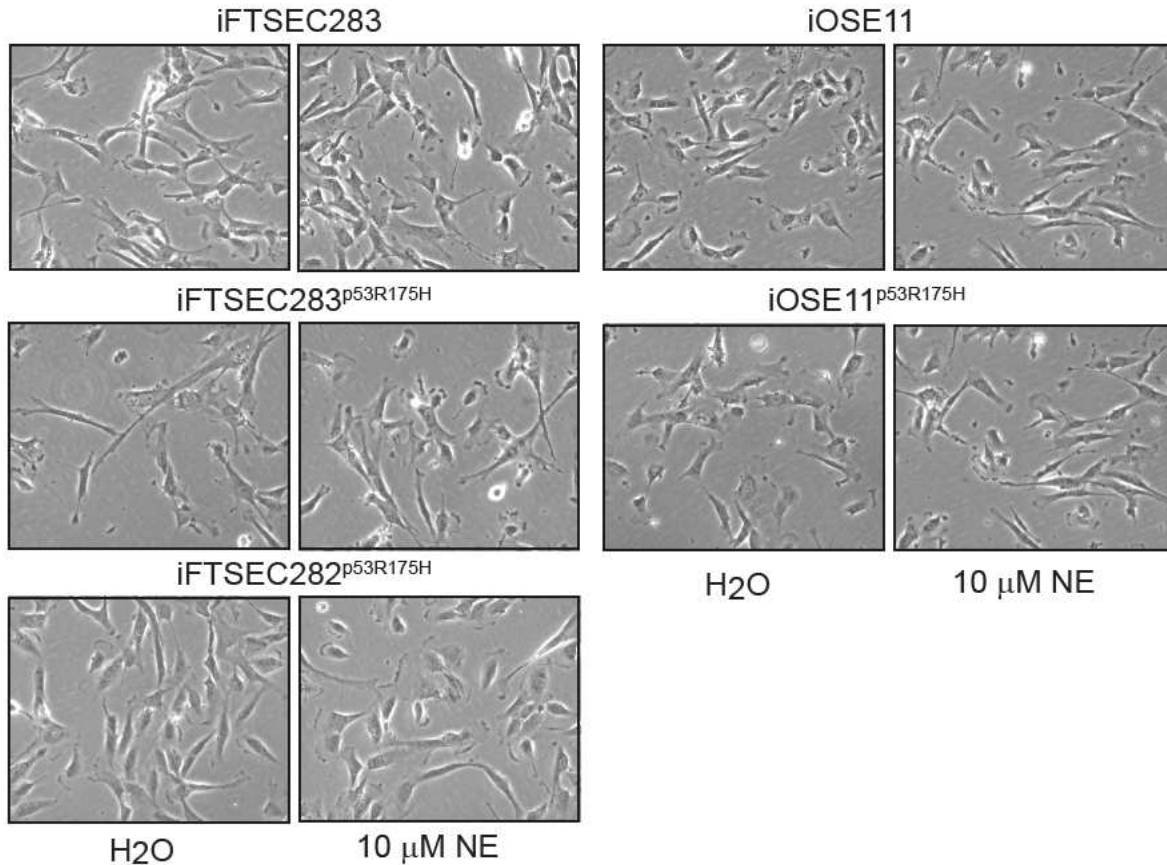
Figure 3.3. Effect of long-term exposure to NE on cell morphology. Phase contrast microscopy showing cell morphology under phase contrast microscopy at the end of the treatment period. (Adapted from (254))

Long-term NE treatment leads to increased proliferation and colony formation in fallopian tube cell lines:

All three fallopian tube cell lines (iFTSEC283, iFTSEC283^{p53R175H}, and iFTSEC282^{p53R175H}) showed an increase in proliferation after four months of treatment with 1 μM or 10 μM NE compared to vehicle control, but only two cell lines (iFTSEC283 and iFTSEC282^{p53R175H}) displayed increased proliferation at 100 nM NE (Figure 3.4A). In contrast, the ovarian surface epithelial cells, iOSE11 and iOSE11^{p53R175H}, showed decreased proliferation when treated with 10 μM NE for four months compared to vehicle

control, but no difference in the proliferation capacity was observed between control-treated cells vs. cells exposed to 1 µM or 100 nM NE (Figure 3.4B).
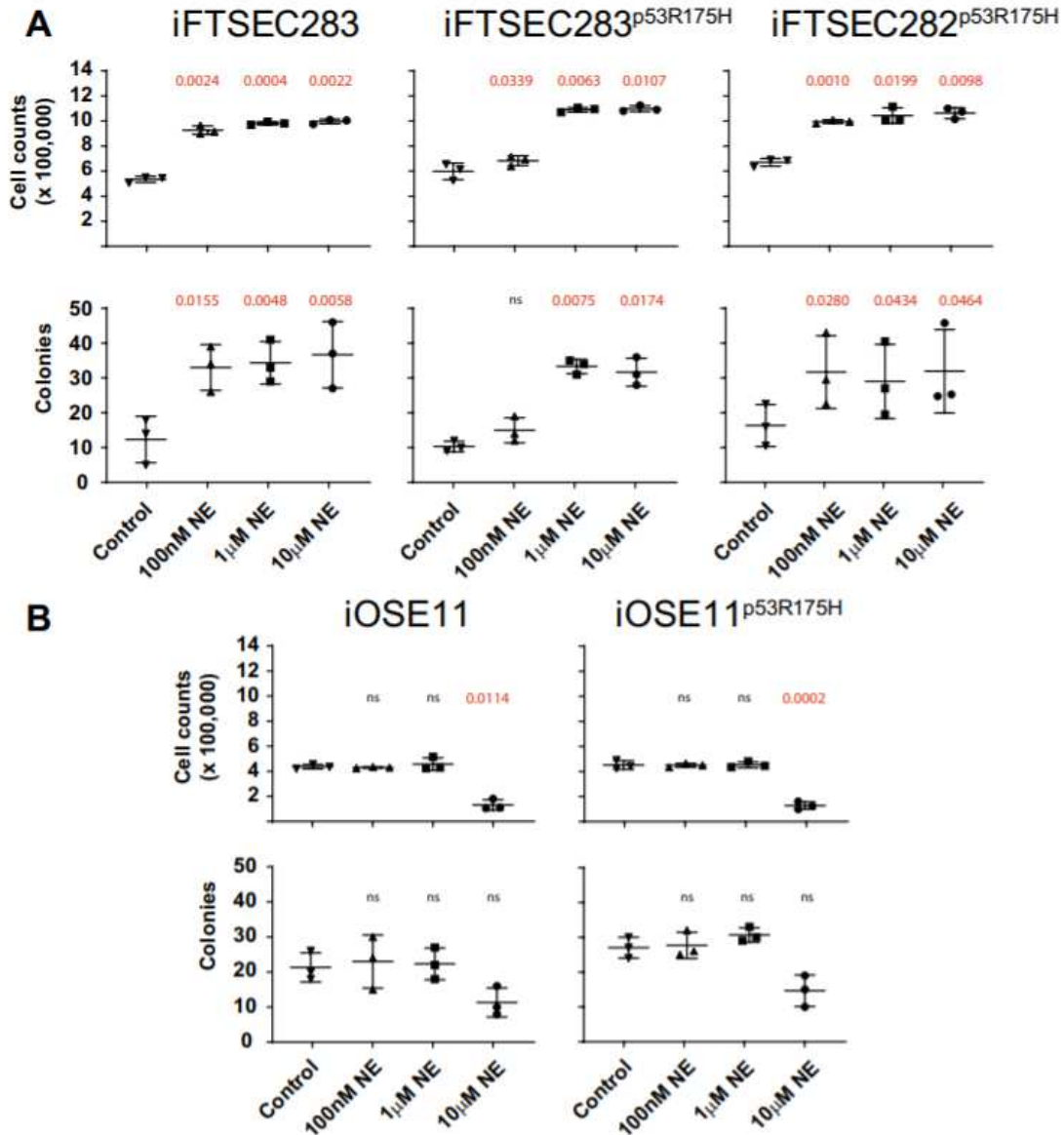
Figure 3.4. Effect of long-term exposure to NE on cell survival. (**A**) Proliferation and (**B**) colony forming assays capacity of cells treated with NE (100 nM, 1 µM, 10 µM) or mock treated for 4 months. Short-term proliferation and colony forming assays were conducted with the same concentrations (or mock treatment) as the long-term treatment. Statistical significance (p value) in a paired t-test in relation to control is indicated. ns, not significant. (Adapted from (254))

Consistent with the proliferation patterns, the three fallopian tube cell-lines showed increase capacity for colony formation after chronic exposure to NE at 1 µM or 10 µM NE compared to vehicle control, but only two cell-lines (iFTSEC283 and iFTSEC282^{p53R175H}) displayed increased colony forming ability at 100 nM NE (Figure 3.4A). In contrast, the two ovarian surface epithelial cell lines demonstrated no significant difference in colony-forming capacity in treated vs. vehicle control (Figure 3.4B).

Decreased fraction of diploid metaphases in p53R175H-overexpressing fallopian tube cells:

Because fallopian tube cell lines displayed increased proliferation rates, we used these cells for further experiments. Since chronic exposure to NE is shown to induce DNA damage and inhibit repair in different cancer models (160), we hypothesized that long-term treatment could cause genomic instability. We performed karyotyping using solid Giemsa stain to assess chromosomal structural and number abnormalities in long-term treated (10 µM NE) and mock-treated fallopian tube iFTSEC283 and iFTSEC283^{p53R175H} cells.

Mock-treated iFTSEC283 and iFTSEC283^{p53R175H} cells displayed ~ 65% [range 61–67%] of diploid metaphases (n = 46) (Figure 3.5). Long-term treatment (10 µM NE) did not affect the fraction of diploid metaphases (63–64%) in iFTSEC283. In contrast, long-term treatment iFTSEC283^{p53R175H} cells displayed a decrease in the fraction of diploid metaphases (~ 33%; range 22–44%) with a corresponding increase in the fraction

of sub-diploid metaphases (Figure 3.5). No gross abnormalities (e.g., tri-radials, quadri-radials, chromosome fusions) were observed.
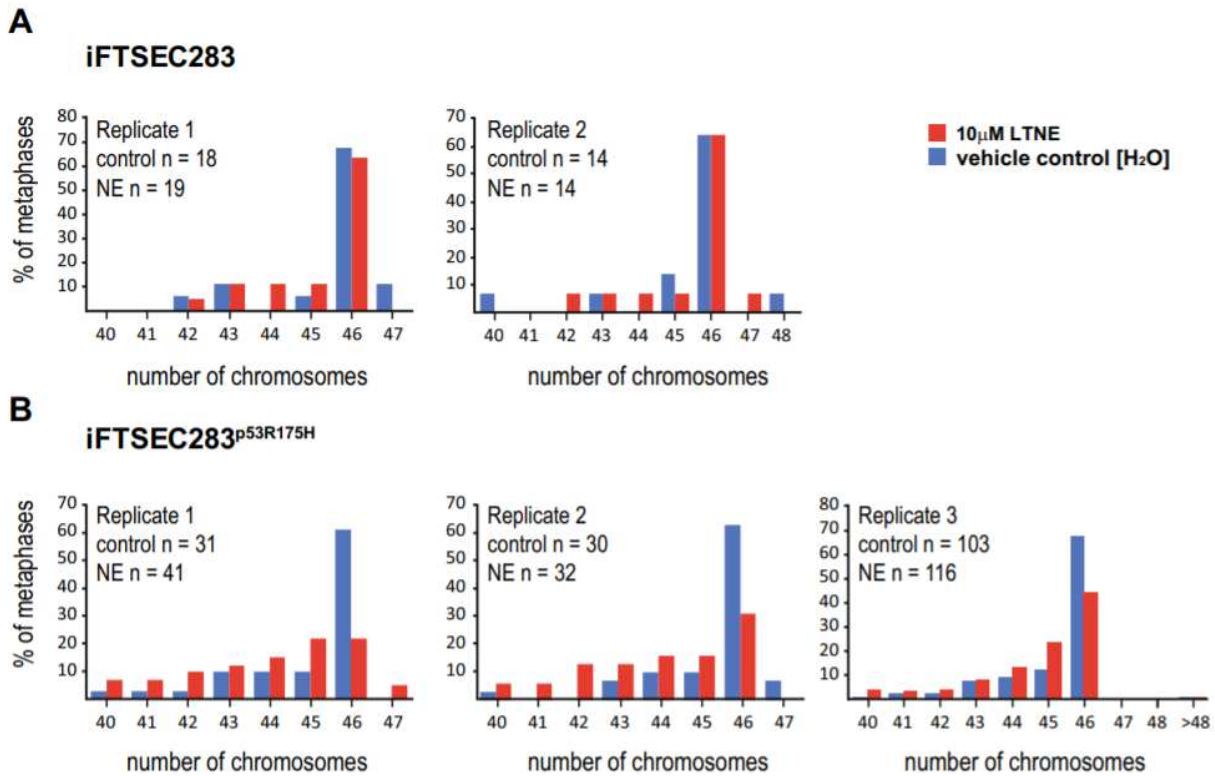
Figure 3.5. Effect of long-term exposure to NE on chromosome number. (**A**) Percentage of metaphase containing the indicated number of chromosomes in 10 µM NE (red bars) and mock-treated (blue bars) iFTSEC283 cells. (**B**) Percentage of metaphase containing the indicated number of chromosomes in 10 µM NE (red bars) and mock-treated (blue bars) iFTSEC283p53R175H cells. Absolute number of metaphases assessed in each condition is also shown. (Adapted from (254))

Transcriptomic profile generated by RNA-Seq:

Next, we performed transcriptomic analysis following RNA sequencing on iFTSEC283 and iFTSEC283[p53R175H] cell lines long-term treated with 10 µM NE or mock-treated to identify genes that are differentially expressed by long-term NE treatment in p53+ and in p53- backgrounds (Figure 3.6A).

In iFTSEC283 cells, 123 genes were differentially expressed in cells treated for long term with 10 µM NE when compared to mock-treated cells (FDR < 0.1) (Figure 3.6B) (Table 3.2). Four known p53 target genes were differentially regulated in iFTSEC283 cells compared to mock-treated cells, but not in their p53-mutant counterpart, after long-term 10 µM NE treatment (https://p53.iarc.fr/TargetGenes.aspx). *CDKN1A* (p21), *BBC3* (PUMA), and *APOBEC3C* were downregulated, and *TP53I3* was upregulated in response to LTNE treatment in iFTSEC283 cells compared to mock-treated cells (Table 3.2).

In iFTSEC283[p53R175H] cells, 23 genes were differentially expressed in cells treated long-term with 10 µM NE versus mock-treated cells. Five upregulated (*PLAC8*, *MCAM, MAPK13, COBLL1* and *LRRC17*) and 4 downregulated (*RCAN2, POSTN, ABI3BP* and *BGN*) genes had ≥ twofold change in expression (Table 3.3) (Figure 3.6C). Consistent with the ectopic overexpression of mutant p53, *TP53* levels were 18X higher in iFTSEC283[p53R175H] cells in both treatment conditions than in iFTSEC283 cells of the same condition and the p53 target genes (found to be differentially regulated in iFTSEC283 cells compared to mock-treated cells) were not differentially expressed, after long-term 10 µM NE treatment in the iFTSEC283[p53R175H] cells.
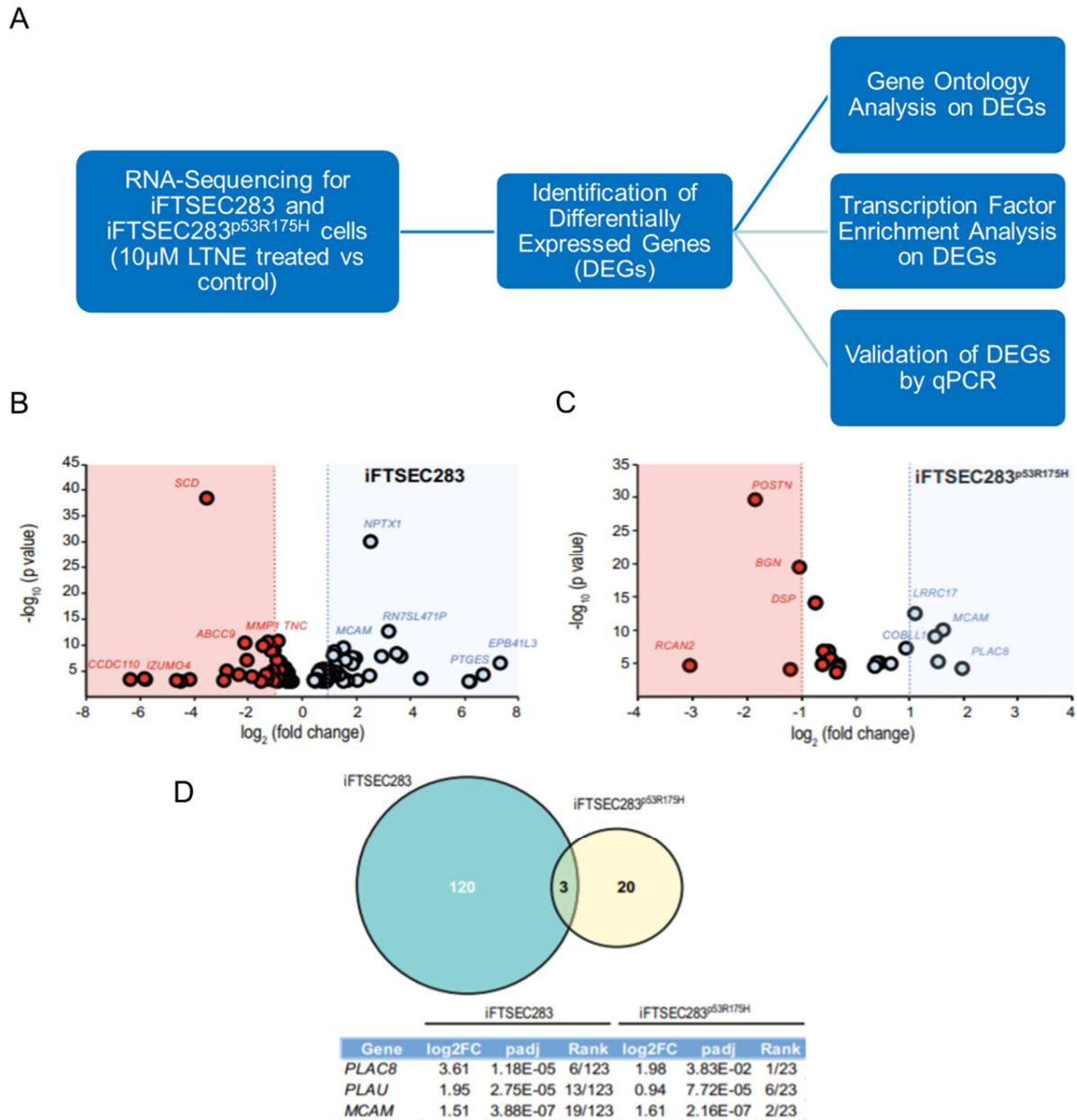
Figure 3.6. Transcriptomic profile. (**A**) Schematic of analysis performed after RNA-sequencing (**B**) Volcano plots of genes differentially expressed in iFTSEC283 (**B**) iFTSEC283[p53R175H] cells (mock versus 10 µM NE treatment). (**C**) Venn diagram showing differentially expressed genes in response to chronic norepinephrine (NE) treatment in iFTSEC283 and iFTSEC283[p53R175H] cells.(Adapted from (254))

Table 3.2: Differentially expressed genes in iFTSEC283 cells (mock versus 10μM NE treated)

Gene	log2FoldChange	p-value	p-value adjusted
EPB41L3	7.30461943	2.06E-07	0.0001299
PTGES	6.67662196	3.93E-05	0.0106956
Y_RNA	6.18430746	0.0007156	0.0899189
RP11-327P2.5	6.13992595	0.000727	0.090094
CTD-2286N8.2	4.36773298	0.0001921	0.0370271
PLAC8	3.61445629	1.27E-08	1.18E-05
OSBP2	3.45987021	3.48E-09	4.03E-06
RN7SL471P	3.19142093	1.76E-13	8.12E-10
HSD17B2	2.90826454	1.27E-08	1.18E-05
NPTX1	2.52180443	7.31E-31	5.07E-27
CNR1	2.46072236	5.45E-05	0.0134952
SVIL	2.02382596	0.0004855	0.0687571
PLAU	1.94859803	3.37E-08	2.75E-05
LIMS2	1.85042122	1.64E-08	1.42E-05
KIAA1199	1.82769226	4.28E-07	0.0002582
PLCB4	1.63900569	0.0005389	0.0747981
PLEKHA7	1.57422358	6.19E-08	4.53E-05
KRT7	1.51452333	0.0002148	0.040834
MCAM	1.5093055	2.23E-10	3.88E-07
KRT80	1.50333893	0.0008563	0.0990472
ARL10	1.3624982	3.81E-05	0.010564
TES	1.22025845	5.61E-07	0.0003245
GATA3	1.21084967	1.28E-05	0.0045664
FHOD3	1.1785617	7.46E-05	0.016968
EDN1	1.1601579	1.29E-09	1.63E-06
ID1	1.12457985	6.91E-09	7.38E-06
HIST1H3J	1.09394105	6.30E-05	0.0150733
HIST1H2BE	0.98189819	0.0001488	0.0312932
CD55	0.96511524	4.05E-06	0.0019955
ATOH8	0.93825563	3.14E-06	0.0016408
HIST1H2BB	0.87894788	0.0008365	0.0990472
ID2	0.87593446	0.0005676	0.0764851
DNAJB9	0.86740438	5.18E-05	0.0131675

Table 3.2 (continued)

Gene	log2FoldChange	p-value	p-value adjusted
NEDD4L	0.84856636	0.0001067	0.022792
PCDH9	0.8321394	5.22E-05	0.0131675
IL7R	0.82725475	2.64E-05	0.00823
HIST1H2AL	0.8264469	0.000175	0.0346964
ID3	0.76552468	3.19E-06	0.0016408
HIST1H2AH	0.70582122	0.0007082	0.0899189
BTN2A1	0.70048327	0.0002521	0.0454322
ANGPT1	0.68454895	8.99E-05	0.020121
RCAN1	0.68228442	6.87E-05	0.0161579
RN7SL3	0.66097992	4.17E-06	0.0019955
ATF5	0.65655309	0.000155	0.0316446
MUL1	0.63623583	9.85E-05	0.0217047
HSD17B10	0.62522671	0.0001537	0.0316446
STC2	0.62223913	0.0003595	0.0573579
MYL6	0.61387674	7.40E-05	0.016968
TPM2	0.59120187	0.0001588	0.0319464
FAM167A	0.56678193	2.18E-05	0.0073705
TP53I3	0.55026238	0.000338	0.0551869
SERPINE1	0.47463274	0.0005623	0.0764851
PVRL3	0.45146847	0.0007772	0.0954568
CSRP1	0.41972259	0.0003851	0.0600564
CTPS1	0.41677408	0.0005812	0.0768271
IRF2BP2	-0.4029449	0.0007875	0.0958769
TRHDE	-0.4531721	0.0006375	0.0819184
LIX1L	-0.4545487	0.0008658	0.0993126
PDGFRA	-0.4952167	0.0005745	0.0766648
FADS1	-0.4953983	0.0008496	0.0990472
FDFT1	-0.5110106	0.0004578	0.0668758
VEGFB	-0.5142936	0.000831	0.0990472
RP11-572C15.6	-0.5168015	0.0002817	0.0494833
MAN1A1	-0.519105	0.0004358	0.064343
APOBEC3C	-0.5307312	0.0002419	0.0447591
SPATS2	-0.5323444	0.0002779	0.0494451
GFPT2	-0.537678	2.06E-05	0.0071591

Table 3.2 (continued)

Gene	log2FoldChange	p-value	p-value adjusted
CD109	-0.5463987	2.67E-05	0.00823
FAM189B	-0.5540821	0.0007191	0.0899189
EEF2K	-0.5654756	0.0003739	0.0589765
KIF3C	-0.5780892	0.0008849	0.0998476
TRIM5	-0.6024296	0.0006321	0.0819184
THBS2	-0.6051078	2.31E-05	0.0074949
CDKN1A	-0.6067381	3.68E-05	0.0104341
TGFB1	-0.6085283	5.68E-05	0.01382
NFIX	-0.6188309	3.34E-05	0.009661
KCNG1	-0.6228066	0.00059	0.0772569
SLC6A6	-0.6246664	9.41E-06	0.0035295
NMNAT2	-0.6368735	0.0003337	0.0551366
TTC3	-0.6377572	2.32E-05	0.0074949
TFPI2	-0.6529236	2.34E-06	0.0012964
GPR161	-0.6882034	0.0003064	0.0525071
FGD1	-0.6988613	0.0003907	0.0602532
RNF150	-0.7007533	1.14E-05	0.00416
SIX4	-0.7330108	0.0002975	0.0516057
HSPB6	-0.7391023	7.26E-06	0.0028792
IVNS1ABP	-0.7399765	7.09E-06	0.0028792
MSMO1	-0.7498656	0.000348	0.0561646
F2RL2	-0.7633603	3.13E-05	0.0094566
PPARA	-0.7763945	0.0001919	0.0370271
LDLR	-0.8247569	1.43E-07	9.46E-05
LTBP4	-0.8263947	0.0004773	0.0683004
SREBF2	-0.8320374	4.38E-06	0.002027
MEG3	-0.8425737	5.65E-06	0.0024505
MFHAS1	-0.9000153	0.0008415	0.0990472
NPAS2	-0.9192279	0.0004092	0.0624077
BHLHE41	-0.9308066	0.0002214	0.0415338
TNC	-0.9323526	1.22E-11	4.23E-08
VAT1L	-0.9464952	7.95E-08	5.52E-05
LIF	-1.0750089	0.0004714	0.0681573
MALAT1	-1.0822371	9.40E-10	1.31E-06

Table 3.2 (continued)

Gene	log2FoldChange	p-value	p-value adjusted
TMEM154	-1.088146	6.87E-06	0.0028792
INSIG1	-1.1668164	8.72E-10	1.31E-06
UST	-1.2501833	3.31E-05	0.009661
MMP1	-1.2713844	1.75E-11	4.86E-08
TMEM8B	-1.326543	0.0004168	0.0628749
AC112721.2	-1.3626301	4.53E-05	0.011868
BBC3	-1.393831	0.0007661	0.0708123
STARD4	-1.4835531	1.27E-10	2.52E-07
SEPT5	-1.5425287	0.0008816	0.0998476
AC112721.1	-1.8757975	0.0001014	0.0219815
KCNJ2	-2.0518147	6.20E-08	4.53E-05
ABCC9	-2.1538068	3.44E-11	7.95E-08
FBXL16	-2.3563701	4.23E-05	0.0112974
C1orf54	-2.8042485	8.70E-06	0.0033552
CTD-2207P18.2	-2.919004	0.0004986	0.0699026
SCD	-3.5739387	2.85E-39	3.95E-35
C12orf79	-4.1835466	0.0004342	0.064343
ABCG2	-4.5385054	0.0008564	0.0990472
SOBP	-4.6621109	0.0005617	0.0764851
PLAC1	-5.8067114	0.0003316	0.0551366
IZUMO4	-5.8514736	0.0002507	0.0454322
CCDC110	-6.364799	0.0003222	0.0545353

Table 3.3: Differentially expressed genes in iFTSEC283[p53R175H] cells (mock versus 10µM NE treated)

Gene	log2FoldChange	p-value	p-value adjusted
PLAC8	1.976572	6.14E-05	0.038343
MCAM	1.613428	8.66E-11	2.16E-07
MAPK13	1.515934	4.46E-06	0.005067
COBLL1	1.471578	7.92E-10	1.65E-06
LRRC17	1.097049	3.07E-13	9.57E-10
PLAU	0.936077	4.32E-08	7.72E-05

Table 3.3 (continued)

Gene	log2FoldChange	p-value	p-value adjusted
PLAC8	1.976572	6.14E-05	0.038343
MCAM	1.613428	8.66E-11	2.16E-07
MAPK13	1.515934	4.46E-06	0.005067
COBLL1	1.471578	7.92E-10	1.65E-06
LRRC17	1.097049	3.07E-13	9.57E-10
PLAU	0.936077	4.32E-08	7.72E-05
KYNU	0.645658	9.85E-06	0.008787
KRT18	0.436963	7.80E-06	8.12E-03
ITGA2	0.382147	8.60E-06	0.008261
HIST1H2AJ	0.351522	3.21E-05	0.022289
LOX	-0.31901	1.34E-05	1.05E-02
CITED2	-0.3223	3.87E-05	2.54E-02
FBLN5	-0.35133	1.78E-04	0.096886
CYR61	-0.35471	1.74E-04	0.096886
EGR1	-0.47226	2.03E-06	0.002534
DUSP1	-0.50799	1.29E-07	2.02E-04
AHNAK2	-0.60377	1.50E-07	0.000208
SCARA3	-0.60971	1.22E-05	0.010166
DSP	-0.73793	8.40E-15	3.50E-11
BGN	-1.03539	3.15E-20	1.96E-16
ABI3BP	-1.20989	6.81E-05	0.040497
POSTN	-1.86558	2.24E-30	2.80E-26
RCAN2	-3.07217	2.29E-05	0.016851

Three genes were differentially expressed in cells treated with 10 µM NE independent of p53 background (i.e., they were differentially expressed in long-term NE treated iFTSEC283 and iFTSEC283[p53R145H] when compared to their mock-treated controls): *PLAC8*, *PLAU*, and *MCAM*. All three genes were upregulated and were among the most highly differentially expressed genes in relation to mock-treated cells (Figure 3.6D). The low number of overlapping genes between iFTSEC283 and

iFTSEC283^{p53R145H} suggests that p53 status is a critical determinant of the cellular response to NE.

Gene ontology and pathway analysis:

Panther database was used to perform Gene Ontology analysis on differentially expressed genes identified by RNA-seq in iFTSEC283 and iFTSEC283^{p53R175H} cells when comparing mock- to long-term 10 µM NE treatment.

In iFTSEC283 cells, GO Biological Process analysis of the upregulated genes in NE treated cells showed enrichment of 36 biological processes (Table 3.4). The most significantly enriched processes (Fold enrichment ≥ 3) were regulation of apoptotic process (GO:0,042,981) and regulation of programmed cell death (GO:0,043,067). GO Cellular Component analysis revealed 'nucleosome (GO:0,000,786)' and 'DNA packaging complex (GO:0,044,815)' to be significantly overrepresented (Table 3.5), and the only Panther Protein Class to be significantly enriched (Table 3.6) was the histone (PC00118) class with a 28.61-fold enrichment. Interestingly, five histone transcripts were upregulated in response to NE in iFTSEC283 cells: *HIST1H3J, HIST1H2BE, HIST1H2BB, HIST1H2AL* and *HIST1H2AH* (Table 3.2). In addition, the most significantly overrepresented Reactome Pathway was HDACs deacetylate histones (R-HSA-3214815) (Table 3.7). These results suggest that long-term NE treatment modulates the epigenetic state of iFTSEC283 cells. GO biological process and Reactome Pathway analysis of the downregulated genes in iFTSEC283 cells showed overrepresentation of

processes and pathways involved in lipid metabolism and steroid biosynthesis (Tables 3.8 and 3.9).

Table 3.4: Panther GO biological process analysis of upregulated genes in iFTSEC283 cells (mock versus 10 μM NE treated)

GO biological process complete	Fold Enrichment	Raw p-value	FDR
anatomical structure development (GO:0048856)	2.15	3.15E-06	1.00E-02
regulation of apoptotic process (GO:0042981)	3.78	5.21E-06	1.03E-02
system development (GO:0048731)	2.44	6.59E-07	1.05E-02
regulation of programmed cell death (GO:0043067)	3.73	6.17E-06	1.09E-02
anatomical structure formation involved in morphogenesis (GO:0048646)	5.25	2.10E-06	1.11E-02
developmental process (GO:0032502)	2.05	5.14E-06	1.17E-02
cellular developmental process (GO:0048869)	2.56	1.65E-06	1.31E-02
cell differentiation (GO:0030154)	2.5	5.02E-06	1.33E-02
multicellular organism development (GO:0007275)	2.15	8.93E-06	1.42E-02
muscle tissue development (GO:0060537)	9.15	1.13E-05	1.49E-02
circulatory system development (GO:0072359)	4.92	1.11E-05	1.61E-02
regulation of developmental process (GO:0050793)	2.8	1.62E-05	1.84E-02
regulation of cell death (GO:0010941)	3.44	1.60E-05	1.96E-02
anatomical structure morphogenesis (GO:0009653)	3.04	1.88E-05	1.99E-02
actin filament-based process (GO:0030029)	5.83	2.08E-05	2.07E-02
regulation of smooth muscle cell-matrix adhesion (GO:2000097)	> 100	2.84E-05	2.65E-02
positive regulation of cell differentiation (GO:0045597)	4.28	3.95E-05	3.31E-02
circadian rhythm (GO:0007623)	13.38	3.77E-05	3.33E-02
cell development (GO:0048468)	3.33	4.85E-05	3.50E-02
regulation of cell population proliferation (GO:0042127)	3.3	5.32E-05	3.52E-02
tube morphogenesis (GO:0035239)	5.29	4.44E-05	3.53E-02
positive regulation of cell migration (GO:0030335)	5.98	5.28E-05	3.65E-02
regulation of cell differentiation (GO:0045595)	3.13	4.82E-05	3.65E-02
negative regulation of endothelial cell apoptotic process (GO:2000352)	39.34	6.61E-05	4.04E-02
regulation of multicellular organismal process (GO:0051239)	2.43	7.30E-05	4.14E-02
negative regulation of transcription, DNA-templated (GO:0045892)	3.64	8.09E-05	4.28E-02
positive regulation of cell motility (GO:2000147)	5.71	7.29E-05	4.29E-02

Table 3.4 (continued)

GO biological process complete	Fold Enrichment	Raw p-value	FDR
positive regulation of cellular component movement (GO:0051272)	5.54	8.99E-05	4.33E-02
striated muscle tissue development (GO:0014706)	8.25	8.80E-05	4.37E-02
animal organ development (GO:0048513)	2.41	8.08E-05	4.43E-02
positive regulation of locomotion (GO:0040017)	5.56	8.78E-05	4.50E-02
negative regulation of RNA biosynthetic process (GO:1902679)	3.52	1.12E-04	4.94E-02
tissue development (GO:0009888)	3.09	1.07E-04	4.98E-02
negative regulation of nucleic acid-templated transcription (GO:1903507)	3.52	1.10E-04	5.01E-02
negative regulation of biological process (GO:0048519)	1.96	5.76E-05	3.66E-02
multicellular organismal process (GO:0032501)	1.93	2.34E-06	9.29E-03

Table 3.5: Panther GO cellular component analysis of upregulated genes in iFTSEC283 cells (mock versus 10 µM NE treated)

GO cellular component complete	Fold Enrichment	Raw p-value	FDR
nucleosome (GO:0000786)	25.88	1.60E-06	3.20E-03
DNA packaging complex (GO:0044815)	23.42	2.59E-06	2.60E-03
protein-DNA complex (GO:0032993)	10.99	9.50E-05	4.76E-02
anchoring junction (GO:0070161)	4.71	4.25E-05	2.84E-02

Table 3.6: Panther GO cellular component analysis of upregulated genes in iFTSEC283 cells (mock versus 10 µM NE treated)

PANTHER Protein Class	Fold Enrichment	Raw p-value	FDR
histone (PC00118)	28.61	1.28E-05	0.00249

Table 3.7: Panther Reactome pathways analysis of upregulated genes in iFTSEC283 cells (mock versus 10 µM NE treated)

Reactome pathways	Fold Enrichment	Raw p-value	FDR
Dissolution of Fibrin Clot (R-HSA-75205)	60.53	5.24E-04	4.61E-02
RNA Polymerase I Promoter Opening (R-HSA-73728)	36.88	7.99E-05	2.03E-02
DNA methylation (R-HSA-5334118)	34.71	9.56E-05	2.18E-02

Table 3.7 (continued)

Reactome pathways	Fold Enrichment	Raw p-value	FDR
Activated PKN1 stimulates transcription of AR (androgen receptor) regulated genes KLK2 and KLK3 (R-HSA-5625886)	32.78	1.13E-04	2.35E-02
HDACs deacetylate histones (R-HSA-3214815)	32.78	5.05E-07	1.15E-03
SIRT1 negatively regulates rRNA expression (R-HSA-427359)	31.9	1.22E-04	2.15E-02
PRC2 methylates histones and DNA (R-HSA-212300)	28.1	1.78E-04	2.90E-02
Condensation of Prophase Chromosomes (R-HSA-2299718)	28.1	1.78E-04	2.70E-02
ERCC6 (CSB) and EHMT2 (G9a) positively regulate rRNA expression (R-HSA-427389)	26.23	2.17E-04	3.10E-02
RHO GTPases activate PKNs (R-HSA-5625740)	24.98	2.17E-05	7.07E-03
HCMV Late Events (R-HSA-9610379)	24.9	1.93E-06	2.20E-03
RMTs methylate histone arginines (R-HSA-3214858)	24.09	2.78E-04	3.53E-02
Meiotic recombination (R-HSA-912446)	21.08	4.10E-04	4.46E-02
Transcriptional regulation of granulopoiesis (R-HSA-9616222)	20.35	4.54E-04	4.72E-02
B-WICH complex positively regulates rRNA expression (R-HSA-5250924)	20.35	4.54E-04	4.51E-02
RNA Polymerase I Promoter Escape (R-HSA-73772)	20	4.77E-04	4.54E-02
Formation of the beta-catenin:TCF transactivating complex (R-HSA-201722)	19.67	5.01E-04	4.58E-02
HCMV Early Events (R-HSA-9609690)	19.67	6.01E-06	4.58E-03
Pre-NOTCH Transcription and Translation (R-HSA-1912408)	19.04	5.51E-04	4.66E-02
HATs acetylate histones (R-HSA-3214847)	18.21	8.70E-06	4.97E-03
RUNX1 regulates transcription of genes involved in differentiation of HSCs (R-HSA-8939236)	16.06	1.19E-04	2.26E-02
HCMV Infection (R-HSA-9609646)	15.86	1.68E-05	6.41E-03
Estrogen-dependent gene expression (R-HSA-9018519)	13.34	2.41E-04	3.23E-02
Ub-specific processing proteases (R-HSA-5689880)	11.57	1.36E-05	6.20E-03
Deubiquitination (R-HSA-5688426)	8.4	7.99E-05	2.28E-02
Chromatin modifying enzymes (R-HSA-3247509)	8.2	3.66E-04	4.40E-02
Chromatin organization (R-HSA-4839726)	8.2	3.66E-04	4.18E-02

Table 3.8: Panther GO biological process analysis of downregulated genes in iFTSEC283 cells (mock versus 10 µM NE treated)

GO biological process complete	Fold Enrichment	Raw p-value	FDR
regulation of steroid biosynthetic process (GO:0050810)	18.68	7.90E-06	3.13E-02
positive regulation of lipid metabolic process (GO:0045834)	12.69	8.38E-06	2.66E-02
regulation of steroid metabolic process (GO:0019218)	16.54	1.86E-06	1.48E-02
regulation of lipid biosynthetic process (GO:0046890)	11.95	2.10E-06	1.11E-02
regulation of lipid metabolic process (GO:0019216)	9.04	3.34E-08	5.30E-04

Table 3.9: Panther Reactome pathways analysis of downregulated genes in iFTSEC283 cells (mock versus 10 µM NE treated)

Reactome pathways	Fold Enrichment	Raw p-value	FDR
BMAL1:CLOCK,NPAS2 activates circadian gene expression (R-HSA-1368108)	37.37	7.76E-05	2.95E-02
Activation of gene expression by SREBF (SREBP) (R-HSA-2426168)	33.63	6.91E-06	5.26E-03
Regulation of cholesterol biosynthesis by SREBP (SREBF) (R-HSA-1655829)	31.73	6.09E-07	6.95E-04
Metabolism of steroids (R-HSA-8957322)	15.91	3.17E-07	7.24E-04
PPARA activates gene expression (R-HSA-1989781)	14.75	2.44E-05	1.39E-02
Regulation of lipid metabolism by PPARalpha (R-HSA-400206)	14.62	2.54E-05	1.16E-02

In iFTSEC283^{p53R175H} cells, analysis of the 23 differentially expressed genes according to GO biological process, molecular function, and cellular component revealed processes involved in extracellular structure and matrix organization to be significantly overrepresented (Table 3.10–3.12). Many of the genes involved in these processes were downregulated in response to long-term treatment with 10 µM NE, including intercellular tight junction component desmoplakin (*DSP*), collagen interacting proteoglycan biglycan (*BGN*), extracellular matrix protein ABI3 binding protein (*ABI3BP*), and integrin binding

protein periostin (*POSTN*) (Table 3.3). Analysis of only the upregulated genes did not show any significantly overrepresented process or pathway.

Table 3.10: Panther GO biological process analysis of differentially expressed genes in iFTSEC283^{p53R175H} cells (mock versus 10 µM NE treated)

GO biological process complete	Fold Enrichment	Raw p-value	FDR
extracellular matrix organization (GO:0030198)	16.08	1.77E-07	2.81E-03
extracellular structure organization (GO:0043062)	16.04	1.80E-07	1.43E-03
wound healing (GO:0042060)	13.18	6.71E-07	3.55E-03
response to wounding (GO:0009611)	10.73	2.61E-06	8.29E-03
tissue development (GO:0009888)	5.2	2.29E-06	9.06E-03
response to stress (GO:0006950)	3.19	1.67E-05	4.43E-02

Table 3.11: Panther GO molecular function analysis of differentially expressed genes in iFTSEC283^{p53R175H} cells (mock versus 10 µM NE treated)

GO molecular function complete	Fold Enrichment	Raw p-value	FDR
extracellular matrix structural constituent (GO:0005201)	29.61	4.40E-08	2.10E-04
cell adhesion molecule binding (GO:0050839)	10.77	2.55E-06	4.06E-03
structural molecule activity (GO:0005198)	9.4	1.16E-06	2.77E-03

Table 3.12: Panther GO cellular component analysis of differentially expressed genes in iFTSEC283^{p53R175H} cells (mock versus 10 µM NE treated)

GO cellular component complete	Fold Enrichment	Raw p-value	FDR
extracellular space (GO:0005615)	3.2	0.0000409	0.0205
collagen-containing extracellular matrix (GO:0062023)	11.8	0.00000898	0.006
extracellular region (GO:0005576)	3.03	0.0000043	0.00431
extracellular matrix (GO:0031012)	13.26	0.000000011	2.21E-05

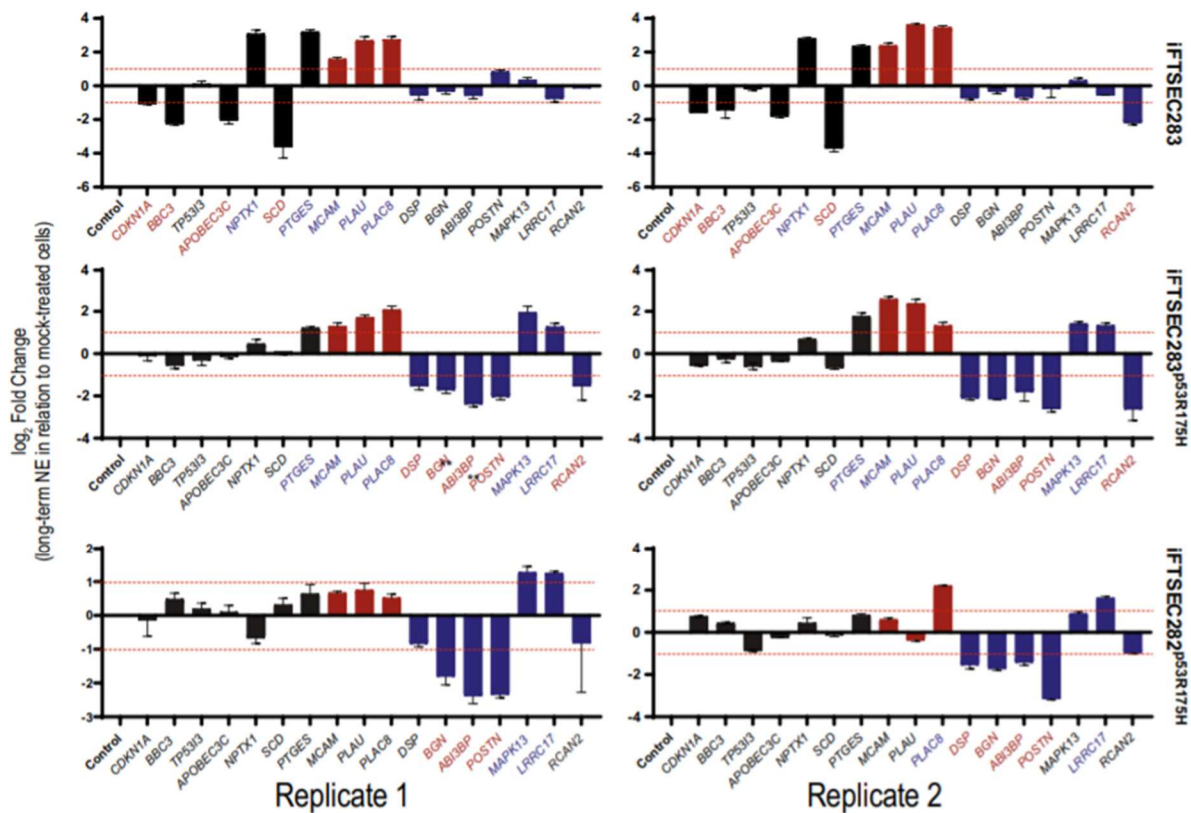**Validation of differentially expressed genes:**

To validate the pattern of differentially expressed genes upon long-term NE treatment with an alternative method, we tested gene expression in mock-treated and long-term [10 µM] NE treated iFTSEC283 and iFTSEC283^{p53R175H} cells by qPCR for several genes. First, we assessed the seven genes differentially expressed (FDR < 0.1)

in iFTSEC283 cells, including *PTGES* and *NPTX1* (among the 10 most upregulated genes), *SCD* (a top downregulated gene), and four p53 target genes (*CDKN1A, BBC3, APOBEC3C* and *TP53I3*). Second, we assessed the three genes (*PLAU, MCAM, PLAC8*) differentially regulated (FDR < 0.1) irrespective of p53 status (Figure 3.7), and third, seven of the top 5 most up- or downregulated genes (FDR < 0.1, *MAPK13, LRRC17, DSP, BGN, ABI3BP, POSTN, RCAN2*) in iFTSEC283[p53R175H] cells. We considered a gene to be differentially regulated when levels of expression in mock-treated cells were significantly (p < 0.05) different from long-term NE treated cells and the Log2 fold change was < -1 or > 1.

Overall, 13/17 (76%) of the genes chosen for validation were consistent across qPCR and RNA-Seq results. Consistent with the RNA-seq results, *PTGES* and *NPTX1* were upregulated and *CDKN1A* (coding for p21), *BBC3* (coding for p53-upregulated modulator of apoptosis (*PUMA*)), *APOBEC3C* and *SCD* were downregulated in long-term [10 µM] NE treated iFTSEC283 cells compared with control in independent replicates using qPCR (Figure 3.7, black bars); while in NE treated iFTSEC283[p53R175H], with the exception of *PTGES*, the expression of these genes remained unaltered compared with mock-treated controls (Figure 3.7, black bars). Expression levels of p53 target genes (*CDKN1A, BBC3* and *APOBEC3C*) were significantly lower in mock treated iFTSEC283[p53R175H] compared to mock treated iFTSEC283 cells and treatment with NE did not further alter their levels (Figure 3.8). Results for *TP53I3* were inconsistent with the RNA-Seq data, with qPCR expression levels being unaltered in IFTSEC283 cells (Figure 3.7, black bars). The three genes differentially regulated irrespective of p53 status, *MCAM, PLAC8* and *PLAU,* were shown to be significantly upregulated in iFTSEC283 and

iFTSEC283^p53R175H in both replicates (Figure 3.7, red bars) consistent with RNA-Seq data. Differential gene expression for *DSP, BGN, ABI3BP, POSTN, MAPK13* and *LRRC17* was also consistent with the RNA-seq data (Figure 3.7, blue bars). Results for RCAN2 which was downregulated in iFTSEC283^p53R175H cells and in one replicate of iFTSEC283 cells were inconsistent with the RNA-Seq results (Figure 3.7, blue bars). Additionally, *PTGES* was found to be upregulated in iFTSEC283^p53R175H cells in qPCR, but not in RNA-Seq.

Figure 3.7. qPCR validation of RNA-Seq data. Genes considered to be differentially (− 1 > Log2FoldChange > 1; p < 0.05) up and down regulated are denoted by blue and red font, respectively. Bars are colored according to (a) genes differentially expressed (FDR < 0.1) in iFTSEC283 cells (black bars); (b) the three genes differentially regulated (FDR < 0.1) irrespective of p53 status (red bars); and (c) and seven genes differentially expressed (FDR < 0.1) in iFTSEC283^p53R175H cells (blue bars). (Adapted from (254))
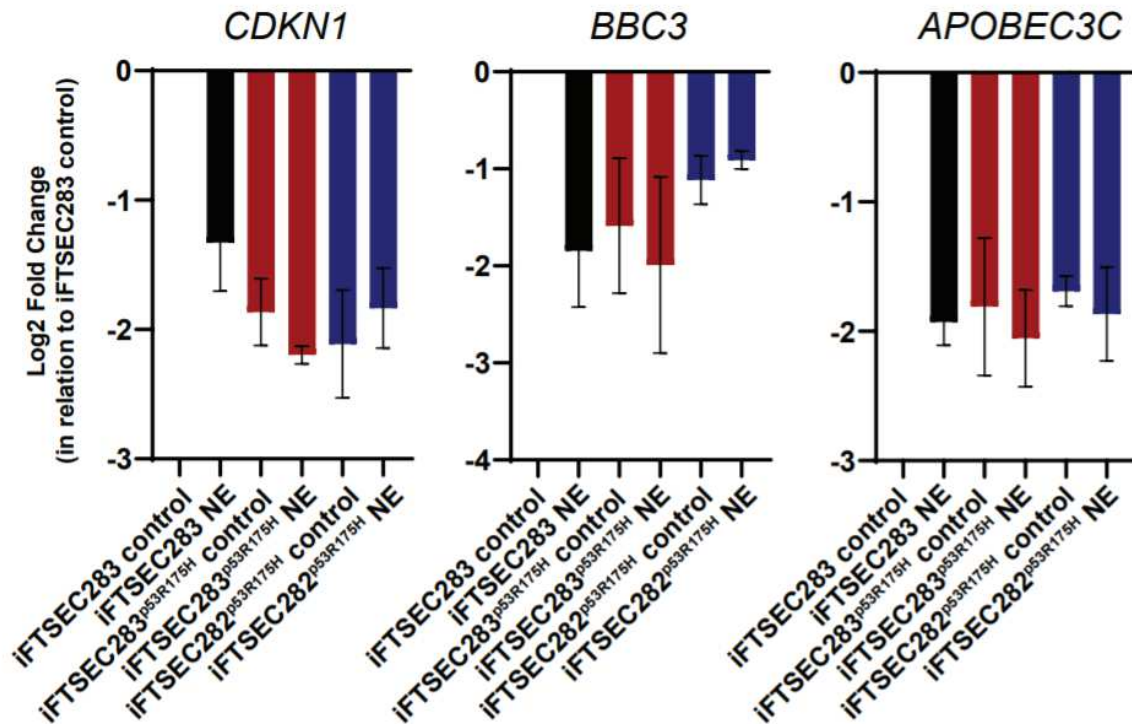
Figure 3.8. Comparative expression of TP53 target genes. *CDKN1A*, *BBC3*, and *APOBEC3*. Gene expression is plotted in reference to the iFTSEC283 control (no NE) (Adapted from (254))

Finally, to explore how robust these changes were across different cell lines, we performed qPCR gene expression analysis on iFTSEC282^{p53R175H} cells. Six out of the seven genes differentially expressed in iFTSEC283 cells only showed no significant change in expression in either p53R175H cell lines (Figure 3.7; compare black bars). However, the three genes differentially regulated irrespective of p53 status in the iFTSEC283 cells were not regulated in iFTSEC282^{p53R175H} (Figure 3.7; compare red bars). Finally, the seven genes differentially expressed in iFTSEC283^{p53R175H} cells behaved similarly in iFTSEC282^{p53R175H} (Figure 3.7; compare blue bars). Although limited

to a few select genes, the data suggest a strong similarity (13/17 genes tested) between the p53 mutant expressing cells but not with p53 wild type cells.

Regulatory motif enrichment analysis:

To identify gene regulatory mechanisms induced by long-term exposure to NE, we performed transcription factor enrichment analysis on the 123 and 23 genes differentially expressed in iFTSEC283 and iFTSEC283^{p53R175H} cells, respectively, compared to mock-treated cells using the oPOSSUM database (250).

In iFTSEC283 cells, we identified four transcription factors having enriched binding sites in our dataset with a Z-score higher than two standard deviations above the mean: MZF1_1-4, Pax4, Myc, and Klf4 (Figure 3.9A). When ranked by Fisher scores, 17 transcription factors had a score higher than one standard deviation above the mean, with transcription factors Myc and Klf4 also being identified (Figure 3.9B).

In iFTSEC283^{p53R175H} cells, we identified transcription factor FoxA1 among the top three enriched transcription factors when ranked by both z-score and Fisher Score (Figure 3.9A). In addition, when the transcription factor enrichment was ranked based on Fisher-score, Myc::Max heterodimer was among the 19 transcription factors that had a Fisher score higher than one standard deviation above the mean (Figure 3.9B).
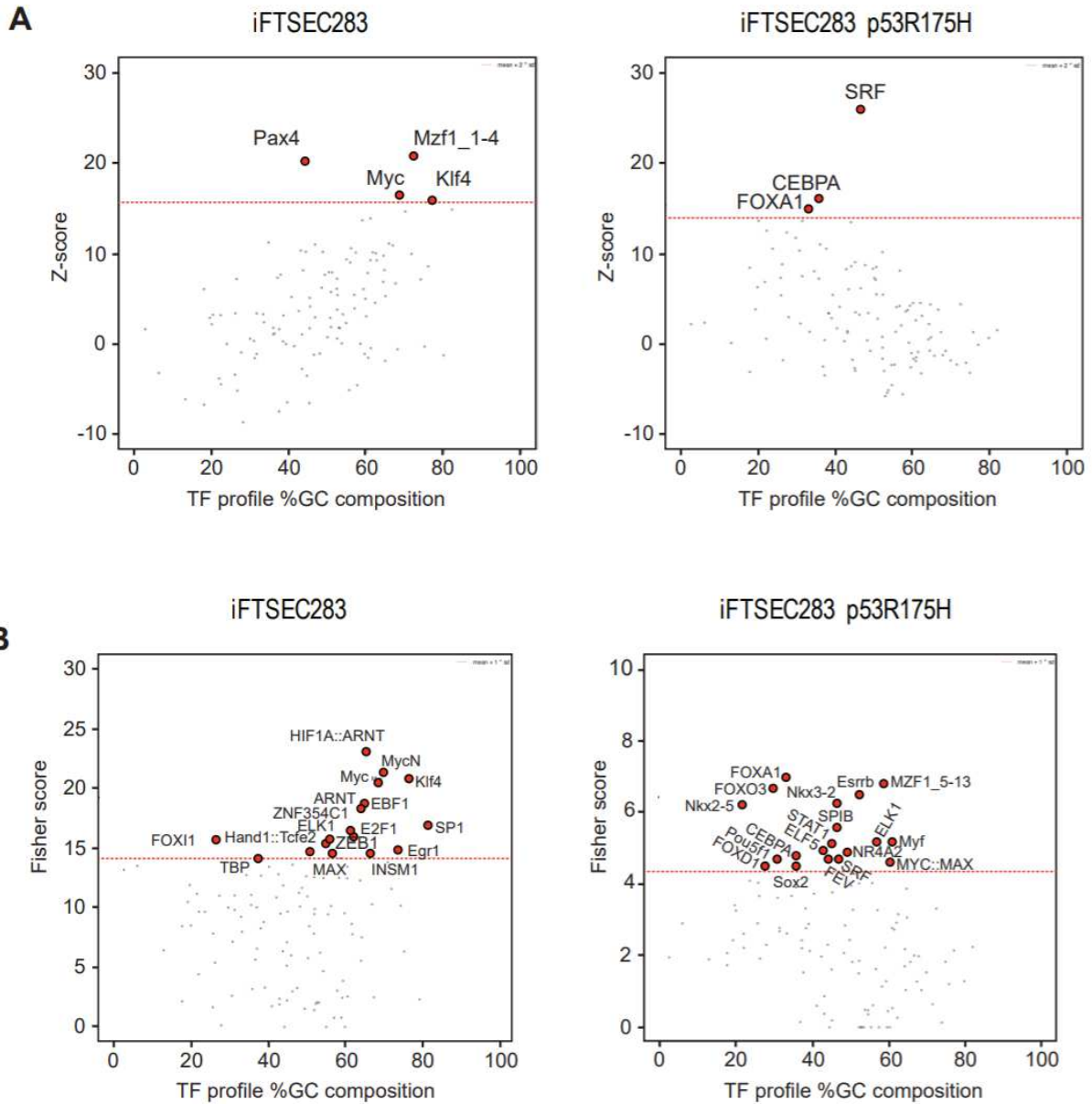
Figure 3.9. Regulatory motif enrichment analysis. Significantly enriched transcription factors identified using oPOSSUM by (**A**) Z-score and (**B**) Fisher score (Adapted from (254))

The only commonality between the two cell lines was the enrichment of genes with Myc binding sites in their promoters in iFTSEC283 cells and with Myc::Max in iFTSEC283[p53R175H]. A total of 68 differentially expressed genes in iFTSEC283 cells

contain predicted Myc binding sites, including *CDKN1A, HIST1H2BB, MEG3* and *PLAU*. In iFTSEC283^{p53R175H}, eight differentially expressed genes contain predicted Myc::Max binding sites (*PLAU, CITED2, CYR61, EGR1, SCARA3, DSP, ABI3BP* and *LRRC17*). Reflecting the low overlap between the two isogenic cell lines in differentially expressed genes upon NE treatment, enriched transcription factors were also largely distinct and support the notion that p53 status is an important determinant of the cellular response to NE. Additionally, in contrast to short-term NE treatment, HoxA5 was not among the significantly enriched transcription factors.

Suppression of *HOXA5* induction after short-term NE treatment following long-term NE exposure:

Since LTNE cells did not show HoxA5 transcription factor enrichment, we performed short-term NE treatment time course study on long-term mock vs LTNE treated normal and partially transformed fallopian tube cells. We treated 137 days mock and 10μM NE treated cells with H_2O or 10μM NE for 15 mins, 1 h, 2 h, 3 h and 4 h. The long-term mock treated cells showed induction of *HOXA5* transcript in response to short-term NE treatment (Figure 3.10A). This *HOXA5* induction curve was similar to the one observed during short-term NE treatment in normal and partially transformed cells (Figure 2.6A and Figure 2.8A). In contrast, 10μM LTNE cells displayed abrogation of *HOXA5* induction in response to short-term NE treatment (Figure 3.10B). This was similar to the one observed during short-term NE treatment in ovarian cancer cells (Figure 2.8B). These results show that after long-term treatment with NE, the induction of *HOXA5* transcript observed during short-term NE treatment is abrogated.

A
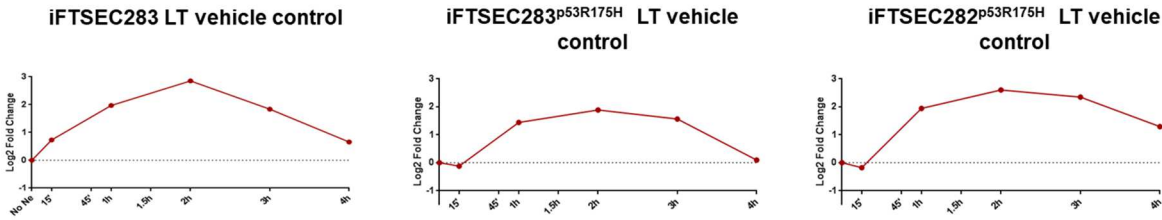
B
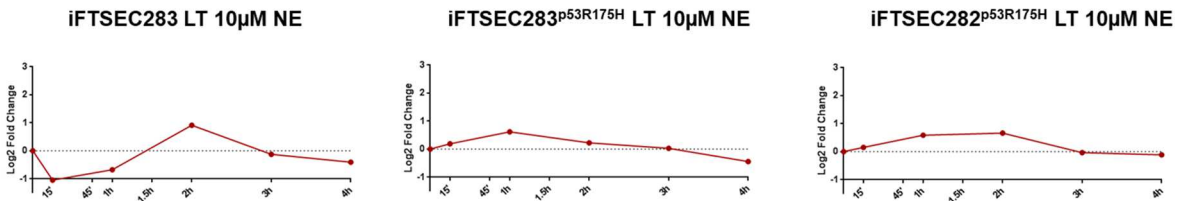
Figure 3.10. *HOXA5* induction. Short-term *HOXA5* induction time course by 10µM NE in (**A**) Long-term mock treated and (**B**) Long-term 10µM NE treated normal and partially transformed fallopian tube cells.

Summary

In this chapter, we evaluated the long-term in vitro effects of norepinephrine (NE) treatment in cells postulated to be the precursors of ovarian cancer – the fallopian tube epithelial cells (iFTSEC283) and ovarian surface epithelial cells (iOSE11), and isogenic cell lines with oncogenic dominant-negative mutant p53 p.R175H to assess the extent to which *TP53* status influences transcriptional responses after long-term exposure to NE. Overall, we observed no morphological changes in iFTSEC283, iFTSEC283[p53R175H], iFTSEC282[p53R175H], iOSE11 and iOSE11[p53R175H] cells, although long-term treatment with 1 µM and 10 µM NE increased proliferation and colony-forming capacity of the fallopian tube epithelial cells with and without p53 mutation. In contrast, ovarian surface epithelial cells showed reduced proliferation and colony-forming capability, even in the p53 mutant

background. This suggests that fallopian tube cells may be more susceptible to oncogenic effects of NE than ovarian surface epithelial cells.

Interestingly, a decrease in the percentage of metaphase spreads containing 46 chromosomes was observed after chronic 10 μM NE treatment only in fallopian tube cells expressing mutant p53. These results suggest that NE and oncogenic p53 alterations can act in combination to promote chromosomal number changes. Additionally, transcriptomic profiling of 10 μM LTNE in iFTSEC283 and iFTSEC283^{p53R175H} cells revealed very low overlap in gene expression compared to mock-treated controls between the two cell lines, with only three genes differentially expressed (*PLAC8*, *PLAU*, *MCAM*), suggesting that p53 status is a critical determinant of the response to NE.

Transcription factor enrichment analysis by oPOSSUM revealed enrichment of distinct transcription factors in p53 wild type and p53R175H overexpressing cells. In contrast to short-term NE treatment, none of the long-term NE treated fallopian tube cell lines showed enrichment of the transcription factor HoxA5. Additionally, when LT 10μM NE treated cells were exposed to short-term 10μM NE treatment time course, the induction of *HOXA5* transcript was attenuated. This was similar to the induction time course observed in ovarian cancer cells. In contrast, LT mock treated cells displayed similar *HOXA5* induction curve as was observed in short-term 10μM NE treatment of normal and partially transformed cells. Additionally, the ADRB2 receptor levels remained unaltered with LTNE treatment. These results suggest that NE signaling is altered after LT 10μM NE treatment.

CHAPTER FOUR

REGULATION OF *HOXA5* BY NOREPINEPHRINE

Note to reader:

A manuscript (Dash *et al*) containing portions of this section is in preparation.

Introduction

Since long-term NE treated fallopian tube cells showed attenuated *HOXA5* induction curve following acute NE treatment when compared with short-term NE treated cells, and that this attenuation was similar to the ones observed in ovarian cancer cells, we decided to study the mechanism by which NE regulates *HOXA5* induction. *HOXA5* gene belongs to a large family of genes known as homeotic genes that play essential roles during embryo morphogenesis and organogenesis.

Homeotic Genes:

Homeotic genes are evolutionarily conserved genes that code for Hox transcription factors and contribute to development of bilaterian organisms (260, 261). The *Hox* genes were first discovered in the third chromosome of fruit fly *Drosophila melanogaster* through

a series of genetic crossings (262). These genes were found to be clustered in two complexes, Antennapedia complex (ANT-C) and Bithorax complex (BX-C), with each complex being approximately 300kb in length (261, 263). Both complexes were named after phenotypes obtained for different alleles and the genomic arrangement of *Hox* genes followed an order of spatial collinearity with activity along the body axis from anterior to posterior direction (261, 263, 264). Subsequently, the presence of *Hox* genes was discovered in all bilaterian organisms (265). These genes coded for Hox proteins, which are transcription factors containing a conserved helix-turn-helix motif capable of binding to specific DNA sequences (265, 266). This DNA binding domain was termed 'homeodomain' and in addition to its presence in all Hox transcription factors, it was also subsequently discovered in other transcription factors (267, 268). The complex interplay between Hox transcription factors with other homeodomain containing proteins is hypothesized to contribute to diversity in bilaterian organisms (267, 269).

In humans, there are thirty-nine *HOX* genes that are organized in four clusters in different chromosome (270). *HOXA* family is located on chromosome 7, *HOXB* family is on chromosome 17, *HOXC* family is present on chromosome 12 and *HOXD* family on chromosome 2 (270). Hox proteins can either bind to DNA as monomers or homodimers, or they can partner with other cofactors such as TALE (three amino acids loop extension) homeodomain transcription factors and bind to DNA as heterodimers or heterotrimers (271, 272). Among TALE transcription factors subfamily, Pre-B-cell Leukemia Homeobox (PBX) partners preferentially with Hox proteins 1-11, while Myeloid Eco-tropic Viral Integration Site 1 Homolog (MEIS) proteins bind to Hox proteins 9-13 (271, 272). These cofactors can influence various transcriptional events such as the recruitment of RNA

polymerases to promote transcription of target genes, or they can also repress transcription by recruitment of transcriptional inhibitors such as histone deacetylases (HDACs) (271, 272).

Alterations in *HOX* family of genes are associated with several developmental disorders such as hand-foot-genital syndrome (HFGS), Charcot–Marie–tooth disease (CMT) and synpolydactyly (SPD) (273-275). Apart from playing a role in development, *HOX* family of genes are also expressed in adulthood and they regulate pathways in many different cellular processes such as stem cell renewal and cellular identity in tissues (276-279). Different *HOX* genes have also been shown to be deregulated in various cancers (280-282). The different mechanisms by which *HOX* genes can become deregulated include: loss of spatiotemporal expression control, gene dominance and epigenetic alterations (283).

HOX genes in ovarian cancer:

HOX genes have been implicated in the oncogenesis of various hematological and solid cancers (281). Broadly classified, *HOXA* family of genes are frequently altered in breast and ovarian cancers, *HOXB* family in colon cancer, *HOXC* genes in prostate and lung cancers, and *HOXD* family of genes in breast cancers (284).

In the human female reproductive system, *HOX* genes 9-13 are expressed uniformly during embryonic development. In adults, the expression of these tandemly arranged *HOX* genes become spatially restricted to specific organs: *HOXA9* in fallopian tubes, *HOXA10* in uterus, *HOXA11* in cervix and *HOXA13* in vagina (285). Work by Cheng *et al* showed that dysregulated expression of these genes was an early step in

development of epithelial ovarian neoplasia (286). *HOXA9* expression promoted development of serous ovarian carcinoma, *HOXA10* lead to development of ovarian endometrioid subtype and *HOXA11* promoted ovarian mucinous subtype (286). *HOXA7* expression was associated with LGSOC, although it was also expressed in HGSOC and high-grade ovarian endometrioid subtype too (286). Comprehensive analysis of *HOX* genes in 73 high grade ovarian carcinoma patients identified a 'HOX signature' consisting of 5 genes – *HOXA13, HOXB6, HOXC13, HOXD1* and *HOXD13* – to be associated with poor survival (287).

Different *HOX* genes have been shown to have a pro-tumorigenic or anti-tumorigenic role in ovarian cancer. For example, *HOXB7* and *HOXB13* were shown to increase tumor growth by upregulating basic fibroblast growth factor and Ras pathway respectively (288, 289). Similarly, *HOXA9* expression was shown to suppresses anti-tumor immune responses and the presence of *HOXD10* resulted in increased migration and invasion (290-292). On the other hand, *HOXA5* was shown to decrease cell growth and increase apoptosis, thus acting as a tumor suppressor (293).

HOXA5:

HOXA5 gene is located near the middle of the *HOXA* cluster of genes present on human chromosome 7 and it encodes a 270 amino acid protein (294). GTEx analysis of *HOXA5* expression in various normal tissues showed fallopian tube as the tissue having highest *HOXA5* expression (Figure 4.1).
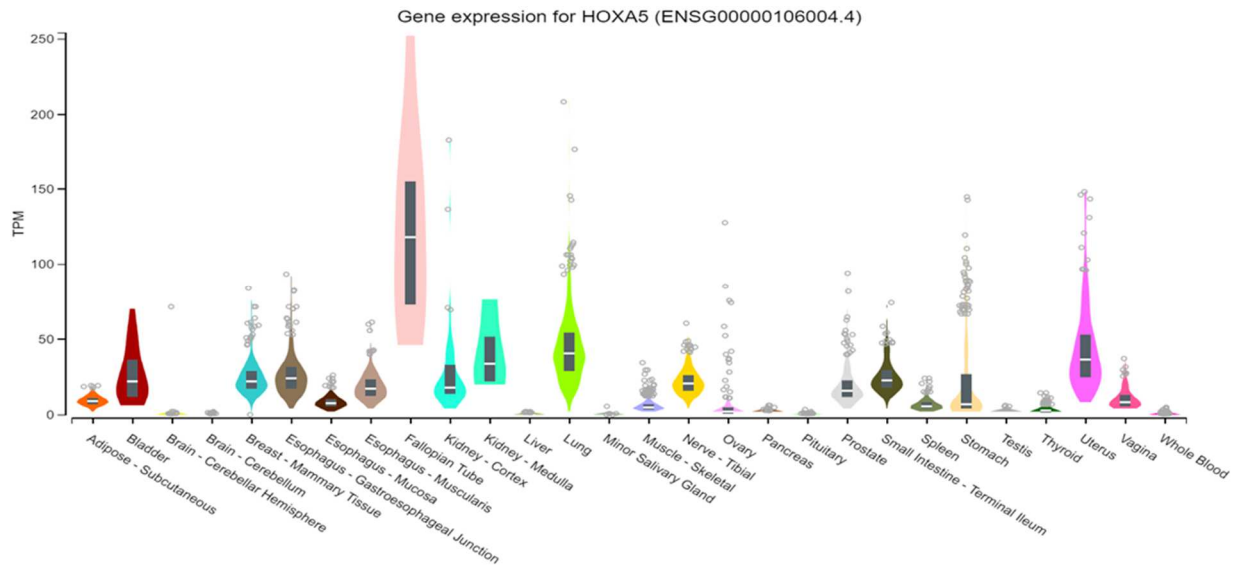
Figure 4.1. GTEx analysis. *HOXA5* mRNA expression in different normal tissues in human

Several studies have shown *HOXA5* to play a tumor suppressive role in various cancers (295). In breast cancer tissues, low *HOXA5* gene expression levels were significantly correlated with progression to higher-grade carcinomas (296). In colorectal cancer mouse models, *HOXA5* expression was shown to prevent tumor progression and metastasis by inducing loss of the colorectal cancer stem-like cell traits (297). In osteosarcoma patients, lower *HOXA5* expression was associated with poor outcome (298). In 45 women diagnosed with endometrial cancer, higher grade cancers had lower *HOXA5* mRNA and protein expression compared to control (299). Upregulation of *HOXA5* in acute myeloid leukemia cells and tissue samples induced apoptosis and reduced proliferation of cancer cells (300). Reduced *HOXA5* expression was observed in non-small cell lung cancer (NSCLC) tissues compared with adjacent normal tissues (301). Finally, downregulation of *HOXA5* in ovarian cancer tissues lead to increased viability, faster proliferation and reduction of apoptosis (293). Additionally, although *Hoxa5*-null

119

mice were not prone to development of spontaneous mammary tumors, hyperplasia was observed in the mammary glands of these mice, suggesting that presence of HoxA5 could reduce breast cancer predisposition (302).

HOXA5 has been shown to mediate tumor suppressive effects through various mechanisms (295). Several studies in different cancers have shown that HoxA5 protein can regulate p53 by directly binding to the 'TAAT' motif present in the promoter region of *TP53* gene (303-306). Additionally, apart from indirectly regulating p21 through its action on p53, HoxA5 protein was also shown to directly bind to the promoter region and regulate p21 in NSCLC, thereby inhibiting cell proliferation (301). Studies have also shown that *HOXA5* can regulate other pathways such as Wnt-signaling and p38α MAPK pathway to bring about its effects (297, 303, 304, 307).

Several studies have shown *HOXA5* promoter region to be hypermethylated in various cancers such as triple-negative breast cancer, ductal carcinoma in situ, lung adenocarcinoma, colorectal cancer and myeloid leukemia (308-312). A study in AML samples showed that long non-coding RNA (lncRNA), HOTAIR, recruits Dnmt3b to *HOXA5* promoter and increases methylation, thereby downregulating *HOXA5* (300). Other recently identified regulators of *HOXA5* include lncRNA GAS5 and microRNAs miR-196-5p and miR-196a (293, 298). Additionally, transcription factors such as YY1 have also been shown to regulate HOXA5 gene (313, 314).

In this chapter, we performed various assays to decipher the mechanism through which NE regulates *HOXA5* expression in short-term and long-term treated cells.

Materials and Methods

HOXA5 **promoter identification:**

As described in chapter 2, three experimentally validated promoters for *HOXA5* were identified using Eukaryotic Promoter Database (EPD) and an approximately 2500 bp region including these promoters as well as a part of *HOXA5* coding region was cloned into pGL3 enhancer vector (Promega) (Figure 2.2). We dissected this segment to six different regions and cloned them individually into pGL3 enhancer vector (Figure 4.2).
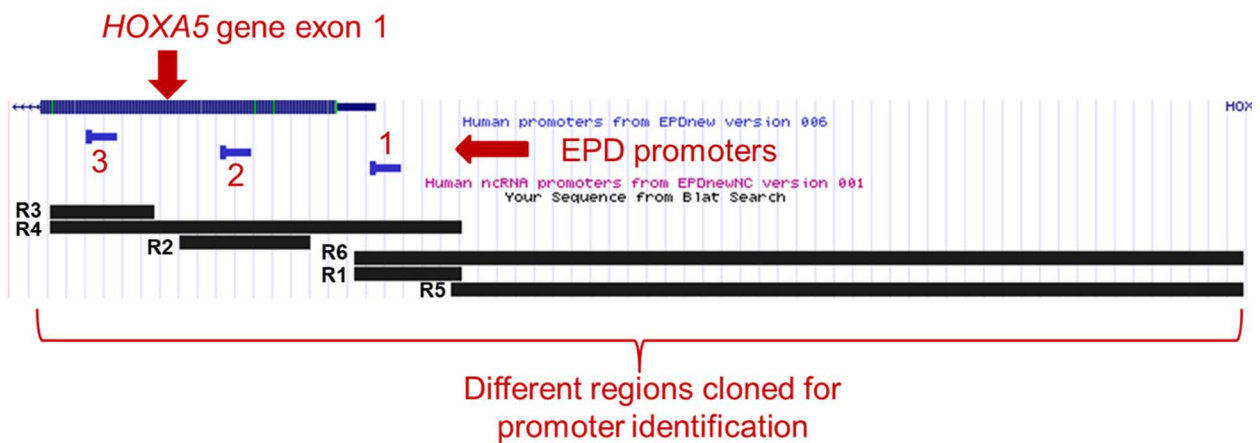
Figure 4.2. Promoter identification. *HOXA5* regulatory region constructs design (hg38 genome). R1 – Promoter 1 (chr7: 27143643-27143844), R2 – Promoter 2 (chr7:27143311-27143559), R3 – Promoter 3 (chr7:27143065-27143262), R4 – all 3 EPD promoters (chr7:27143065-27143844), R5 – Without EPD promoters (chr7:27143825-27145331) and R6 – R1+R5 (chr7: 27143643-27145331). These constructs were cloned into pGL3 enhancer vector.

Region R1 was 202bp in length and contained Promoter 1. Region R2 was 249bp in length and contained Promoter 2. Region R3 was 198bp in length and contained Promoter 3. Region R4 was 780bp in length and contained all three EPD promoters.

121

Region R5 was 1507bp in length and contained region without the three EPD promoters. Finally, Region R6 was 1689bp in length and contained regions R5 and R1. The whole region was labelled as R7.

Luciferase assay:

8000 iFTSEC283 cells each were plated in 96 well plates in 8 technical replicates. After overnight incubation, they were transfected with different *HOXA5* promoter regions containing pGL3 vector (50ng per well) (Promega) and pRL renilla luciferase vector (20ng per well) (Promega), which was used as internal control. pGL3 control vector (50 ng per well) (Promega) was used as positive control for the assay. Cells with the transfection medium containing Opti-MEM (Gibco), FuGENE HD (Promega) and the vectors were centrifuged for 30 mins at 1000 rpm before incubating for 48 hrs. Following incubation, the cells were treated with 10uM norepinephrine (Sigma-Aldrich) or vehicle (H2O) control containing fresh medium and incubated for 4 h. After treatment, Dual-Glo® Luciferase Assay System (Promega) was used to measure luciferase activity following manufacturer's protocol. SpectraMax L microplate reader was used for reading the output and firefly luciferase/renilla luciferase ratio was calculated.

Results

Short-term NE treatment showed differential regulation of R6 region of *HOXA5* whole segment:

iFTSEC283 cells were transfected with pGL3 enhancer vector containing 6 different parts of the *HOXA5* regulatory region (Figure 4.1) as well as the whole regulatory region (Figure 2.2) and treated with 10μM NE for 4 h followed by luciferase assay. Luciferase data suggested that among all three EPD promoters, Promoter 1 contained in the region R1 region had highest activity in both mock- and NE- treated cells, suggesting that in this model, Promoter 1 is involved in *HOXA5* gene regulation and could be considered as the minimal promoter (Figure 4.3). In contrast, region containing Promoter 2, R2, showed no luciferase activity in either condition, suggesting that this region is not involved in *HOXA5* upregulation and rather may contain negative regulators of *HOXA5* gene (Figure 4.3). Regions R3, R4 and R5 showed modest luciferase activity without any difference between mock vs treated cells, suggesting these regions are not regulated in response to NE (Figure 4.3). We identified R6, which contains R1 and R5 regions, as the region showing highest luciferase activity among all regions in addition to having an increased luciferase activity NE treated cells compared with mock-treated cells (Figure 4.3). Since both R1 and R5 individually did not show altered luciferase activity in response to NE, the data suggests that NE induces *HOXA5* through a minimal promoter region containing Promoter 1 by acting on an additional regulatory element present in R6.
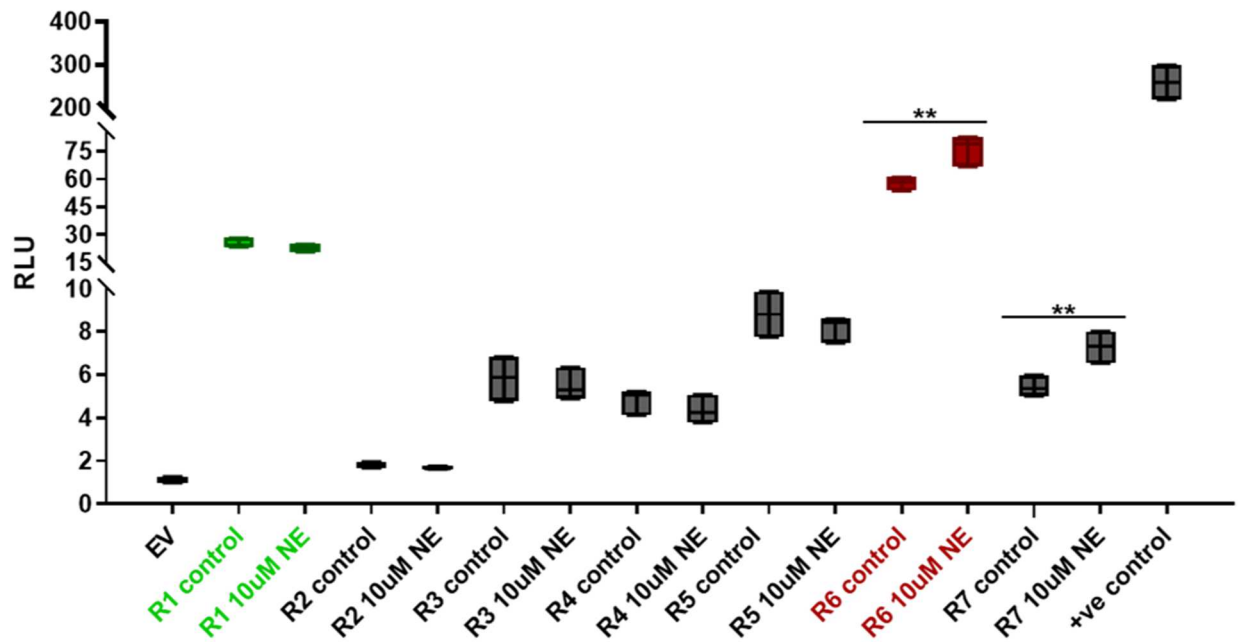
Figure 4.3. Luciferase assay for promoter identification. Six different *HOXA5* regulatory region constructs containing pGL3 enhancer vector and the whole region (R7) containing pGL3 enhancer vector were transfected into iFTSEC283 cells for 48 h followed by treatment with 10μM NE for 4 h and luciferase assay measurement.

Next, we used the Human Genome Browser database to get an overview on different regulatory elements that might be present in the R6 region (Figure 4.4). Using ChIP-seq data from ENCODE track on Human Genome Browser, we identified 74 transcription factors that have binding sites in the R6 region (Figure 4.4). In addition, we also identified 5 putative cis-regulatory proximal enhancer regions – E2542592/enhP, E2542593/enhP, E2542594/enhP, E2542595/enhP, E2542596/enhP (Figure 4.4). These data suggest that the R6 region has several regulatory elements and some of them may be responsible for the induction of *HOXA5* by NE.

124

Figure 4.4. Human genome browser. R6 region analysis using Human Genome Browser (GRCh38/hg38) Assembly. ENCODE candidate cis regulatory elements – enhancers are shown in orange box and promoters in red box. ENCODE Transcription Factors data - each peak cluster of transcription factor occupancy is enclosed by a gray box. The darkness of the box is proportional to the maximum signal strength.

Summary

In this chapter, we identified a minimal promoter region – R1 (202bp) - that positively regulates *HOXA5* expression in iFTSEC283 cells irrespective of NE treatment. We also identified a larger segment containing the minimal promoter region - R6 (1689bp) - that leads to higher upregulation of *HOXA5* expression compared with R1, suggesting that R6 may contain additional regulatory elements such as enhancers. In addition, the R6 region also showed differential *HOXA5* upregulation after NE treatment compared to control-treated cells, suggesting that NE may act on R6 to induce *HOXA5*. Future work includes dissecting the R6 region and identifying the regulatory elements used by NE to induce *HOXA5* in short-term NE treated cells. Additionally, the attenuation of *HOXA5* induction observed after short-term NE treatment in the 'long-term NE treated' (LTNE) cells and in ovarian cancer cells will also be studied.

CHAPTER FIVE

DISCUSSION AND FUTURE DIRECTION

HGSOC is the most common ovarian cancer subtype and is associated with poor prognosis (2, 5, 9). Most of the HGSOC cases are detected at advanced stages that are more aggressive and difficult to control (7, 9). In addition, lack of effective screening modalities to detect HGSOC at early stages and resistance to current standard of care leads to higher mortality rate (3, 80, 81). Therefore, identifying mechanisms that lead to initiation of HGSOC would help identify novel biomarkers that can aid early diagnosis.

As described in Chapter 1, epidemiological studies have reported that, conditions which cause chronic Sympathetic Nervous System (SNS) activation such as depression and PTSD, are associated with a higher risk of developing ovarian cancer (125, 126, 218-220). Additionally, stress hormone NE was found to be the most abundant catecholamine present in the normal rodent ovary and in aging mice, a spontaneous increase in SNS activity was observed which in turn led to increased NE levels and development of a polycystic condition (211-216). The effect of NE stimulation in ovarian cancer progression is also very well established (189, 193, 195-201, 203, 210). Although very little is known about the role of NE in ovarian cancer initiation, most of the mechanisms disrupted by NE

to promote cancer progression, can also potentially cause tumor initiation. For example, dysregulation of DNA damage repair pathways and oncogene activation are key processes involved in cancer initiation (238). This suggests that chronic NE stimulation might play a role in tumor initiation.

In this study we explored the possible mechanisms by which NE could influence ovarian cancer initiation by evaluating the in vitro effects of NE treatment on cell lines postulated to be the precursors of ovarian cancer— iFTSEC283 and iOSE11. Additionally, since ~96% of HGSOC patients have *TP53* alterations and these alterations happen early in the development of HGSOC (10-13, 41), we also evaluated the effects of NE treatment on precursor cells over-expressing a dominant-negative *TP53* mutant (p.R175H). We subcategorized our study into three groups – unraveling the effects of 1) short-term/ acute NE treatment, 2) long-term/chronic NE treatment and 3) identifying molecular mechanisms that are distinct between the two conditions.

To understand the effects of short-term NE exposure, we focused on early transcriptional changes induced in iOSE11 and iFTSEC283 cells by NE. We identified differentially expressed genes after 1 h and 4 h treatment with NE in both cell lines. iFTSEC283 cells had much higher number of differentially expressed genes in response to NE – 234 genes and 313 genes at 1 h and 4 h time points respectively, compared to iOSE11 cells – 53 and 34 genes after 1 h and 4 h of NE treatment respectively. Although there was a significant difference between the total number of differentially expressed genes identified in both cell lines, 45/53 genes (84.9%) at 1 h time point and 22/34 genes (64.7%) at 4 h time point identified in the iOSE11 cell lines overlapped with the differentially expressed genes identified in the iFTSEC283 cell line at respective time

points. Additionally, transcription factor enrichment analysis identified HoxA5 as a significantly enriched transcription factor common to both cell lines at both time points. These data suggest some degree of overlap between both cell lines in response to short term NE treatment.

Since iFTSEC283 cells displayed higher total number of differentially expressed genes in response to short-term NE treatment compared to iOSE11 cells and the fact that numerous evidences have shown that majority of the HGSOC arise from epithelium of distal fallopian tube (33, 36-38, 40, 43), we generated transcriptomic profile of long-term NE treated vs control iFTSEC283 cells (137 days) and compared it to the short-term transcriptomic profiles. A total of 123 differentially regulated genes were identified in response to chronic NE treatment. While 71 differentially expressed genes in response to short-term NE treatment were common to 1 h and 4 h time points suggesting some degree of overlap between the two time points, only 11 genes were common between 1 h time point and long-term NE treated iFTSEC283 cells and only 9 genes were common between 4 h time point and long-term NE treated cells. These data suggest that the transcriptional response to acute NE treatment is distinct from the transcriptional response observed after chronic exposure to NE.

The differences between the transcriptomic profile of the acute vs chronic NE treated iFTSEC283 cells can be explained by multiple mechanisms such as selection of clonal populations with altered signaling pathways or altered epigenetic regulation by prolonged NE treatment. Performing single cell analysis such as single-cell RNA seq or single cell ATAC seq could help identify these differences. Another question that remains to be answered is whether the observed alterations brought about by chronic exposure

129

to NE are sufficient for ovarian cancer initiation. Interestingly, in long-term NE treated iFTSEC283 cells, canonical p53 target genes (315) – *CDKN1A* (coding for p21) and *BBC3* (coding for PUMA) – were downregulated in response to NE. Both p21 and PUMA are induced by p53 in response to DNA damage and are involved in cell cycle arrest and apoptosis respectively (316, 317). Deregulation of these genes leads to continued cell proliferation and reduced apoptosis even in the presence of DNA damage, thereby increasing the frequency of acquiring alterations in the DNA that could lead to tumor initiation (316-319). In addition to canonical p53 target genes, five histone transcripts were upregulated in iFTSEC283 cells in response to long-term NE exposure. Gene Ontology Reactome Pathway analysis revealed an overrepresentation of 'Chromatin Modifying Enzymes', HDACs, HATs and 'DNA Methylation' pathways. These results suggest that NE may play a role in epigenetic regulation of iFTSEC283 cells.

Next, we compared the transcriptomic profiles of long-term treated iFTSEC283 cells and long-term treated iFTSEC283[p53R175H] cells. Only 23 differentially expressed genes were identified in iFTSEC283[p53R175H] cells in response to NE, out of which only 3 genes – *PLAU*, *MCAM* and *PLAC8* – overlapped with iFTSEC283 cells, suggesting that the p53 status determines the response to chronic NE treatment. The top downregulated genes identified in iFTSEC283[p53R175H] cells coded for proteins that are involved in cell-cell junction and extracellular matrix/structure organization such as intercellular tight junction component desmoplakin (*DSP*), collagen interacting proteoglycan biglycan (*BGN*), extracellular matrix protein ABI3 binding protein (*ABI3BP*), and integrin binding protein periostin (*POSTN*). Loss of *DSP* has been shown to increase local tumor invasion and cell proliferation (320, 321). Similarly, *ABI3BP* overexpression in vitro and in vivo was

shown to decrease tumor growth by inducing senescence and its expression is lost in most carcinomas (322, 323). *BGN* has been shown to have either oncogenic or tumor suppressive role depending on the cancer type and cellular origin (324). The downregulation of these gene combined with upregulation of extracellular matrix-degrading urokinase *PLAU* and cell adhesion molecule *MCAM* in iFTSEC283[p53R175H] can lead to degradation of the extracellular matrix and loss of cell adhesion, thereby promoting local cell invasion. In addition, iFTSEC283[p53R175H] cells also upregulated a stress activated p38 isoform, *MAPK13*, which has been shown to be positively associated with initiation of skin tumors and colitis-associated colon cancer (325, 326).

In addition to having a distinct transcriptomic profile compared to wild-type p53 containing iFTSEC283 cells, iFTSEC283[p53R175H] cells also displayed a decrease in the percentage of metaphase spreads containing diploid number of chromosomes after chronic exposure to 10µM NE. These results suggest that NE and oncogenic p53 alterations can act synergistically to promote chromosomal abnormalities. Chromosomal instability (CIN) is frequently observed in HGSOC (16-20). In addition, several in vivo studies have shown that chromosomal instability (CIN) is sufficient to induce tumor initiation (327-329). This raises the possibility that chronic exposure to NE in the presence of oncogenic p53 alteration, which is the earliest genetic alteration found in precursor lesions of HGSOC (11, 13, 41), could lead to initiation and development of HGSOC through increased chromosomal number alterations.

To summarize, the transcriptomic data suggests a difference between the acute vs chronic NE response. Additionally, p53 status was implicated to be critical to chronic NE response. Next, we wanted to study the molecular mechanisms underlying these

differences. First, we focused on understanding the differences between response to acute vs chronic NE treatment irrespective of p53 status. As mentioned previously, transcription factor enrichment analysis identified HoxA5 transcription factor to be significantly enriched at both 1 h and 4 h time points in iFTSEC283 and iOSE11 cells. A qPCR time course study revealed that *HOXA5* transcript was induced by acute NE treatment in iOSE11, iOSE11[p53R175H], iFTSEC283, iFTSEC283[p53R175H] and iFTSEC282[p53R175H] cells. In all five cell lines, the induction of *HOXA5* by 10μM NE started around 45 mins to 1h, peaked at around 2 h to 3 h and returned to baseline levels by 4 h. The induction of *HOXA5* by NE was confirmed by increased luciferase activity in iOSE11 and iFTSEC283 cells in response to NE treatment when a ~2500bp *HOXA5* cis regulatory region was cloned into pGL3 enhancer vector and used for luciferase reporter assay time course study. These results indicate that acute NE treatment induces *HOXA5* irrespective of the p53 status.

When we performed transcription factor enrichment analysis on the differentially expressed genes identified in response to long-term NE treatment in iFTSEC283 and iFTSEC283[p53R175H] cells, neither cell line exhibited enrichment of HoxA5. Additionally, when LT 10μM NE treated cells were further exposed to short-term 10μM NE treatment qPCR time course described above, the induction of *HOXA5* transcript was attenuated. In contrast, LT mock treated cells displayed similar *HOXA5* induction curve as was observed in short-term 10μM NE treatment of normal and partially transformed cells. Additionally, the NE-binding receptor, ADRB2, levels remained unaltered after long-term NE treatment compared to long-term mock treated cells, suggesting that the attenuation of *HOXA5* induction was not due to loss of receptor. The attenuation of *HOXA5* induction

by NE was also observed in ovarian cancer cells – OVCAR8 and SKOV3, and these cells had similar ADRB2 levels as normal and partially transformed iFTSEC283 and iOSE11 cell. These results suggest that long-term exposure to NE could lead to altered *HOXA5* regulation which is more similar to cancer cells and distinct from short-term response to NE.

As described in chapter 4, *HOXA5* has been shown to mediate tumor suppressive effects through various mechanisms (295). Several studies in different cancers have shown that HoxA5 protein can regulate p53 by directly binding to the 'TAAT' motif present in the promoter region of *TP53* gene (303-306). Additionally, apart from indirectly regulating p21 through its action on p53, HoxA5 protein was also shown to directly bind to the promoter region and regulate p21 in NSCLC, thereby inhibiting cell proliferation (301). It is possible that the downregulation of p21 and PUMA identified in our long-term NE treated iFTSEC283 cells transcriptomic data could be associated with attenuation of *HOXA5* induction observed in long-term NE treated cells. In contrast, in our short-term NE treated iFTSEC283 cells, six genes – *TSC22D3*, *CSF3*, *FRMD4A*, *MAML3*, *PPAP2B* and *PRKCE* – were identified to be regulated by HoxA5 in response to NE through combination of ChIP-seq, RNA-Seq, oPOSSUM, MEME and FIMO analysis. This suggests that a part of acute NE response is mediated by HoxA5.

Next, we focused on identifying the mechanism by which *HOXA5* is induced after acute NE treatment. We dissected the ~2500kb *HOXA5* proximal cis regulatory region into smaller regions to identify regulatory elements present in near *HOXA5* gene. Through luciferase assays, we identified a minimal promoter region – R1 (202bp) - that positively regulates *HOXA5* expression in iFTSEC283 cells, but this region did not respond to NE

treatment. We then identified a larger segment containing the minimal promoter region - R6 (1689bp) - that leads to higher upregulation of *HOXA5* expression compared with R1, suggesting that R6 may contain additional regulatory elements such as enhancers. In addition, the R6 region also showed differential *HOXA5* upregulation after NE treatment compared to control-treated cells, suggesting that NE may act on R6 to induce *HOXA5*.

Ongoing work in the lab includes dissecting the R6 region in order to understand the mechanism by which NE regulates *HOXA5*. Once the region is established, it will be followed by in silico analysis and site directed mutagenesis to identify transcription factors that may be responsible for mediating *HOXA5* regulation by NE.

Future work includes identifying mechanisms that lead to differences in *HOXA5* regulation in acute vs chronic NE treatment response. Several studies have shown *HOXA5* promoter region to be hypermethylated in various cancers such as triple-negative breast cancer, ductal carcinoma in situ, lung adenocarcinoma, colorectal cancer and myeloid leukemia (308-312). Therefore, it can be hypothesized that the attenuation of *HOXA5* induction after chronic NE exposure could be due to hypermethylation of the promoter region or other epigenetic changes. Additionally, transcription factors regulating *HOXA5* in response to acute NE treatment could be deregulated after chronic NE treatment. Experiments such as promoter bashing, site directed mutagenesis, ATAC-seq and methylation specific PCR would help identify the mechanism underlying *HOXA5* regulation in chronic NE treated cells.

In summary, this study focuses on delineating the effects of short-term and long-term stress responses, through the actions of NE, on precursor cells of HGSOC. By generating global transcriptomic profiles, we found that the responses to acute and

chronic NE treatment were distinct from each other. We also showed that the transcription factor HoxA5 was induced in response to acute NE treatment in *TP53* wildtype and mut-*TP53* overexpressing normal cell lines, and, in turn, partially mediated the acute NE stress response through its action on target genes. On the other hand, chronic NE treated cells showed abrogation of HoxA5 induction, and this phenomenon was also observed in ovarian cancer cells. Since various studies have shown HoxA5 to primarily have anti-tumorigenic roles, we hypothesize that abrogation of HoxA5 induction in chronic NE treated cells could lead to tumor development through loss of anti-tumorigenic effects. The overall summary of this study is depicted in Figure 5.
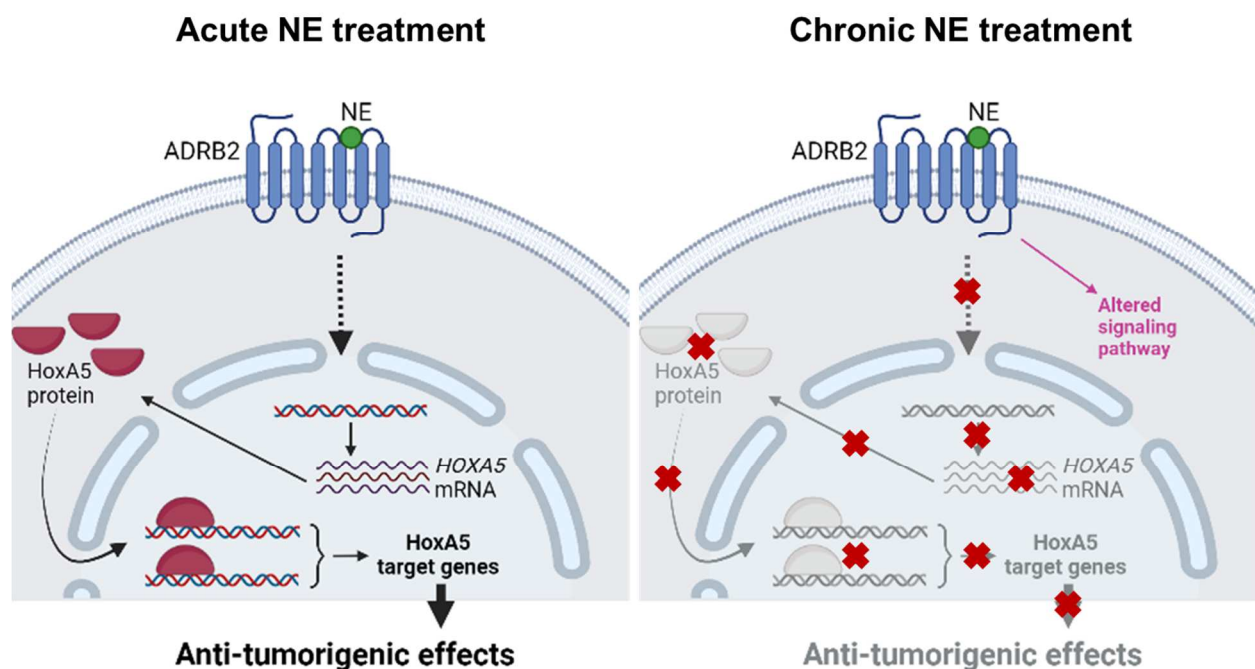
Figure 5. Overall summary. (Created with BioRender.com)

While there are certain limitations, such as the lack of *in vivo* studies and patient data, this study highlights the differences between acute and chronic response to NE treatment at the molecular level in ovarian surface epithelial and fallopian tube cell line

models. Further research would help in understanding the role of chronic stress in ovarian cancer initiation. This can ultimately lead to the identification of more specific and sensitive biomarkers, and aid in early detection of ovarian cancer in patients.

REFERENCES

1.   Momenimovahed Z, Tiznobaik A, Taheri S, Salehiniya H. Ovarian cancer in the world: epidemiology and risk factors. Int J Womens Health. 2019;11:287-99. Epub 2019/05/24. doi: 10.2147/ijwh.S197604. PubMed PMID: 31118829; PubMed Central PMCID: PMCPMC6500433.

2.   Siegel RL, Miller KD, Fuchs HE, Jemal A. Cancer Statistics, 2021. CA Cancer J Clin. 2021;71(1):7-33. Epub 2021/01/13. doi: 10.3322/caac.21654. PubMed PMID: 33433946.

3.   De Leo A, Santini D, Ceccarelli C, Santandrea G, Palicelli A, Acquaviva G, et al. What Is New on Ovarian Carcinoma: Integrated Morphologic and Molecular Analysis Following the New 2020 World Health Organization Classification of Female Genital Tumors. Diagnostics (Basel). 2021;11(4). Epub 2021/05/01. doi: 10.3390/diagnostics11040697. PubMed PMID: 33919741; PubMed Central PMCID: PMCPMC8070731.

4.   Torre LA, Trabert B, DeSantis CE, Miller KD, Samimi G, Runowicz CD, et al. Ovarian cancer statistics, 2018. CA Cancer J Clin. 2018;68(4):284-96. Epub 2018/05/29. doi: 10.3322/caac.21456. PubMed PMID: 29809280; PubMed Central PMCID: PMCPMC6621554.

5. Prat J, D'Angelo E, Espinosa I. Ovarian carcinomas: at least five different diseases with distinct histological features and molecular genetics. Hum Pathol. 2018;80:11-27. Epub 2018/06/27. doi: 10.1016/j.humpath.2018.06.018. PubMed PMID: 29944973.

6. Prat J, Mutch DG. Pathology of cancers of the female genital tract including molecular pathology. Int J Gynaecol Obstet. 2018;143 Suppl 2:93-108. Epub 2018/10/12. doi: 10.1002/ijgo.12617. PubMed PMID: 30306579.

7. Prat J. Staging Classification for Cancer of the Ovary, Fallopian Tube, and Peritoneum: Abridged Republication of Guidelines From the International Federation of Gynecology and Obstetrics (FIGO). Obstet Gynecol. 2015;126(1):171-4. Epub 2015/08/05. doi: 10.1097/aog.0000000000000917. PubMed PMID: 26241270.

8. Kurman RJ, Shih Ie M. The Dualistic Model of Ovarian Carcinogenesis: Revisited, Revised, and Expanded. Am J Pathol. 2016;186(4):733-47. Epub 2016/03/26. doi: 10.1016/j.ajpath.2015.11.011. PubMed PMID: 27012190; PubMed Central PMCID: PMCPMC5808151.

9. Lisio MA, Fu L, Goyeneche A, Gao ZH, Telleria C. High-Grade Serous Ovarian Cancer: Basic Sciences, Clinical and Therapeutic Standpoints. Int J Mol Sci. 2019;20(4). Epub 2019/03/01. doi: 10.3390/ijms20040952. PubMed PMID: 30813239; PubMed Central PMCID: PMCPMC6412907.

10. Ahmed AA, Etemadmoghadam D, Temple J, Lynch AG, Riad M, Sharma R, et al. Driver mutations in TP53 are ubiquitous in high grade serous carcinoma of the ovary. J Pathol. 2010;221(1):49-56. Epub 2010/03/17. doi: 10.1002/path.2696. PubMed PMID: 20229506; PubMed Central PMCID: PMCPMC3262968.

11.   Brachova P, Thiel KW, Leslie KK. The consequence of oncomorphic TP53 mutations in ovarian cancer. Int J Mol Sci. 2013;14(9):19257-75. Epub 2013/09/26. doi: 10.3390/ijms140919257. PubMed PMID: 24065105; PubMed Central PMCID: PMCPMC3794832.

12.   Seagle BL, Yang CP, Eng KH, Dandapani M, Odunsi-Akanji O, Goldberg GL, et al. TP53 hot spot mutations in ovarian cancer: selective resistance to microtubule stabilizers in vitro and differential survival outcomes from The Cancer Genome Atlas. Gynecol   Oncol.   2015;138(1):159-64.   Epub   2015/05/11.   doi: 10.1016/j.ygyno.2015.04.039. PubMed PMID: 25958320; PubMed Central PMCID: PMCPMC5303002.

13.   Zhang Y, Cao L, Nguyen D, Lu H. TP53 mutations in epithelial ovarian cancer. Transl Cancer Res. 2016;5(6):650-63. Epub 2016/12/01. doi: 10.21037/tcr.2016.08.40. PubMed PMID: 30613473; PubMed Central PMCID: PMCPMC6320227.

14.   Hoogstraat M, de Pagter MS, Cirkel GA, van Roosmalen MJ, Harkins TT, Duran K, et al. Genomic and transcriptomic plasticity in treatment-naive ovarian cancer. Genome Res. 2014;24(2):200-11. Epub 2013/11/14. doi: 10.1101/gr.161026.113. PubMed PMID: 24221193; PubMed Central PMCID: PMCPMC3912411.

15.   Integrated genomic analyses of ovarian carcinoma. Nature. 2011;474(7353):609-15. Epub 2011/07/02. doi: 10.1038/nature10166. PubMed PMID: 21720365; PubMed Central PMCID: PMCPMC3163504.

16.   Bayani J, Paderova J, Murphy J, Rosen B, Zielenska M, Squire JA. Distinct patterns of structural and numerical chromosomal instability characterize sporadic ovarian   cancer.   Neoplasia.   2008;10(10):1057-65.   Epub   2008/09/25.   doi:

10.1593/neo.08584. PubMed PMID: 18813350; PubMed Central PMCID: PMCPMC2546587.

17.   Bashashati A, Ha G, Tone A, Ding J, Prentice LM, Roth A, et al. Distinct evolutionary trajectories of primary high-grade serous ovarian cancers revealed through spatial mutational profiling. J Pathol. 2013;231(1):21-34. Epub 2013/06/20. doi: 10.1002/path.4230. PubMed PMID: 23780408; PubMed Central PMCID: PMCPMC3864404.

18.   Bayani J, Brenton JD, Macgregor PF, Beheshti B, Albert M, Nallainathan D, et al. Parallel analysis of sporadic primary ovarian carcinomas by spectral karyotyping, comparative genomic hybridization, and expression microarrays. Cancer Res. 2002;62(12):3466-76. Epub 2002/06/18. PubMed PMID: 12067990.

19.   Penner-Goeke S, Lichtensztejn Z, Neufeld M, Ali JL, Altman AD, Nachtigal MW, et al. The temporal dynamics of chromosome instability in ovarian cancer cell lines and primary patient samples. PLoS Genet. 2017;13(4):e1006707. Epub 2017/04/05. doi: 10.1371/journal.pgen.1006707. PubMed PMID: 28376088; PubMed Central PMCID: PMCPMC5395197.

20.   Testa U, Petrucci E, Pasquini L, Castelli G, Pelosi E. Ovarian Cancers: Genetic Abnormalities, Tumor Heterogeneity and Progression, Clonal Evolution and Cancer Stem Cells. Medicines (Basel). 2018;5(1). Epub 2018/02/02. doi: 10.3390/medicines5010016. PubMed PMID: 29389895; PubMed Central PMCID: PMCPMC5874581.

21.   Ahn G, Folkins AK, McKenney JK, Longacre TA. Low-grade Serous Carcinoma of the Ovary: Clinicopathologic Analysis of 52 Invasive Cases and Identification of a

Possible Noninvasive Intermediate Lesion. Am J Surg Pathol. 2016;40(9):1165-76. Epub 2016/08/05. doi: 10.1097/pas.0000000000000693. PubMed PMID: 27487741.

22.   Santandrea G, Piana S, Valli R, Zanelli M, Gasparini E, De Leo A, et al. Immunohistochemical Biomarkers as a Surrogate of Molecular Analysis in Ovarian Carcinomas: A Review of the Literature. Diagnostics (Basel). 2021;11(2). Epub 2021/02/13. doi: 10.3390/diagnostics11020199. PubMed PMID: 33572888; PubMed Central PMCID: PMCPMC7911119.

23.   Cheasley D, Nigam A, Zethoven M, Hunter S, Etemadmoghadam D, Semple T, et al. Genomic analysis of low-grade serous ovarian carcinoma to identify key drivers and therapeutic vulnerabilities. J Pathol. 2021;253(1):41-54. Epub 2020/09/10. doi: 10.1002/path.5545. PubMed PMID: 32901952.

24.   Kandoth C, Schultz N, Cherniack AD, Akbani R, Liu Y, Shen H, et al. Integrated genomic characterization of endometrial carcinoma. Nature. 2013;497(7447):67-73. Epub 2013/05/03. doi: 10.1038/nature12113. PubMed PMID: 23636398; PubMed Central PMCID: PMCPMC3704730.

25.   Pierson WE, Peters PN, Chang MT, Chen LM, Quigley DA, Ashworth A, et al. An integrated molecular profile of endometrioid ovarian cancer. Gynecol Oncol. 2020;157(1):55-61. Epub 2020/03/07. doi: 10.1016/j.ygyno.2020.02.011. PubMed PMID: 32139151.

26.   Iida Y, Okamoto A, Hollis RL, Gourley C, Herrington CS. Clear cell carcinoma of the ovary: a clinical and molecular perspective. Int J Gynecol Cancer. 2021;31(4):605-16. Epub 2020/09/20. doi: 10.1136/ijgc-2020-001656. PubMed PMID: 32948640.

27.   Morice P, Gouy S, Leary A. Mucinous Ovarian Carcinoma. N Engl J Med. 2019;380(13):1256-66. Epub 2019/03/28. doi: 10.1056/NEJMra1813254. PubMed PMID: 30917260.

28.   Cheasley D, Wakefield MJ, Ryland GL, Allan PE, Alsop K, Amarasinghe KC, et al. The molecular origin and taxonomy of mucinous ovarian carcinoma. Nat Commun. 2019;10(1):3935. Epub 2019/09/04. doi: 10.1038/s41467-019-11862-x. PubMed PMID: 31477716; PubMed Central PMCID: PMCPMC6718426.

29.   Klotz DM, Wimberger P. Cells of origin of ovarian cancer: ovarian surface epithelium or fallopian tube? Arch Gynecol Obstet. 2017;296(6):1055-62. Epub 2017/09/25. doi: 10.1007/s00404-017-4529-z. PubMed PMID: 28940023.

30.   Lengyel E. Ovarian cancer development and metastasis. Am J Pathol. 2010;177(3):1053-64. Epub 2010/07/24. doi: 10.2353/ajpath.2010.100105. PubMed PMID: 20651229; PubMed Central PMCID: PMCPMC2928939.

31.   Ahmed N, Abubaker K, Findlay J, Quinn M. Cancerous ovarian stem cells: obscure targets for therapy but relevant to chemoresistance. J Cell Biochem. 2013;114(1):21-34. Epub 2012/08/14. doi: 10.1002/jcb.24317. PubMed PMID: 22887554.

32.   Kuhn E, Kurman RJ, Shih IM. Ovarian Cancer Is an Imported Disease: Fact or Fiction? Curr Obstet Gynecol Rep. 2012;1(1):1-9. Epub 2012/04/17. doi: 10.1007/s13669-011-0004-1. PubMed PMID: 22506137; PubMed Central PMCID: PMCPMC3322388.

33.   Kurman RJ, Shih Ie M. The origin and pathogenesis of epithelial ovarian cancer: a proposed unifying theory. Am J Surg Pathol. 2010;34(3):433-43. Epub 2010/02/16. doi:

10.1097/PAS.0b013e3181cf3d79. PubMed PMID: 20154587; PubMed Central PMCID: PMCPMC2841791.

34.   Zhang S, Dolgalev I, Zhang T, Ran H, Levine DA, Neel BG. Both fallopian tube and ovarian surface epithelium are cells-of-origin for high-grade serous ovarian carcinoma. Nat Commun. 2019;10(1):5367. Epub 2019/11/28. doi: 10.1038/s41467-019-13116-2. PubMed PMID: 31772167; PubMed Central PMCID: PMCPMC6879755 Pharmaceuticals and Northern Biologics, Inc. He also is a member of the Scientific Advisory Board, and receives consulting fees and equity from Avrinas, Inc, and is an expert witness for the Johnson and Johnson ovarian cancer talc litigation. His spouse has equity in Mirati Therapuetics, Amgen, Inc., Arvinas, Inc. and Array Biopharma. The other authors declare no competing interests.

35.   Piek JM, van Diest PJ, Zweemer RP, Jansen JW, Poort-Keesom RJ, Menko FH, et al. Dysplastic changes in prophylactically removed Fallopian tubes of women predisposed to developing ovarian cancer. J Pathol. 2001;195(4):451-6. Epub 2001/12/18. doi: 10.1002/path.1000. PubMed PMID: 11745677.

36.   Carlson JW, Miron A, Jarboe EA, Parast MM, Hirsch MS, Lee Y, et al. Serous tubal intraepithelial carcinoma: its potential role in primary peritoneal serous carcinoma and serous cancer prevention. J Clin Oncol. 2008;26(25):4160-5. Epub 2008/09/02. doi: 10.1200/jco.2008.16.4814. PubMed PMID: 18757330; PubMed Central PMCID: PMCPMC2654373.

37.   Pisanic TR, 2nd, Wang Y, Sun H, Considine M, Li L, Wang TH, et al. Methylomic Landscapes of Ovarian Cancer Precursor Lesions. Clin Cancer Res. 2020;26(23):6310-

20. Epub 2020/08/21. doi: 10.1158/1078-0432.Ccr-20-0270. PubMed PMID: 32817081; PubMed Central PMCID: PMCPMC7710556.

38.   Kim J, Park EY, Kim O, Schilder JM, Coffey DM, Cho CH, et al. Cell Origins of High-Grade Serous Ovarian Cancer. Cancers (Basel). 2018;10(11). Epub 2018/11/15. doi: 10.3390/cancers10110433. PubMed PMID: 30424539; PubMed Central PMCID: PMCPMC6267333.

39.   Lee Y, Miron A, Drapkin R, Nucci MR, Medeiros F, Saleemuddin A, et al. A candidate precursor to serous carcinoma that originates in the distal fallopian tube. J Pathol. 2007;211(1):26-35. Epub 2006/11/23. doi: 10.1002/path.2091. PubMed PMID: 17117391.

40.   Kyo S, Ishikawa N, Nakamura K, Nakayama K. The fallopian tube as origin of ovarian cancer: Change of diagnostic and preventive strategies. Cancer Med. 2020;9(2):421-31. Epub 2019/11/27. doi: 10.1002/cam4.2725. PubMed PMID: 31769234; PubMed Central PMCID: PMCPMC6970023.

41.   Shih IM, Wang Y, Wang TL. The Origin of Ovarian Cancer Species and Precancerous Landscape. Am J Pathol. 2021;191(1):26-39. Epub 2020/10/05. doi: 10.1016/j.ajpath.2020.09.006. PubMed PMID: 33011111; PubMed Central PMCID: PMCPMC7786078.

42.   Salvador S, Rempel A, Soslow RA, Gilks B, Huntsman D, Miller D. Chromosomal instability in fallopian tube precursor lesions of serous carcinoma and frequent monoclonality of synchronous ovarian and fallopian tube mucosal serous carcinoma. Gynecol   Oncol.   2008;110(3):408-17.   Epub   2008/07/04.   doi: 10.1016/j.ygyno.2008.05.010. PubMed PMID: 18597838.

43.   Labidi-Galy SI, Papp E, Hallberg D, Niknafs N, Adleff V, Noe M, et al. High grade serous ovarian carcinomas originate in the fallopian tube. Nat Commun. 2017;8(1):1093. Epub 2017/10/25. doi: 10.1038/s41467-017-00962-1. PubMed PMID: 29061967; PubMed Central PMCID: PMCPMC5653668 Advisory Board and Board of Directors. V.E.V. owns Personal Genome Diagnostics stock, which is subject to certain restrictions under university policy. The terms of this arrangement is managed by the Johns Hopkins University in accordance with its conflict of interest policies. The remaining authors declare no competing financial interests.

44.   Jarboe E, Folkins A, Nucci MR, Kindelberger D, Drapkin R, Miron A, et al. Serous carcinogenesis in the fallopian tube: a descriptive classification. Int J Gynecol Pathol. 2008;27(1):1-9. Epub 2007/12/25. doi: 10.1097/pgp.0b013e31814b191f. PubMed PMID: 18156967.

45.   Jarboe EA, Folkins AK, Drapkin R, Ince TA, Agoston ES, Crum CP. Tubal and ovarian pathways to pelvic epithelial cancer: a pathological perspective. Histopathology. 2008;53(2):127-38. Epub 2008/02/27. doi: 10.1111/j.1365-2559.2007.02938.x. PubMed PMID: 18298580.

46.   Yates MS, Meyer LA, Deavers MT, Daniels MS, Keeler ER, Mok SC, et al. Microscopic and early-stage ovarian cancers in BRCA1/2 mutation carriers: building a model for early BRCA-associated tumorigenesis. Cancer Prev Res (Phila). 2011;4(3):463-70. Epub 2011/02/01. doi: 10.1158/1940-6207.Capr-10-0266. PubMed PMID: 21278312; PubMed Central PMCID: PMCPMC3048908.

47.   Kindelberger DW, Lee Y, Miron A, Hirsch MS, Feltmate C, Medeiros F, et al. Intraepithelial carcinoma of the fimbria and pelvic serous carcinoma: Evidence for a

causal relationship. Am J Surg Pathol. 2007;31(2):161-9. Epub 2007/01/27. doi: 10.1097/01.pas.0000213335.40358.47. PubMed PMID: 17255760.

48. Dubeau L. The cell of origin of ovarian epithelial tumors and the ovarian surface epithelium dogma: does the emperor have no clothes? Gynecol Oncol. 1999;72(3):437-42. Epub 1999/03/04. doi: 10.1006/gyno.1998.5275. PubMed PMID: 10053122.

49. Dubeau L. The cell of origin of ovarian epithelial tumours. Lancet Oncol. 2008;9(12):1191-7. Epub 2008/11/29. doi: 10.1016/s1470-2045(08)70308-5. PubMed PMID: 19038766; PubMed Central PMCID: PMCPMC4176875.

50. Auersperg N. The origin of ovarian carcinomas: a unifying hypothesis. Int J Gynecol Pathol. 2011;30(1):12-21. Epub 2010/12/07. doi: 10.1097/PGP.0b013e3181f45f3e. PubMed PMID: 21131839.

51. Flesken-Nikitin A, Hwang CI, Cheng CY, Michurina TV, Enikolopov G, Nikitin AY. Ovarian surface epithelium at the junction area contains a cancer-prone stem cell niche. Nature. 2013;495(7440):241-5. Epub 2013/03/08. doi: 10.1038/nature11979. PubMed PMID: 23467088; PubMed Central PMCID: PMCPMC3982379.

52. Szabova L, Yin C, Bupp S, Guerin TM, Schlomer JJ, Householder DB, et al. Perturbation of Rb, p53, and Brca1 or Brca2 cooperate in inducing metastatic serous epithelial ovarian cancer. Cancer Res. 2012;72(16):4141-53. Epub 2012/05/24. doi: 10.1158/0008-5472.Can-11-3834. PubMed PMID: 22617326; PubMed Central PMCID: PMCPMC3421072.

53. Tanwar PS, Mohapatra G, Chiang S, Engler DA, Zhang L, Kaneko-Tarui T, et al. Loss of LKB1 and PTEN tumor suppressor genes in the ovarian surface epithelium induces papillary serous ovarian cancer. Carcinogenesis. 2014;35(3):546-53. Epub

2013/10/31. doi: 10.1093/carcin/bgt357. PubMed PMID: 24170201; PubMed Central PMCID: PMCPMC3941742.

54.   Amante S, Santos F, Cunha TM. Low-grade serous epithelial ovarian cancer: a comprehensive review and update for radiologists. Insights Imaging. 2021;12(1):60. Epub 2021/05/12. doi: 10.1186/s13244-021-01004-7. PubMed PMID: 33974157; PubMed Central PMCID: PMCPMC8113429.

55.   Singer G, Oldt R, 3rd, Cohen Y, Wang BG, Sidransky D, Kurman RJ, et al. Mutations in BRAF and KRAS characterize the development of low-grade ovarian serous carcinoma. J Natl Cancer Inst. 2003;95(6):484-6. Epub 2003/03/20. doi: 10.1093/jnci/95.6.484. PubMed PMID: 12644542.

56.   Tsang YT, Deavers MT, Sun CC, Kwan SY, Kuo E, Malpica A, et al. KRAS (but not BRAF) mutations in ovarian serous borderline tumour are associated with recurrent low-grade serous carcinoma. J Pathol. 2013;231(4):449-56. Epub 2014/02/20. doi: 10.1002/path.4252. PubMed PMID: 24549645; PubMed Central PMCID: PMCPMC4095747.

57.   Elsherif S, Javadi S, Viswanathan C, Faria S, Bhosale P. Low-grade epithelial ovarian cancer: what a radiologist should know. Br J Radiol. 2019;92(1095):20180571. Epub 2019/01/04. doi: 10.1259/bjr.20180571. PubMed PMID: 30604635; PubMed Central PMCID: PMCPMC6541194.

58.   Sainz de la Cuesta R, Eichhorn JH, Rice LW, Fuller AF, Jr., Nikrui N, Goff BA. Histologic transformation of benign endometriosis to early epithelial ovarian cancer. Gynecol Oncol. 1996;60(2):238-44. Epub 1996/02/01. doi: 10.1006/gyno.1996.0032. PubMed PMID: 8631545.

59.   Jiang X, Morland SJ, Hitchcock A, Thomas EJ, Campbell IG. Allelotyping of endometriosis with adjacent ovarian carcinoma reveals evidence of a common lineage. Cancer Res. 1998;58(8):1707-12. Epub 1998/05/01. PubMed PMID: 9563487.

60.   Matias-Guiu X, Stewart CJR. Endometriosis-associated ovarian neoplasia. Pathology. 2018;50(2):190-204. Epub 2017/12/16. doi: 10.1016/j.pathol.2017.10.006. PubMed PMID: 29241974.

61.   Cybulska P, Paula ADC, Tseng J, Leitao MM, Jr., Bashashati A, Huntsman DG, et al. Molecular profiling and molecular classification of endometrioid ovarian carcinomas. Gynecol Oncol. 2019;154(3):516-23. Epub 2019/07/26. doi: 10.1016/j.ygyno.2019.07.012. PubMed PMID: 31340883; PubMed Central PMCID: PMCPMC6736779.

62.   Meng B, Hoang LN, McIntyre JB, Duggan MA, Nelson GS, Lee CH, et al. POLE exonuclease domain mutation predicts long progression-free survival in grade 3 endometrioid carcinoma of the endometrium. Gynecol Oncol. 2014;134(1):15-9. Epub 2014/05/23. doi: 10.1016/j.ygyno.2014.05.006. PubMed PMID: 24844595.

63.   Church DN, Stelloo E, Nout RA, Valtcheva N, Depreeuw J, ter Haar N, et al. Prognostic significance of POLE proofreading mutations in endometrial cancer. J Natl Cancer Inst. 2015;107(1):402. Epub 2014/12/17. doi: 10.1093/jnci/dju402. PubMed PMID: 25505230; PubMed Central PMCID: PMCPMC4301706.

64.   Pawlik TM, Raut CP, Rodriguez-Bigas MA. Colorectal carcinogenesis: MSI-H versus MSI-L. Dis Markers. 2004;20(4-5):199-206. Epub 2004/11/06. doi: 10.1155/2004/368680. PubMed PMID: 15528785; PubMed Central PMCID: PMCPMC3839332.

65.   Imai K, Yamamoto H. Carcinogenesis and microsatellite instability: the interrelationship between genetics and epigenetics. Carcinogenesis. 2008;29(4):673-80. Epub 2007/10/19. doi: 10.1093/carcin/bgm228. PubMed PMID: 17942460.

66.   Latham A, Srinivasan P, Kemel Y, Shia J, Bandlamudi C, Mandelker D, et al. Microsatellite Instability Is Associated With the Presence of Lynch Syndrome Pan-Cancer. J Clin Oncol. 2019;37(4):286-95. Epub 2018/10/31. doi: 10.1200/jco.18.00283. PubMed PMID: 30376427; PubMed Central PMCID: PMCPMC6553803.

67.   Leskela S, Romero I, Cristobal E, Pérez-Mies B, Rosa-Rosa JM, Gutierrez-Pecharroman A, et al. Mismatch Repair Deficiency in Ovarian Carcinoma: Frequency, Causes, and Consequences. Am J Surg Pathol. 2020;44(5):649-56. Epub 2020/04/16. doi: 10.1097/pas.0000000000001432. PubMed PMID: 32294063.

68.   Wu RC, Ayhan A, Maeda D, Kim KR, Clarke BA, Shaw P, et al. Frequent somatic mutations of the telomerase reverse transcriptase promoter in ovarian clear cell carcinoma but not in other major types of gynaecological malignancy. J Pathol. 2014;232(4):473-81. Epub 2013/12/18. doi: 10.1002/path.4315. PubMed PMID: 24338723; PubMed Central PMCID: PMCPMC3946218.

69.   Dondi G, Coluccelli S, De Leo A, Ferrari S, Gruppioni E, Bovicelli A, et al. An Analysis of Clinical, Surgical, Pathological and Molecular Characteristics of Endometrial Cancer According to Mismatch Repair Status. A Multidisciplinary Approach. Int J Mol Sci. 2020;21(19). Epub 2020/10/03. doi: 10.3390/ijms21197188. PubMed PMID: 33003368; PubMed Central PMCID: PMCPMC7582893.

70.   Hollis RL, Thomson JP, Stanley B, Churchman M, Meynert AM, Rye T, et al. Molecular stratification of endometrioid ovarian carcinoma predicts clinical outcome. Nat

Commun. 2020;11(1):4995. Epub 2020/10/07. doi: 10.1038/s41467-020-18819-5. PubMed PMID: 33020491; PubMed Central PMCID: PMCPMC7536188 interests in AstraZeneca and Tesaro. C.G.: discloses research funding from AstraZeneca, Aprea, Nucana, Tesaro and Novartis; honoraria/consultancy fees from Roche, AstraZeneca, M.S.D., Tesaro, Nucana, Clovis, Foundation One, Cor2Ed and Sierra Oncology; named on issued/pending patents related to predicting treatment response in ovarian cancer outside the scope of the work described here. All other authors declare no conflicts of interest.

71.   Kurman RJ, Shih Ie M. Molecular pathogenesis and extraovarian origin of epithelial ovarian cancer--shifting the paradigm. Hum Pathol. 2011;42(7):918-31. Epub 2011/06/21. doi: 10.1016/j.humpath.2011.03.003. PubMed PMID: 21683865; PubMed Central PMCID: PMCPMC3148026.

72.   McConechy MK, Anglesio MS, Kalloger SE, Yang W, Senz J, Chow C, et al. Subtype-specific mutation of PPP2R1A in endometrial and ovarian carcinomas. J Pathol. 2011;223(5):567-73. Epub 2011/03/08. doi: 10.1002/path.2848. PubMed PMID: 21381030.

73.   McConechy MK, Ding J, Senz J, Yang W, Melnyk N, Tone AA, et al. Ovarian and endometrial endometrioid carcinomas have distinct CTNNB1 and PTEN mutation profiles. Mod Pathol. 2014;27(1):128-34. Epub 2013/06/15. doi: 10.1038/modpathol.2013.107. PubMed PMID: 23765252; PubMed Central PMCID: PMCPMC3915240.

74.   Gadducci A, Guerrieri ME. Immune Checkpoint Inhibitors in Gynecological Cancers: Update of Literature and Perspectives of Clinical Research. Anticancer Res.

2017;37(11):5955-65. Epub 2017/10/25. doi: 10.21873/anticanres.12042. PubMed PMID: 29061774.

75.   Chui MH, Gilks CB, Cooper K, Clarke BA. Identifying Lynch syndrome in patients with ovarian carcinoma: the significance of tumor subtype. Adv Anat Pathol. 2013;20(6):378-86. Epub 2013/10/12. doi: 10.1097/PAP.0b013e3182a92cf8. PubMed PMID: 24113308.

76.   Mackenzie R, Kommoss S, Winterhoff BJ, Kipp BR, Garcia JJ, Voss J, et al. Targeted deep sequencing of mucinous ovarian tumors reveals multiple overlapping RAS-pathway activating mutations in borderline and cancerous neoplasms. BMC Cancer. 2015;15:415. Epub 2015/05/20. doi: 10.1186/s12885-015-1421-8. PubMed PMID: 25986173; PubMed Central PMCID: PMCPMC4494777.

77.   Jelovac D, Armstrong DK. Recent progress in the diagnosis and treatment of ovarian cancer. CA Cancer J Clin. 2011;61(3):183-203. Epub 2011/04/28. doi: 10.3322/caac.20113. PubMed PMID: 21521830; PubMed Central PMCID: PMCPMC3576854.

78.   Goff BA, Mandel L, Muntz HG, Melancon CH. Ovarian carcinoma diagnosis. Cancer. 2000;89(10):2068-75. Epub 2000/11/07. doi: 10.1002/1097-0142(20001115)89:10<2068::aid-cncr6>3.0.co;2-z. PubMed PMID: 11066047.

79.   Goff B. Symptoms associated with ovarian cancer. Clin Obstet Gynecol. 2012;55(1):36-42. Epub 2012/02/22. doi: 10.1097/GRF.0b013e3182480523. PubMed PMID: 22343227.

80.   Goff BA. Ovarian cancer: screening and early detection. Obstet Gynecol Clin North Am. 2012;39(2):183-94. Epub 2012/05/30. doi: 10.1016/j.ogc.2012.02.007. PubMed PMID: 22640710.

81.   Doubeni CA, Doubeni AR, Myers AE. Diagnosis and Management of Ovarian Cancer. Am Fam Physician. 2016;93(11):937-44. Epub 2016/06/10. PubMed PMID: 27281838.

82.   Liu JH, Zanotti KM. Management of the adnexal mass. Obstet Gynecol. 2011;117(6):1413-28. Epub 2011/05/25. doi: 10.1097/AOG.0b013e31821c62b6. PubMed PMID: 21606754.

83.   Timmerman D, Ameye L, Fischerova D, Epstein E, Melis GB, Guerriero S, et al. Simple ultrasound rules to distinguish between benign and malignant adnexal masses before surgery: prospective validation by IOTA group. Bmj. 2010;341:c6839. Epub 2010/12/16. doi: 10.1136/bmj.c6839. PubMed PMID: 21156740; PubMed Central PMCID: PMCPMC3001703.

84.   Ameye L, Timmerman D, Valentin L, Paladini D, Zhang J, Van Holsbeke C, et al. Clinically oriented three-step strategy for assessment of adnexal pathology. Ultrasound Obstet Gynecol. 2012;40(5):582-91. Epub 2012/04/19. doi: 10.1002/uog.11177. PubMed PMID: 22511559.

85.   Clarke-Pearson DL. Clinical practice. Screening for ovarian cancer. N Engl J Med. 2009;361(2):170-7. Epub 2009/07/10. doi: 10.1056/NEJMcp0901926. PubMed PMID: 19587342.

86.   Andersen MR, Goff BA, Lowe KA, Scholler N, Bergan L, Drescher CW, et al. Use of a Symptom Index, CA125, and HE4 to predict ovarian cancer. Gynecol Oncol.

2010;116(3):378-83. Epub 2009/12/01. doi: 10.1016/j.ygyno.2009.10.087. PubMed PMID: 19945742; PubMed Central PMCID: PMCPMC2822097.

87.   Moss EL, Hollingworth J, Reynolds TM. The role of CA125 in clinical practice. J Clin Pathol. 2005;58(3):308-12. Epub 2005/03/01. doi: 10.1136/jcp.2004.018077. PubMed PMID: 15735166; PubMed Central PMCID: PMCPMC1770590.

88.   Wei SU, Li H, Zhang B. The diagnostic value of serum HE4 and CA-125 and ROMA index in ovarian cancer. Biomed Rep. 2016;5(1):41-4. Epub 2016/06/28. doi: 10.3892/br.2016.682. PubMed PMID: 27347403; PubMed Central PMCID: PMCPMC4906902.

89.   Screening for ovarian cancer: recommendation statement. U.S. Preventive Services Task Force. Am Fam Physician. 2005;71(4):759-62. Epub 2005/03/11. PubMed PMID: 15756773.

90.   Jia MM, Deng J, Cheng XL, Yan Z, Li QC, Xing YY, et al. Diagnostic accuracy of urine HE4 in patients with ovarian cancer: a meta-analysis. Oncotarget. 2017;8(6):9660-71. Epub 2017/01/01. doi: 10.18632/oncotarget.14173. PubMed PMID: 28039447; PubMed Central PMCID: PMCPMC5354761.

91.   Campbell S, Gentry-Maharaj A. The role of transvaginal ultrasound in screening for ovarian cancer. Climacteric. 2018;21(3):221-6. Epub 2018/03/02. doi: 10.1080/13697137.2018.1433656. PubMed PMID: 29490504.

92.   Žilovič D, Čiurlienė R, Sabaliauskaitė R, Jarmalaitė S. Future Screening Prospects for Ovarian Cancer. Cancers (Basel). 2021;13(15). Epub 2021/08/08. doi: 10.3390/cancers13153840. PubMed PMID: 34359740; PubMed Central PMCID: PMCPMC8345180.

93.   Chui MH, Momeni Boroujeni A, Mandelker D, Ladanyi M, Soslow RA. Characterization of TP53-wildtype tubo-ovarian high-grade serous carcinomas: rare exceptions to the binary classification of ovarian serous carcinoma. Mod Pathol. 2021;34(2):490-501. Epub 2020/08/18. doi: 10.1038/s41379-020-00648-y. PubMed PMID: 32801341.

94.   Young RC, Walton LA, Ellenberg SS, Homesley HD, Wilbanks GD, Decker DG, et al. Adjuvant therapy in stage I and stage II epithelial ovarian cancer. Results of two prospective randomized trials. N Engl J Med. 1990;322(15):1021-7. Epub 1990/04/12. doi: 10.1056/nejm199004123221501. PubMed PMID: 2181310.

95.   Ozols RF, Bundy BN, Greer BE, Fowler JM, Clarke-Pearson D, Burger RA, et al. Phase III trial of carboplatin and paclitaxel compared with cisplatin and paclitaxel in patients with optimally resected stage III ovarian cancer: a Gynecologic Oncology Group study.   J   Clin   Oncol.   2003;21(17):3194-200.   Epub   2003/07/16.   doi: 10.1200/jco.2003.02.153. PubMed PMID: 12860964.

96.   Hoskins P, Vergote I, Cervantes A, Tu D, Stuart G, Zola P, et al. Advanced ovarian cancer: phase III randomized study of sequential cisplatin-topotecan and carboplatin-paclitaxel vs carboplatin-paclitaxel. J Natl Cancer Inst. 2010;102(20):1547-56. Epub 2010/10/13. doi: 10.1093/jnci/djq362. PubMed PMID: 20937992.

97.   Monk BJ, Minion LE, Coleman RL. Anti-angiogenic agents in ovarian cancer: past, present, and future. Ann Oncol. 2016;27 Suppl 1(Suppl 1):i33-i9. Epub 2016/05/04. doi: 10.1093/annonc/mdw093. PubMed PMID: 27141068; PubMed Central PMCID: PMCPMC6283356.

98.   Elies A, Rivière S, Pouget N, Becette V, Dubot C, Donnadieu A, et al. The role of neoadjuvant chemotherapy in ovarian cancer. Expert Rev Anticancer Ther. 2018;18(6):555-66. Epub 2018/04/11. doi: 10.1080/14737140.2018.1458614. PubMed PMID: 29633903.

99.   Bian C, Yao K, Li L, Yi T, Zhao X. Primary debulking surgery vs. neoadjuvant chemotherapy followed by interval debulking surgery for patients with advanced ovarian cancer. Arch Gynecol Obstet. 2016;293(1):163-8. Epub 2015/07/23. doi: 10.1007/s00404-015-3813-z. PubMed PMID: 26198168.

100.   Sato S, Itamochi H. Neoadjuvant chemotherapy in advanced ovarian cancer: latest results and place in therapy. Ther Adv Med Oncol. 2014;6(6):293-304. Epub 2014/11/05. doi: 10.1177/1758834014544891. PubMed PMID: 25364394; PubMed Central PMCID: PMCPMC4206650.

101.   Alberts DS, Liu PY, Hannigan EV, O'Toole R, Williams SD, Young JA, et al. Intraperitoneal cisplatin plus intravenous cyclophosphamide versus intravenous cisplatin plus intravenous cyclophosphamide for stage III ovarian cancer. N Engl J Med. 1996;335(26):1950-5. Epub 1996/12/26. doi: 10.1056/nejm199612263352603. PubMed PMID: 8960474.

102.   Armstrong DK, Bundy B, Wenzel L, Huang HQ, Baergen R, Lele S, et al. Intraperitoneal cisplatin and paclitaxel in ovarian cancer. N Engl J Med. 2006;354(1):34-43. Epub 2006/01/06. doi: 10.1056/NEJMoa052985. PubMed PMID: 16394300.

103.   Bell J, Brady MF, Young RC, Lage J, Walker JL, Look KY, et al. Randomized phase III trial of three versus six cycles of adjuvant carboplatin and paclitaxel in early stage epithelial ovarian carcinoma: a Gynecologic Oncology Group study. Gynecol Oncol.

2006;102(3):432-9. Epub 2006/07/25. doi: 10.1016/j.ygyno.2006.06.013. PubMed PMID: 16860852.

104.   Burger RA, Brady MF, Bookman MA, Fleming GF, Monk BJ, Huang H, et al. Incorporation of bevacizumab in the primary treatment of ovarian cancer. N Engl J Med. 2011;365(26):2473-83. Epub 2011/12/30. doi: 10.1056/NEJMoa1104390. PubMed PMID: 22204724.

105.   Perren TJ, Swart AM, Pfisterer J, Ledermann JA, Pujade-Lauraine E, Kristensen G, et al. A phase 3 trial of bevacizumab in ovarian cancer. N Engl J Med. 2011;365(26):2484-96. Epub 2011/12/30. doi: 10.1056/NEJMoa1103799. PubMed PMID: 22204725.

106.   Aghajanian C, Blank SV, Goff BA, Judson PL, Teneriello MG, Husain A, et al. OCEANS: a randomized, double-blind, placebo-controlled phase III trial of chemotherapy with or without bevacizumab in patients with platinum-sensitive recurrent epithelial ovarian, primary peritoneal, or fallopian tube cancer. J Clin Oncol. 2012;30(17):2039-45. Epub 2012/04/25. doi: 10.1200/jco.2012.42.0505. PubMed PMID: 22529265; PubMed Central PMCID: PMCPMC3646321 found at the end of this article.

107.   Trillsch F, Mahner S, Hilpert F, Davies L, García-Martínez E, Kristensen G, et al. Prognostic and predictive effects of primary versus secondary platinum resistance for bevacizumab treatment for platinum-resistant ovarian cancer in the AURELIA trial. Ann Oncol. 2016;27(9):1733-9. Epub 2016/06/12. doi: 10.1093/annonc/mdw236. PubMed PMID: 27287207.

108.   Graybill W, Sood AK, Monk BJ, Coleman RL. State of the science: Emerging therapeutic strategies for targeting angiogenesis in ovarian cancer. Gynecol Oncol.

2015;138(2):223-6. Epub 2015/07/15. doi: 10.1016/j.ygyno.2015.07.008. PubMed PMID: 26166806.

109.   Vanacker H, Harter P, Labidi-Galy SI, Banerjee S, Oaknin A, Lorusso D, et al. PARP-inhibitors in epithelial ovarian cancer: Actual positioning and future expectations. Cancer Treat Rev. 2021;99:102255. Epub 2021/08/01. doi: 10.1016/j.ctrv.2021.102255. PubMed PMID: 34332292.

110.   Morales J, Li L, Fattah FJ, Dong Y, Bey EA, Patel M, et al. Review of poly (ADP-ribose) polymerase (PARP) mechanisms of action and rationale for targeting in cancer and other diseases. Crit Rev Eukaryot Gene Expr. 2014;24(1):15-28. Epub 2014/03/04. doi: 10.1615/critreveukaryotgeneexpr.2013006875. PubMed PMID: 24579667; PubMed Central PMCID: PMCPMC4806654.

111.   Roy R, Chun J, Powell SN. BRCA1 and BRCA2: different roles in a common pathway of genome protection. Nat Rev Cancer. 2011;12(1):68-78. Epub 2011/12/24. doi: 10.1038/nrc3181. PubMed PMID: 22193408; PubMed Central PMCID: PMCPMC4972490.

112.   Helleday T, Petermann E, Lundin C, Hodgson B, Sharma RA. DNA repair pathways as targets for cancer therapy. Nat Rev Cancer. 2008;8(3):193-204. Epub 2008/02/08. doi: 10.1038/nrc2342. PubMed PMID: 18256616.

113.   Mansour WY, Rhein T, Dahm-Daphi J. The alternative end-joining pathway for repair of DNA double-strand breaks requires PARP1 but is not dependent upon microhomologies. Nucleic Acids Res. 2010;38(18):6065-77. Epub 2010/05/21. doi: 10.1093/nar/gkq387. PubMed PMID: 20483915; PubMed Central PMCID: PMCPMC2952854.

114.   Luijsterburg MS, de Krijger I, Wiegant WW, Shah RG, Smeenk G, de Groot AJL, et al. PARP1 Links CHD2-Mediated Chromatin Expansion and H3.3 Deposition to DNA Repair by Non-homologous End-Joining. Mol Cell. 2016;61(4):547-62. Epub 2016/02/20. doi: 10.1016/j.molcel.2016.01.019. PubMed PMID: 26895424; PubMed Central PMCID: PMCPMC4769320.

115.   Ronson GE, Piberger AL, Higgs MR, Olsen AL, Stewart GS, McHugh PJ, et al. PARP1 and PARP2 stabilise replication forks at base excision repair intermediates through Fbh1-dependent Rad51 regulation. Nat Commun. 2018;9(1):746. Epub 2018/02/23. doi: 10.1038/s41467-018-03159-2. PubMed PMID: 29467415; PubMed Central PMCID: PMCPMC5821833.

116.   Murai J, Huang SY, Das BB, Renaud A, Zhang Y, Doroshow JH, et al. Trapping of PARP1 and PARP2 by Clinical PARP Inhibitors. Cancer Res. 2012;72(21):5588-99. Epub 2012/11/03. doi: 10.1158/0008-5472.Can-12-2753. PubMed PMID: 23118055; PubMed Central PMCID: PMCPMC3528345.

117.   Jungmichel S, Rosenthal F, Altmeyer M, Lukas J, Hottiger MO, Nielsen ML. Proteome-wide identification of poly(ADP-Ribosyl)ation targets in different genotoxic stress responses. Mol Cell. 2013;52(2):272-85. Epub 2013/09/24. doi: 10.1016/j.molcel.2013.08.026. PubMed PMID: 24055347.

118.   Kaufman B, Shapira-Frommer R, Schmutzler RK, Audeh MW, Friedlander M, Balmaña J, et al. Olaparib monotherapy in patients with advanced cancer and a germline BRCA1/2 mutation. J Clin Oncol. 2015;33(3):244-50. Epub 2014/11/05. doi: 10.1200/jco.2014.56.2728. PubMed PMID: 25366685; PubMed Central PMCID: PMCPMC6057749.

119.   Pazzaglia S, Pioli C. Multifaceted Role of PARP-1 in DNA Repair and Inflammation: Pathological and Therapeutic Implications in Cancer and Non-Cancer Diseases. Cells. 2019;9(1). Epub 2019/12/28. doi: 10.3390/cells9010041. PubMed PMID: 31877876; PubMed Central PMCID: PMCPMC7017201.

120.   Ray-Coquard I, Pautier P, Pignata S, Pérol D, González-Martín A, Berger R, et al. Olaparib plus Bevacizumab as First-Line Maintenance in Ovarian Cancer. N Engl J Med. 2019;381(25):2416-28. Epub 2019/12/19. doi: 10.1056/NEJMoa1911361. PubMed PMID: 31851799.

121.   Mirza MR, Monk BJ, Herrstedt J, Oza AM, Mahner S, Redondo A, et al. Niraparib Maintenance Therapy in Platinum-Sensitive, Recurrent Ovarian Cancer. N Engl J Med. 2016;375(22):2154-64. Epub 2016/10/09. doi: 10.1056/NEJMoa1611310. PubMed PMID: 27717299.

122.   Moore KN, Secord AA, Geller MA, Miller DS, Cloven N, Fleming GF, et al. Niraparib monotherapy for late-line treatment of ovarian cancer (QUADRA): a multicentre, open-label, single-arm, phase 2 trial. Lancet Oncol. 2019;20(5):636-48. Epub 2019/04/06. doi: 10.1016/s1470-2045(19)30029-4. PubMed PMID: 30948273.

123.   Swisher EM, Lin KK, Oza AM, Scott CL, Giordano H, Sun J, et al. Rucaparib in relapsed, platinum-sensitive high-grade ovarian carcinoma (ARIEL2 Part 1): an international, multicentre, open-label, phase 2 trial. Lancet Oncol. 2017;18(1):75-87. Epub 2016/12/03. doi: 10.1016/s1470-2045(16)30559-9. PubMed PMID: 27908594.

124.   La Vecchia C. Ovarian cancer: epidemiology and risk factors. Eur J Cancer Prev. 2017;26(1):55-62. Epub 2016/01/06. doi: 10.1097/cej.0000000000000217. PubMed PMID: 26731563.

125. Avgerinos KI, Spyrou N, Mantzoros CS, Dalamaga M. Obesity and cancer risk: Emerging biological mechanisms and perspectives. Metabolism. 2019;92:121-35. Epub 2018/11/18. doi: 10.1016/j.metabol.2018.11.001. PubMed PMID: 30445141.

126. Lee JE, Nam CM, Lee SG, Park S, Kim TH, Park EC. The Health Burden of Cancer Attributable to Obesity in Korea: A Population-Based Cohort Study. Cancer Res Treat. 2019;51(3):933-40. Epub 2018/10/05. doi: 10.4143/crt.2018.301. PubMed PMID: 30282445; PubMed Central PMCID: PMCPMC6639210.

127. Shi J, Liu B, Wang H, Zhang T, Yang L. Association of metformin use with ovarian cancer incidence and prognosis: a systematic review and meta-analysis. Int J Gynecol Cancer. 2019;29(1):140-6. Epub 2019/01/15. doi: 10.1136/ijgc-2018-000060. PubMed PMID: 30640696.

128. Webb PM, Jordan SJ. Epidemiology of epithelial ovarian cancer. Best Pract Res Clin Obstet Gynaecol. 2017;41:3-14. Epub 2016/10/17. doi: 10.1016/j.bpobgyn.2016.08.006. PubMed PMID: 27743768.

129. Roberts AL, Huang T, Koenen KC, Kim Y, Kubzansky LD, Tworoger SS. Posttraumatic Stress Disorder Is Associated with Increased Risk of Ovarian Cancer: A Prospective and Retrospective Longitudinal Cohort Study. Cancer Res. 2019;79(19):5113-20. Epub 2019/09/07. doi: 10.1158/0008-5472.Can-19-1222. PubMed PMID: 31488422; PubMed Central PMCID: PMCPMC6774860.

130. Trudel-Fitzgerald C, Poole EM, Sood AK, Okereke OI, Kawachi I, Kubzansky LD, et al. Social Integration, Marital Status, and Ovarian Cancer Risk: A 20-Year Prospective Cohort Study. Psychosom Med. 2019;81(9):833-40. Epub 2019/10/09. doi:

10.1097/psy.0000000000000747. PubMed PMID: 31592935; PubMed Central PMCID: PMCPMC6832885.

131. Jones MR, Kamara D, Karlan BY, Pharoah PDP, Gayther SA. Genetic epidemiology of ovarian cancer and prospects for polygenic risk prediction. Gynecol Oncol. 2017;147(3):705-13. Epub 2017/10/22. doi: 10.1016/j.ygyno.2017.10.001. PubMed PMID: 29054568.

132. Kuchenbaecker KB, Hopper JL, Barnes DR, Phillips KA, Mooij TM, Roos-Blom MJ, et al. Risks of Breast, Ovarian, and Contralateral Breast Cancer for BRCA1 and BRCA2 Mutation Carriers. Jama. 2017;317(23):2402-16. Epub 2017/06/21. doi: 10.1001/jama.2017.7112. PubMed PMID: 28632866.

133. Ramus SJ, Song H, Dicks E, Tyrer JP, Rosenthal AN, Intermaggio MP, et al. Germline Mutations in the BRIP1, BARD1, PALB2, and NBN Genes in Women With Ovarian Cancer. J Natl Cancer Inst. 2015;107(11). Epub 2015/09/01. doi: 10.1093/jnci/djv214. PubMed PMID: 26315354; PubMed Central PMCID: PMCPMC4643629.

134. Yang X, Leslie G, Doroszuk A, Schneider S, Allen J, Decker B, et al. Cancer Risks Associated With Germline PALB2 Pathogenic Variants: An International Study of 524 Families. J Clin Oncol. 2020;38(7):674-85. Epub 2019/12/17. doi: 10.1200/jco.19.01907. PubMed PMID: 31841383; PubMed Central PMCID: PMCPMC7049229.

135. Yang X, Song H, Leslie G, Engel C, Hahnen E, Auber B, et al. Ovarian and Breast Cancer Risks Associated With Pathogenic Variants in RAD51C and RAD51D. J Natl Cancer Inst. 2020;112(12):1242-50. Epub 2020/02/29. doi: 10.1093/jnci/djaa030. PubMed PMID: 32107557; PubMed Central PMCID: PMCPMC7735771.

136.	Møller P, Seppälä TT, Bernstein I, Holinski-Feder E, Sala P, Gareth Evans D, et al. Cancer risk and survival in path_MMR carriers by gene and gender up to 75 years of age: a report from the Prospective Lynch Syndrome Database. Gut. 2018;67(7):1306-16. Epub 2017/07/30. doi: 10.1136/gutjnl-2017-314057. PubMed PMID: 28754778; PubMed Central PMCID: PMCPMC6031262.

137.	Kumle M, Weiderpass E, Braaten T, Adami HO, Lund E. Risk for invasive and borderline epithelial ovarian neoplasias following use of hormonal contraceptives: the Norwegian-Swedish Women's Lifestyle and Health Cohort Study. Br J Cancer. 2004;90(7):1386-91. Epub 2004/04/01. doi: 10.1038/sj.bjc.6601715. PubMed PMID: 15054460; PubMed Central PMCID: PMCPMC2409682.

138.	Havrilesky LJ, Moorman PG, Lowery WJ, Gierisch JM, Coeytaux RR, Urrutia RP, et al. Oral contraceptive pills as primary prevention for ovarian cancer: a systematic review and meta-analysis. Obstet Gynecol. 2013;122(1):139-47. Epub 2013/06/08. doi: 10.1097/AOG.0b013e318291c235. PubMed PMID: 23743450.

139.	Schrijver LH, Antoniou AC, Olsson H, Mooij TM, Roos-Blom MJ, Azarang L, et al. Oral contraceptive use and ovarian cancer risk for BRCA1/2 mutation carriers: an international cohort study. Am J Obstet Gynecol. 2021;225(1):51.e1-.e17. Epub 2021/01/26. doi: 10.1016/j.ajog.2021.01.014. PubMed PMID: 33493488; PubMed Central PMCID: PMCPMC8278569.

140.	Beral V, Doll R, Hermon C, Peto R, Reeves G. Ovarian cancer and oral contraceptives: collaborative reanalysis of data from 45 epidemiological studies including 23,257 women with ovarian cancer and 87,303 controls. Lancet. 2008;371(9609):303-14. Epub 2008/02/26. doi: 10.1016/s0140-6736(08)60167-1. PubMed PMID: 18294997.

141.   ACOG Practice Bulletin No. 110: noncontraceptive uses of hormonal contraceptives. Obstet Gynecol. 2010;115(1):206-18. Epub 2009/12/23. doi: 10.1097/AOG.0b013e3181cb50b5. PubMed PMID: 20027071.

142.   Cibula D, Widschwendter M, Májek O, Dusek L. Tubal ligation and the risk of ovarian cancer: review and meta-analysis. Hum Reprod Update. 2011;17(1):55-67. Epub 2010/07/17. doi: 10.1093/humupd/dmq030. PubMed PMID: 20634209.

143.   Antoniou AC, Rookus M, Andrieu N, Brohet R, Chang-Claude J, Peock S, et al. Reproductive and hormonal factors, and ovarian cancer risk for BRCA1 and BRCA2 mutation carriers: results from the International BRCA1/2 Carrier Cohort Study. Cancer Epidemiol Biomarkers Prev. 2009;18(2):601-10. Epub 2009/02/05. doi: 10.1158/1055-9965.Epi-08-0546. PubMed PMID: 19190154.

144.   Thau L, Reddy V, Singh P. Anatomy, Central Nervous System. StatPearls. Treasure Island (FL): StatPearls Publishing

Copyright © 2021, StatPearls Publishing LLC.; 2021.

145.   Waxenbaum JA, Reddy V, Varacallo M. Anatomy, Autonomic Nervous System. StatPearls. Treasure Island (FL): StatPearls Publishing

Copyright © 2021, StatPearls Publishing LLC.; 2021.

146.   Akinrodoye MA, Lui F. Neuroanatomy, Somatic Nervous System. StatPearls. Treasure Island (FL): StatPearls Publishing

Copyright © 2021, StatPearls Publishing LLC.; 2021.

147.   Alshak MN, J MD. Neuroanatomy, Sympathetic Nervous System. StatPearls. Treasure Island (FL): StatPearls Publishing

Copyright © 2021, StatPearls Publishing LLC.; 2021.

148. Tindle J, Tadi P. Neuroanatomy, Parasympathetic Nervous System. StatPearls. Treasure Island (FL): StatPearls Publishing

Copyright © 2021, StatPearls Publishing LLC.; 2021.

149. Paravati S, Rosani A, Warrington SJ. Physiology, Catecholamines. StatPearls. Treasure Island (FL): StatPearls Publishing

Copyright © 2021, StatPearls Publishing LLC.; 2021.

150. Feher J. 9.6 - The Adrenal Medulla and Integration of Metabolic Control. In: Feher J, editor. Quantitative Human Physiology (Second Edition). Boston: Academic Press; 2012. p. 916-23.

151. Hwu PW, Kiening K, Anselm I, Compton DR, Nakajima T, Opladen T, et al. Gene therapy in the putamen for curing AADC deficiency and Parkinson's disease. EMBO Mol Med. 2021:e14712. Epub 2021/08/24. doi: 10.15252/emmm.202114712. PubMed PMID: 34423905.

152. Goto Y, Otani S, Grace AA. The Yin and Yang of dopamine release: a new perspective. Neuropharmacology. 2007;53(5):583-7. Epub 2007/08/22. doi: 10.1016/j.neuropharm.2007.07.007. PubMed PMID: 17709119; PubMed Central PMCID: PMCPMC2078202.

153. Al-Chalabi M, Bass AN, Alsalman I. Physiology, Prolactin. StatPearls. Treasure Island (FL): StatPearls Publishing

Copyright © 2021, StatPearls Publishing LLC.; 2021.

154. Othumpangat S. Catecholamines. In: Wexler P, editor. Encyclopedia of Toxicology (Third Edition). Oxford: Academic Press; 2014. p. 748-50.

155.   Dartt DA. Neural regulation of lacrimal gland secretory processes: relevance in dry eye diseases. Prog Retin Eye Res. 2009;28(3):155-77. Epub 2009/04/21. doi: 10.1016/j.preteyeres.2009.04.003. PubMed PMID: 19376264; PubMed Central PMCID: PMCPMC3652637.

156.   Kenney MJ, Ganta CK. Autonomic nervous system and immune system interactions. Compr Physiol. 2014;4(3):1177-200. Epub 2014/06/20. doi: 10.1002/cphy.c130051. PubMed PMID: 24944034; PubMed Central PMCID: PMCPMC4374437.

157.   Bahler L, Molenaars RJ, Verberne HJ, Holleman F. Role of the autonomic nervous system in activation of human brown adipose tissue: A review of the literature. Diabetes Metab. 2015;41(6):437-45. Epub 2015/09/26. doi: 10.1016/j.diabet.2015.08.005. PubMed PMID: 26404650.

158.   Chistiakov DA, Ashwell KW, Orekhov AN, Bobryshev YV. Innervation of the arterial wall and its modification in atherosclerosis. Auton Neurosci. 2015;193:7-11. Epub 2015/07/15. doi: 10.1016/j.autneu.2015.06.005. PubMed PMID: 26164815.

159.   Tank AW, Lee Wong D. Peripheral and central effects of circulating catecholamines. Compr Physiol. 2015;5(1):1-15. Epub 2015/01/16. doi: 10.1002/cphy.c140007. PubMed PMID: 25589262.

160.   Cole SW, Nagaraja AS, Lutgendorf SK, Green PA, Sood AK. Sympathetic nervous system regulation of the tumour microenvironment. Nat Rev Cancer. 2015;15(9):563-72. Epub 2015/08/25. doi: 10.1038/nrc3978. PubMed PMID: 26299593; PubMed Central PMCID: PMCPMC4828959.

161.   Taylor BN, Cassagnol M. Alpha Adrenergic Receptors.   StatPearls. Treasure Island (FL): StatPearls Publishing

Copyright © 2021, StatPearls Publishing LLC.; 2021.

162.   Alhayek S, Preuss CV. Beta 1 Receptors.   StatPearls. Treasure Island (FL): StatPearls Publishing

Copyright © 2021, StatPearls Publishing LLC.; 2021.

163.   Abosamak NR, Shahin MH. Beta 2 Receptor Agonists/Antagonists.   StatPearls. Treasure Island (FL): StatPearls Publishing

Copyright © 2021, StatPearls Publishing LLC.; 2021.

164.   Hanoun M, Maryanovich M, Arnal-Estapé A, Frenette PS. Neural regulation of hematopoiesis, inflammation, and cancer. Neuron. 2015;86(2):360-73. Epub 2015/04/24. doi: 10.1016/j.neuron.2015.01.026. PubMed PMID: 25905810; PubMed Central PMCID: PMCPMC4416657.

165.   Dalal R, Grujic D. Epinephrine.   StatPearls. Treasure Island (FL): StatPearls Publishing

Copyright © 2021, StatPearls Publishing LLC.; 2021.

166.   Richter SD, Schürmeyer TH, Schedlowski M, Hädicke A, Tewes U, Schmidt RE, et al. Time kinetics of the endocrine response to acute psychological stress. J Clin Endocrinol   Metab.   1996;81(5):1956-60.   Epub   1996/05/01.   doi: 10.1210/jcem.81.5.8626864. PubMed PMID: 8626864.

167.   Wingenfeld K, Whooley MA, Neylan TC, Otte C, Cohen BE. Effect of current and lifetime posttraumatic stress disorder on 24-h urinary catecholamines and cortisol: results

from the Mind Your Heart Study. Psychoneuroendocrinology. 2015;52:83-91. Epub 2014/12/03. doi: 10.1016/j.psyneuen.2014.10.023. PubMed PMID: 25459895; PubMed Central PMCID: PMCPMC4297502.

168.   Sloan EK, Capitanio JP, Tarara RP, Mendoza SP, Mason WA, Cole SW. Social stress enhances sympathetic innervation of primate lymph nodes: mechanisms and implications for viral pathogenesis. J Neurosci. 2007;27(33):8857-65. Epub 2007/08/19. doi: 10.1523/jneurosci.1247-07.2007. PubMed PMID: 17699667; PubMed Central PMCID: PMCPMC6672171.

169.   Sloan EK, Capitanio JP, Tarara RP, Cole SW. Social temperament and lymph node innervation. Brain Behav Immun. 2008;22(5):717-26. Epub 2007/12/11. doi: 10.1016/j.bbi.2007.10.010. PubMed PMID: 18068331; PubMed Central PMCID: PMCPMC2519873.

170.   Powell ND, Sloan EK, Bailey MT, Arevalo JM, Miller GE, Chen E, et al. Social stress up-regulates inflammatory gene expression in the leukocyte transcriptome via β-adrenergic induction of myelopoiesis. Proc Natl Acad Sci U S A. 2013;110(41):16574-9. Epub 2013/09/26. doi: 10.1073/pnas.1310655110. PubMed PMID: 24062448; PubMed Central PMCID: PMCPMC3799381.

171.   Heidt T, Sager HB, Courties G, Dutta P, Iwamoto Y, Zaltsman A, et al. Chronic variable stress activates hematopoietic stem cells. Nat Med. 2014;20(7):754-8. Epub 2014/06/24. doi: 10.1038/nm.3589. PubMed PMID: 24952646; PubMed Central PMCID: PMCPMC4087061.

172. Elenkov IJ, Wilder RL, Chrousos GP, Vizi ES. The sympathetic nerve--an integrative interface between two supersystems: the brain and the immune system. Pharmacol Rev. 2000;52(4):595-638. Epub 2000/12/21. PubMed PMID: 11121511.

173. Cole SW, Arevalo JM, Takahashi R, Sloan EK, Lutgendorf SK, Sood AK, et al. Computational identification of gene-social environment interaction at the human IL6 locus. Proc Natl Acad Sci U S A. 2010;107(12):5681-6. Epub 2010/02/24. doi: 10.1073/pnas.0911515107. PubMed PMID: 20176930; PubMed Central PMCID: PMCPMC2851818.

174. Irwin MR, Cole SW. Reciprocal regulation of the neural and innate immune systems. Nat Rev Immunol. 2011;11(9):625-32. Epub 2011/08/06. doi: 10.1038/nri3042. PubMed PMID: 21818124; PubMed Central PMCID: PMCPMC3597082.

175. Ramsay DS, Woods SC. Clarifying the roles of homeostasis and allostasis in physiological regulation. Psychol Rev. 2014;121(2):225-47. Epub 2014/04/16. doi: 10.1037/a0035942. PubMed PMID: 24730599; PubMed Central PMCID: PMCPMC4166604.

176. Thaker PH, Han LY, Kamat AA, Arevalo JM, Takahashi R, Lu C, et al. Chronic stress promotes tumor growth and angiogenesis in a mouse model of ovarian carcinoma. Nat Med. 2006;12(8):939-44. Epub 2006/07/25. doi: 10.1038/nm1447. PubMed PMID: 16862152.

177. Sloan EK, Priceman SJ, Cox BF, Yu S, Pimentel MA, Tangkanangnukul V, et al. The sympathetic nervous system induces a metastatic switch in primary breast cancer. Cancer Res. 2010;70(18):7042-52. Epub 2010/09/09. doi: 10.1158/0008-5472.Can-10-0522. PubMed PMID: 20823155; PubMed Central PMCID: PMCPMC2940980.

178.   Goldfarb Y, Sorski L, Benish M, Levi B, Melamed R, Ben-Eliyahu S. Improving postoperative immune status and resistance to cancer metastasis: a combined perioperative approach of immunostimulation and prevention of excessive surgical stress responses.   Ann   Surg.   2011;253(4):798-810.   Epub   2011/04/09.   doi: 10.1097/SLA.0b013e318211d7b5. PubMed PMID: 21475023.

179.   Lamkin DM, Sloan EK, Patel AJ, Chiang BS, Pimentel MA, Ma JC, et al. Chronic stress enhances progression of acute lymphoblastic leukemia via β-adrenergic signaling. Brain   Behav   Immun.   2012;26(4):635-41.   Epub   2012/02/07.   doi: 10.1016/j.bbi.2012.01.013.   PubMed   PMID: 22306453;   PubMed   Central   PMCID: PMCPMC3322262.

180.   Hassan S, Karpova Y, Baiz D, Yancey D, Pullikuth A, Flores A, et al. Behavioral stress accelerates prostate cancer development in mice. J Clin Invest. 2013;123(2):874-86. Epub 2013/01/26. doi: 10.1172/jci63324. PubMed PMID: 23348742; PubMed Central PMCID: PMCPMC3561807.

181.   Pasquier E, Street J, Pouchy C, Carre M, Gifford AJ, Murray J, et al. β-blockers increase response to chemotherapy via direct antitumour and anti-angiogenic mechanisms in neuroblastoma. Br J Cancer. 2013;108(12):2485-94. Epub 2013/05/23. doi: 10.1038/bjc.2013.205.   PubMed   PMID: 23695022;   PubMed   Central   PMCID: PMCPMC3694229.

182.   Eng JW, Reed CB, Kokolus KM, Pitoniak R, Utley A, Bucsek MJ, et al. Housing temperature-induced stress drives therapeutic resistance in murine tumour models through β2-adrenergic receptor activation. Nat Commun. 2015;6:6426. Epub 2015/03/11.

doi: 10.1038/ncomms7426. PubMed PMID: 25756236; PubMed Central PMCID: PMCPMC4471870.

183. Cole SW, Sood AK. Molecular pathways: beta-adrenergic signaling in cancer. Clin Cancer Res. 2012;18(5):1201-6. Epub 2011/12/22. doi: 10.1158/1078-0432.Ccr-11-0641. PubMed PMID: 22186256; PubMed Central PMCID: PMCPMC3294063.

184. Hara MR, Kovacs JJ, Whalen EJ, Rajagopal S, Strachan RT, Grant W, et al. A stress response pathway regulates DNA damage through β2-adrenoreceptors and β-arrestin-1. Nature. 2011;477(7364):349-53. Epub 2011/08/23. doi: 10.1038/nature10368. PubMed PMID: 21857681; PubMed Central PMCID: PMCPMC3628753.

185. Hara MR, Sachs BD, Caron MG, Lefkowitz RJ. Pharmacological blockade of a β(2)AR-β-arrestin-1 signaling cascade prevents the accumulation of DNA damage in a behavioral stress model. Cell Cycle. 2013;12(2):219-24. Epub 2013/01/05. doi: 10.4161/cc.23368. PubMed PMID: 23287463; PubMed Central PMCID: PMCPMC3575451.

186. Reeder A, Attar M, Nazario L, Bathula C, Zhang A, Hochbaum D, et al. Stress hormones reduce the efficacy of paclitaxel in triple negative breast cancer through induction of DNA damage. Br J Cancer. 2015;112(9):1461-70. Epub 2015/04/17. doi: 10.1038/bjc.2015.133. PubMed PMID: 25880007; PubMed Central PMCID: PMCPMC4453678.

187. Armaiz-Pena GN, Allen JK, Cruz A, Stone RL, Nick AM, Lin YG, et al. Src activation by β-adrenoreceptors is a key switch for tumour metastasis. Nat Commun. 2013;4:1403. Epub 2013/01/31. doi: 10.1038/ncomms2413. PubMed PMID: 23360994; PubMed Central PMCID: PMCPMC3561638.

188.   Gu L, Lau SK, Loera S, Somlo G, Kane SE. Protein kinase A activation confers resistance to trastuzumab in human breast cancer cell lines. Clin Cancer Res. 2009;15(23):7196-206. Epub 2009/11/19. doi: 10.1158/1078-0432.Ccr-09-0585. PubMed PMID: 19920112; PubMed Central PMCID: PMCPMC2787631.

189.   Shi M, Liu D, Duan H, Qian L, Wang L, Niu L, et al. The β2-adrenergic receptor and Her2 comprise a positive feedback loop in human breast cancer cells. Breast Cancer Res Treat. 2011;125(2):351-62. Epub 2010/03/20. doi: 10.1007/s10549-010-0822-2. PubMed PMID: 20237834.

190.   Sastry KS, Karpova Y, Prokopovich S, Smith AJ, Essau B, Gersappe A, et al. Epinephrine protects cancer cells from apoptosis via activation of cAMP-dependent protein kinase and BAD phosphorylation. J Biol Chem. 2007;282(19):14094-100. Epub 2007/03/14. doi: 10.1074/jbc.M611370200. PubMed PMID: 17353197.

191.   Sood AK, Armaiz-Pena GN, Halder J, Nick AM, Stone RL, Hu W, et al. Adrenergic modulation of focal adhesion kinase protects human ovarian cancer cells from anoikis. J Clin Invest. 2010;120(5):1515-23. Epub 2010/04/15. doi: 10.1172/jci40802. PubMed PMID: 20389021; PubMed Central PMCID: PMCPMC2860925.

192.   Bruzzone A, Piñero CP, Rojas P, Romanato M, Gass H, Lanari C, et al. α(2)-Adrenoceptors enhance cell proliferation and mammary tumor growth acting through both the stroma and the tumor cells. Curr Cancer Drug Targets. 2011;11(6):763-74. Epub 2011/05/24. doi: 10.2174/156800911796191051. PubMed PMID: 21599632.

193.   Calvani M, Pelon F, Comito G, Taddei ML, Moretti S, Innocenti S, et al. Norepinephrine promotes tumor microenvironment reactivity through β3-adrenoreceptors during melanoma progression. Oncotarget. 2015;6(7):4615-32. Epub 2014/12/05. doi:

10.18632/oncotarget.2652. PubMed PMID: 25474135; PubMed Central PMCID: PMCPMC4467103.

194.   Lang K, Drell TLt, Lindecke A, Niggemann B, Kaltschmidt C, Zaenker KS, et al. Induction of a metastatogenic tumor cell type by neurotransmitters and its pharmacological inhibition by established drugs. Int J Cancer. 2004;112(2):231-8. Epub 2004/09/08. doi: 10.1002/ijc.20410. PubMed PMID: 15352035.

195.   Palm D, Lang K, Niggemann B, Drell TLt, Masur K, Zaenker KS, et al. The norepinephrine-driven metastasis development of PC-3 human prostate cancer cells in BALB/c nude mice is inhibited by beta-blockers. Int J Cancer. 2006;118(11):2744-9. Epub 2005/12/29. doi: 10.1002/ijc.21723. PubMed PMID: 16381019.

196.   Yang EV, Sood AK, Chen M, Li Y, Eubank TD, Marsh CB, et al. Norepinephrine up-regulates the expression of vascular endothelial growth factor, matrix metalloproteinase (MMP)-2, and MMP-9 in nasopharyngeal carcinoma tumor cells. Cancer Res. 2006;66(21):10357-64. Epub 2006/11/03. doi: 10.1158/0008-5472.Can-06-2496. PubMed PMID: 17079456.

197.   Nilsson MB, Armaiz-Pena G, Takahashi R, Lin YG, Trevino J, Li Y, et al. Stress hormones regulate interleukin-6 expression by human ovarian carcinoma cells through a Src-dependent mechanism. J Biol Chem. 2007;282(41):29919-26. Epub 2007/08/25. doi: 10.1074/jbc.M611539200. PubMed PMID: 17716980.

198.   Liu J, Deng GH, Zhang J, Wang Y, Xia XY, Luo XM, et al. The effect of chronic stress on anti-angiogenesis of sunitinib in colorectal cancer models. Psychoneuroendocrinology. 2015;52:130-42. Epub 2014/12/02. doi: 10.1016/j.psyneuen.2014.11.008. PubMed PMID: 25437118.

199.   Armaiz-Pena GN, Gonzalez-Villasana V, Nagaraja AS, Rodriguez-Aguayo C, Sadaoui NC, Stone RL, et al. Adrenergic regulation of monocyte chemotactic protein 1 leads to enhanced macrophage recruitment and ovarian carcinoma growth. Oncotarget. 2015;6(6):4266-73. Epub 2015/03/05. doi: 10.18632/oncotarget.2887. PubMed PMID: 25738355; PubMed Central PMCID: PMCPMC4414188.

200.   Cole SW, Korin YD, Fahey JL, Zack JA. Norepinephrine accelerates HIV replication via protein kinase A-dependent effects on cytokine production. J Immunol. 1998;161(2):610-6. Epub 1998/07/22. PubMed PMID: 9670934.

201.   Collado-Hidalgo A, Sung C, Cole S. Adrenergic inhibition of innate anti-viral response: PKA blockade of Type I interferon gene transcription mediates catecholamine support for HIV-1 replication. Brain Behav Immun. 2006;20(6):552-63. Epub 2006/03/01. doi: 10.1016/j.bbi.2006.01.005. PubMed PMID: 16504464.

202.   Lee JW, Shahzad MM, Lin YG, Armaiz-Pena G, Mangala LS, Han HD, et al. Surgical stress promotes tumor growth in ovarian carcinoma. Clin Cancer Res. 2009;15(8):2695-702. Epub 2009/04/09. doi: 10.1158/1078-0432.Ccr-08-2966. PubMed PMID: 19351748; PubMed Central PMCID: PMCPMC2746852.

203.   Inbar S, Neeman E, Avraham R, Benish M, Rosenne E, Ben-Eliyahu S. Do stress responses promote leukemia progression? An animal study suggesting a role for epinephrine and prostaglandin-E2 through reduced NK activity. PLoS One. 2011;6(4):e19246. Epub 2011/05/12. doi: 10.1371/journal.pone.0019246. PubMed PMID: 21559428; PubMed Central PMCID: PMCPMC3084788.

204.   Ayala GE, Dai H, Powell M, Li R, Ding Y, Wheeler TM, et al. Cancer-related axonogenesis and neurogenesis in prostate cancer. Clin Cancer Res. 2008;14(23):7593-603. Epub 2008/12/03. doi: 10.1158/1078-0432.Ccr-08-1164. PubMed PMID: 19047084.

205.   Magnon C, Hall SJ, Lin J, Xue X, Gerber L, Freedland SJ, et al. Autonomic nerve development contributes to prostate cancer progression. Science. 2013;341(6142):1236361. Epub 2013/07/13. doi: 10.1126/science.1236361. PubMed PMID: 23846904.

206.   Voss MJ, Entschladen F. Tumor interactions with soluble factors and the nervous system. Cell Commun Signal. 2010;8:21. Epub 2010/09/09. doi: 10.1186/1478-811x-8-21. PubMed PMID: 20822525; PubMed Central PMCID: PMCPMC2942890.

207.   Lutgendorf SK, DeGeest K, Dahmoush L, Farley D, Penedo F, Bender D, et al. Social isolation is associated with elevated tumor norepinephrine in ovarian carcinoma patients. Brain Behav Immun. 2011;25(2):250-5. Epub 2010/10/20. doi: 10.1016/j.bbi.2010.10.012. PubMed PMID: 20955777; PubMed Central PMCID: PMCPMC3103818.

208.   Lara HE, Dorfman M, Venegas M, Luza SM, Luna SL, Mayerhofer A, et al. Changes in sympathetic nerve activity of the mammalian ovary during a normal estrous cycle and in polycystic ovary syndrome: Studies on norepinephrine release. Microsc Res Tech. 2002;59(6):495-502. Epub 2002/12/06. doi: 10.1002/jemt.10229. PubMed PMID: 12467025.

209.   Lawrence IE, Jr., Burden HW. The origin of the extrinsic adrenergic innervation to the rat ovary. Anat Rec. 1980;196(1):51-9. Epub 1980/01/01. doi: 10.1002/ar.1091960106. PubMed PMID: 7416501.

210. Greiner M, Paredes A, Rey-Ares V, Saller S, Mayerhofer A, Lara HE. Catecholamine uptake, storage, and regulated release by ovarian granulosa cells. Endocrinology. 2008;149(10):4988-96. Epub 2008/06/21. doi: 10.1210/en.2007-1661. PubMed PMID: 18566131.

211. Aguado LI, Petrovic SL, Ojeda SR. Ovarian beta-adrenergic receptors during the onset of puberty: characterization, distribution, and coupling to steroidogenic responses. Endocrinology. 1982;110(4):1124-32. Epub 1982/04/01. doi: 10.1210/endo-110-4-1124. PubMed PMID: 6120828.

212. Mayerhofer A, Dissen GA, Costa ME, Ojeda SR. A role for neurotransmitters in early follicular development: induction of functional follicle-stimulating hormone receptors in newly formed follicles of the rat ovary. Endocrinology. 1997;138(8):3320-9. Epub 1997/08/01. doi: 10.1210/endo.138.8.5335. PubMed PMID: 9231784.

213. Mayerhofer A, Smith GD, Danilchik M, Levine JE, Wolf DP, Dissen GA, et al. Oocytes are a source of catecholamines in the primate ovary: evidence for a cell-cell regulatory loop. Proc Natl Acad Sci U S A. 1998;95(18):10990-5. Epub 1998/09/02. doi: 10.1073/pnas.95.18.10990. PubMed PMID: 9724817; PubMed Central PMCID: PMCPMC28008.

214. Chávez-Genaro R, Lombide P, Domínguez R, Rosas P, Vázquez-Cuevas F. Sympathetic pharmacological denervation in ageing rats: effects on ovulatory response and follicular population. Reprod Fertil Dev. 2007;19(8):954-60. Epub 2007/12/14. doi: 10.1071/rd07075. PubMed PMID: 18076827.

215. Acuña E, Fornes R, Fernandois D, Garrido MP, Greiner M, Lara HE, et al. Increases in norepinephrine release and ovarian cyst formation during ageing in the rat.

Reprod Biol Endocrinol. 2009;7:64. Epub 2009/06/18. doi: 10.1186/1477-7827-7-64. PubMed PMID: 19531218; PubMed Central PMCID: PMCPMC2705370.

216. Lara HE, Ferruz JL, Luza S, Bustamante DA, Borges Y, Ojeda SR. Activation of ovarian sympathetic nerves in polycystic ovary syndrome. Endocrinology. 1993;133(6):2690-5. Epub 1993/12/01. doi: 10.1210/endo.133.6.7902268. PubMed PMID: 7902268.

217. Lambert EA, Teede H, Sari CI, Jona E, Shorakae S, Woodington K, et al. Sympathetic activation and endothelial dysfunction in polycystic ovary syndrome are not explained by either obesity or insulin resistance. Clin Endocrinol (Oxf). 2015;83(6):812-9. Epub 2015/05/01. doi: 10.1111/cen.12803. PubMed PMID: 25926334.

218. Lansdown A, Rees DA. The sympathetic nervous system in polycystic ovary syndrome: a novel therapeutic target? Clin Endocrinol (Oxf). 2012;77(6):791-801. Epub 2012/08/14. doi: 10.1111/cen.12003. PubMed PMID: 22882204.

219. Johansson J, Feng Y, Shao R, Lönn M, Billig H, Stener-Victorin E. Intense electroacupuncture normalizes insulin sensitivity, increases muscle GLUT4 content, and improves lipid profile in a rat model of polycystic ovary syndrome. Am J Physiol Endocrinol Metab. 2010;299(4):E551-9. Epub 2010/07/29. doi: 10.1152/ajpendo.00323.2010. PubMed PMID: 20663984.

220. Mannerås L, Jonsdottir IH, Holmäng A, Lönn M, Stener-Victorin E. Low-frequency electro-acupuncture and physical exercise improve metabolic disturbances and modulate gene expression in adipose tissue in rats with dihydrotestosterone-induced polycystic ovary syndrome. Endocrinology. 2008;149(7):3559-68. Epub 2008/04/05. doi: 10.1210/en.2008-0053. PubMed PMID: 18388196.

221.   Mravec B, Tibensky M. Increased cancer risk in polycystic ovary syndrome: An (un)sympathetic connection? Med Hypotheses. 2020;134:109437. Epub 2019/10/28. doi: 10.1016/j.mehy.2019.109437. PubMed PMID: 31655360.

222.   Gradus JL, Farkas DK, Svensson E, Ehrenstein V, Lash TL, Milstein A, et al. Posttraumatic stress disorder and cancer risk: a nationwide cohort study. Eur J Epidemiol. 2015;30(7):563-8. Epub 2015/05/10. doi: 10.1007/s10654-015-0032-7. PubMed PMID: 25957083; PubMed Central PMCID: PMCPMC4519360.

223.   Huang T, Poole EM, Okereke OI, Kubzansky LD, Eliassen AH, Sood AK, et al. Depression and risk of epithelial ovarian cancer: Results from two large prospective cohort studies. Gynecol Oncol. 2015;139(3):481-6. Epub 2015/10/10. doi: 10.1016/j.ygyno.2015.10.004. PubMed PMID: 26449316; PubMed Central PMCID: PMCPMC4679423.

224.   Huang T, Tworoger SS, Hecht JL, Rice MS, Sood AK, Kubzansky LD, et al. Association of Ovarian Tumor β2-Adrenergic Receptor Status with Ovarian Cancer Risk Factors and Survival. Cancer Epidemiol Biomarkers Prev. 2016;25(12):1587-94. Epub 2016/09/03. doi: 10.1158/1055-9965.Epi-16-0534. PubMed PMID: 27587791; PubMed Central PMCID: PMCPMC5135562.

225.   Davis LZ, Slavich GM, Thaker PH, Goodheart MJ, Bender DP, Dahmoush L, et al. Eudaimonic well-being and tumor norepinephrine in patients with epithelial ovarian cancer. Cancer. 2015;121(19):3543-50. Epub 2015/06/23. doi: 10.1002/cncr.29516. PubMed PMID: 26096769; PubMed Central PMCID: PMCPMC4575608.

226.   Ryan RM, Deci EL. To be happy or to be self-fulfilled: A review of research on hedonic and eudaimonic well-being. Annual review of psychology. 2001;52(16):141-66.

227. Goldstein DS, Levinson P, Keiser HR. Plasma and urinary catecholamines during the human ovulatory cycle. Am J Obstet Gynecol. 1983;146(7):824-9. Epub 1983/08/01. doi: 10.1016/0002-9378(83)91086-4. PubMed PMID: 6869453.

228. Minson CT, Halliwill JR, Young TM, Joyner MJ. Influence of the menstrual cycle on sympathetic activity, baroreflex sensitivity, and vascular transduction in young women. Circulation. 2000;101(8):862-8. Epub 2000/03/01. doi: 10.1161/01.cir.101.8.862. PubMed PMID: 10694525.

229. Lutgendorf SK, DeGeest K, Sung CY, Arevalo JM, Penedo F, Lucci J, 3rd, et al. Depression, social support, and beta-adrenergic transcription control in human ovarian cancer. Brain Behav Immun. 2009;23(2):176-83. Epub 2008/06/14. doi: 10.1016/j.bbi.2008.04.155. PubMed PMID: 18550328; PubMed Central PMCID: PMCPMC2677379.

230. Landen CN, Jr., Lin YG, Armaiz Pena GN, Das PD, Arevalo JM, Kamat AA, et al. Neuroendocrine modulation of signal transducer and activator of transcription-3 in ovarian cancer. Cancer Res. 2007;67(21):10389-96. Epub 2007/11/03. doi: 10.1158/0008-5472.Can-07-0858. PubMed PMID: 17974982.

231. Wu W, Pew T, Zou M, Pang D, Conzen SD. Glucocorticoid receptor-induced MAPK phosphatase-1 (MPK-1) expression inhibits paclitaxel-associated MAPK activation and contributes to breast cancer cell survival. J Biol Chem. 2005;280(6):4117-24. Epub 2004/12/14. doi: 10.1074/jbc.M411200200. PubMed PMID: 15590693.

232. Kang Y, Nagaraja AS, Armaiz-Pena GN, Dorniak PL, Hu W, Rupaimoole R, et al. Adrenergic Stimulation of DUSP1 Impairs Chemotherapy Response in Ovarian Cancer.

Clin Cancer Res. 2016;22(7):1713-24. Epub 2015/11/20. doi: 10.1158/1078-0432.Ccr-15-1275. PubMed PMID: 26581245; PubMed Central PMCID: PMCPMC4818718.

233.   Nagaraja AS, Dorniak PL, Sadaoui NC, Kang Y, Lin T, Armaiz-Pena G, et al. Sustained adrenergic signaling leads to increased metastasis in ovarian cancer via increased PGE2 synthesis. Oncogene. 2016;35(18):2390-7. Epub 2015/08/11. doi: 10.1038/onc.2015.302. PubMed PMID: 26257064; PubMed Central PMCID: PMCPMC4749473.

234.   Lamboy-Caraballo R, Ortiz-Sanchez C, Acevedo-Santiago A, Matta J, A NAM, G NA-P. Norepinephrine-Induced DNA Damage in Ovarian Cancer Cells. Int J Mol Sci. 2020;21(6). Epub 2020/03/28. doi: 10.3390/ijms21062250. PubMed PMID: 32213975; PubMed Central PMCID: PMCPMC7139728.

235.   Shahzad MM, Arevalo JM, Armaiz-Pena GN, Lu C, Stone RL, Moreno-Smith M, et al. Stress effects on FosB- and interleukin-8 (IL8)-driven ovarian cancer growth and metastasis. J Biol Chem. 2010;285(46):35462-70. Epub 2010/09/10. doi: 10.1074/jbc.M110.109579. PubMed PMID: 20826776; PubMed Central PMCID: PMCPMC2975170.

236.   Casas E, Kim J, Bendesky A, Ohno-Machado L, Wolfe CJ, Yang J. Snail2 is an essential mediator of Twist1-induced epithelial mesenchymal transition and metastasis. Cancer Res. 2011;71(1):245-54. Epub 2011/01/05. doi: 10.1158/0008-5472.Can-10-2330. PubMed PMID: 21199805; PubMed Central PMCID: PMCPMC3025803.

237.   Szubert S, Moszynski R, Michalak S, Nowicki M, Sajdak S, Szpurek D. The associations between serum VEGF, bFGF and endoglin levels with microvessel density and expression of proangiogenic factors in malignant and benign ovarian tumors.

Microvasc Res. 2016;107:91-6. Epub 2016/06/18. doi: 10.1016/j.mvr.2016.06.002. PubMed PMID: 27312585.

238. Allen JK, Armaiz-Pena GN, Nagaraja AS, Sadaoui NC, Ortiz T, Dood R, et al. Sustained Adrenergic Signaling Promotes Intratumoral Innervation through BDNF Induction. Cancer Res. 2018;78(12):3233-42. Epub 2018/04/18. doi: 10.1158/0008-5472.Can-16-1701. PubMed PMID: 29661830; PubMed Central PMCID: PMCPMC6004256.

239. Antoni MH, Lutgendorf SK, Cole SW, Dhabhar FS, Sephton SE, McDonald PG, et al. The influence of bio-behavioural factors on tumour biology: pathways and mechanisms. Nat Rev Cancer. 2006;6(3):240-8. Epub 2006/02/25. doi: 10.1038/nrc1820. PubMed PMID: 16498446; PubMed Central PMCID: PMCPMC3146042.

240. Pater MM, Hughes GA, Hyslop DE, Nakshatri H, Pater A. Glucocorticoid-dependent oncogenic transformation by type 16 but not type 11 human papilloma virus DNA. Nature. 1988;335(6193):832-5. Epub 1988/10/27. doi: 10.1038/335832a0. PubMed PMID: 2847052.

241. Moodley M, Moodley J, Chetty R, Herrington CS. The role of steroid contraceptive hormones in the pathogenesis of invasive cervical cancer: a review. Int J Gynecol Cancer. 2003;13(2):103-10. Epub 2003/03/27. doi: 10.1046/j.1525-1438.2003.13030.x. PubMed PMID: 12657108.

242. Falcinelli M, Thaker PH, Lutgendorf SK, Conzen SD, Flaherty RL, Flint MS. The role of psychological stress in cancer initiation: clinical relevance and potential molecular mechanisms. Cancer Res. 2021. Epub 2021/07/17. doi: 10.1158/0008-5472.Can-21-0684. PubMed PMID: 34266894.

243. Karst AM, Levanon K, Drapkin R. Modeling high-grade serous ovarian carcinogenesis from the fallopian tube. Proc Natl Acad Sci U S A. 2011;108(18):7547-52. Epub 2011/04/20. doi: 10.1073/pnas.1017300108. PubMed PMID: 21502498; PubMed Central PMCID: PMCPMC3088633.

244. Lawrenson K, Benjamin E, Turmaine M, Jacobs I, Gayther S, Dafou D. In vitro three-dimensional modelling of human ovarian surface epithelial cells. Cell Prolif. 2009;42(3):385-93. Epub 2009/04/29. doi: 10.1111/j.1365-2184.2009.00604.x. PubMed PMID: 19397591; PubMed Central PMCID: PMCPMC6760819.

245. Lawrenson K, Grun B, Gayther SA. Heterotypic three-dimensional in vitro modeling of stromal-epithelial interactions during ovarian cancer initiation and progression. J Vis Exp. 2012(66):e4206. Epub 2012/09/07. doi: 10.3791/4206. PubMed PMID: 22951414; PubMed Central PMCID: PMCPMC3486769.

246. Lawrenson K, Li Q, Kar S, Seo JH, Tyrer J, Spindler TJ, et al. Cis-eQTL analysis and functional validation of candidate susceptibility genes for high-grade serous ovarian cancer. Nat Commun. 2015;6:8234. Epub 2015/09/24. doi: 10.1038/ncomms9234. PubMed PMID: 26391404; PubMed Central PMCID: PMCPMC4580986.

247. Kim D, Pertea G, Trapnell C, Pimentel H, Kelley R, Salzberg SL. TopHat2: accurate alignment of transcriptomes in the presence of insertions, deletions and gene fusions. Genome Biol. 2013;14(4):R36. Epub 2013/04/27. doi: 10.1186/gb-2013-14-4-r36. PubMed PMID: 23618408; PubMed Central PMCID: PMCPMC4053844.

248. Anders S, Pyl PT, Huber W. HTSeq--a Python framework to work with high-throughput sequencing data. Bioinformatics. 2015;31(2):166-9. Epub 2014/09/28. doi:

10.1093/bioinformatics/btu638. PubMed PMID: 25260700; PubMed Central PMCID: PMCPMC4287950.

249. Love MI, Huber W, Anders S. Moderated estimation of fold change and dispersion for RNA-seq data with DESeq2. Genome Biol. 2014;15(12):550. Epub 2014/12/18. doi: 10.1186/s13059-014-0550-8. PubMed PMID: 25516281; PubMed Central PMCID: PMCPMC4302049.

250. Kwon AT, Arenillas DJ, Worsley Hunt R, Wasserman WW. oPOSSUM-3: advanced analysis of regulatory motif over-representation across genes or ChIP-Seq datasets. G3 (Bethesda). 2012;2(9):987-1002. Epub 2012/09/14. doi: 10.1534/g3.112.003202. PubMed PMID: 22973536; PubMed Central PMCID: PMCPMC3429929.

251. Dreos R, Ambrosini G, Périer RC, Bucher P. The Eukaryotic Promoter Database: expansion of EPDnew and new promoter analysis tools. Nucleic Acids Res. 2015;43(Database issue):D92-6. Epub 2014/11/08. doi: 10.1093/nar/gku1111. PubMed PMID: 25378343; PubMed Central PMCID: PMCPMC4383928.

252. Afgan E, Baker D, Batut B, van den Beek M, Bouvier D, Cech M, et al. The Galaxy platform for accessible, reproducible and collaborative biomedical analyses: 2018 update. Nucleic Acids Res. 2018;46(W1):W537-w44. Epub 2018/05/24. doi: 10.1093/nar/gky379. PubMed PMID: 29790989; PubMed Central PMCID: PMCPMC6030816.

253. Gjyshi A, Dash S, Cen L, Cheng CH, Zhang C, Yoder SJ, et al. Early transcriptional response of human ovarian and fallopian tube surface epithelial cells to norepinephrine. Sci Rep. 2018;8(1):8291. Epub 2018/05/31. doi: 10.1038/s41598-018-26670-4. PubMed PMID: 29844388; PubMed Central PMCID: PMCPMC5974302.

254.   Dash S, Yoder S, Mesa T, Smith A, Cen L, Eschrich S, et al. Effects of long-term norepinephrine treatment on normal immortalized ovarian and fallopian tube cells. Sci Rep. 2021;11(1):14334. Epub 2021/07/14. doi: 10.1038/s41598-021-93506-z. PubMed PMID: 34253763; PubMed Central PMCID: PMCPMC8275603.

255.   Pellerin I, Schnabel C, Catron KM, Abate C. Hox proteins have different affinities for a consensus DNA site that correlate with the positions of their genes on the hox cluster. Mol Cell Biol. 1994;14(7):4532-45. Epub 1994/07/01. doi: 10.1128/mcb.14.7.4532-4545.1994. PubMed PMID: 7911971; PubMed Central PMCID: PMCPMC358825.

256.   Bailey TL, Johnson J, Grant CE, Noble WS. The MEME Suite. Nucleic Acids Res. 2015;43(W1):W39-49. Epub 2015/05/09. doi: 10.1093/nar/gkv416. PubMed PMID: 25953851; PubMed Central PMCID: PMCPMC4489269.

257.   Schmidt C, Kraft K. Beta-endorphin and catecholamine concentrations during chronic and acute stress in intensive care patients. Eur J Med Res. 1996;1(11):528-32. Epub 1996/09/20. PubMed PMID: 9438155.

258.   Lara HE, Belmar J. Release of norepinephrine from the cat ovary: changes after ovulation. Biol Reprod. 1991;44(5):752-9. Epub 1991/05/01. doi: 10.1095/biolreprod44.5.752. PubMed PMID: 1831051.

259.   Heeb RM, Stollhof B, Reichhold J, Thiesen J, Krämer I. Stability of ready-to-administer and ready-to-use epinephrine and norepinephrine injection solutions. Pharmaceutical Technology in Hospital Pharmacy. 2017;2(4):159-71.

260.   Akam M. Hox genes, homeosis and the evolution of segment identity: no need for hopeless monsters. Int J Dev Biol. 1998;42(3):445-51. Epub 1998/07/08. PubMed PMID: 9654030.

261.   Lewis EB. The bithorax complex: the first fifty years. Int J Dev Biol. 1998;42(3):403-15. Epub 1998/07/08. PubMed PMID: 9654025.

262.   Lewis EB. A gene complex controlling segmentation in Drosophila. Nature. 1978;276(5688):565-70. Epub 1978/12/07. doi: 10.1038/276565a0. PubMed PMID: 103000.

263.   Kaufman TC, Seeger MA, Olsen G. Molecular and genetic organization of the antennapedia gene complex of Drosophila melanogaster. Adv Genet. 1990;27:309-62. Epub 1990/01/01. doi: 10.1016/s0065-2660(08)60029-2. PubMed PMID: 1971986.

264.   Maeda RK, Karch F. The bithorax complex of Drosophila an exceptional Hox cluster. Curr Top Dev Biol. 2009;88:1-33. Epub 2009/08/05. doi: 10.1016/s0070-2153(09)88001-0. PubMed PMID: 19651300.

265.   Duboule D. The rise and fall of Hox gene clusters. Development. 2007;134(14):2549-60. Epub 2007/06/08. doi: 10.1242/dev.001065. PubMed PMID: 17553908.

266.   McGinnis W, Levine MS, Hafen E, Kuroiwa A, Gehring WJ. A conserved DNA sequence in homoeotic genes of the Drosophila Antennapedia and bithorax complexes. Nature. 1984;308(5958):428-33. Epub 1984/03/04. doi: 10.1038/308428a0. PubMed PMID: 6323992.

267. Williams RW. Plant homeobox genes: many functions stem from a common motif. Bioessays. 1998;20(4):280-2. Epub 1998/06/10. doi: 10.1002/(sici)1521-1878(199804)20:4<280::Aid-bies2>3.0.Co;2-u. PubMed PMID: 9619098.

268. Suzuki M, Yagi N. DNA recognition code of transcription factors in the helix-turn-helix, probe helix, hormone receptor, and zinc finger families. Proc Natl Acad Sci U S A. 1994;91(26):12357-61. Epub 1994/12/20. doi: 10.1073/pnas.91.26.12357. PubMed PMID: 7809040; PubMed Central PMCID: PMCPMC45436.

269. Holland PW. Did homeobox gene duplications contribute to the Cambrian explosion? Zoological Lett. 2015;1:1. Epub 2015/11/26. doi: 10.1186/s40851-014-0004-x. PubMed PMID: 26605046; PubMed Central PMCID: PMCPMC4604119.

270. Holland P, Booth H, Bruford E. a, 2007. Classification and nomenclature of all human homeobox genes. BMC biology.5:47.

271. Longobardi E, Penkov D, Mateos D, De Florian G, Torres M, Blasi F. Biochemistry of the tale transcription factors PREP, MEIS, and PBX in vertebrates. Dev Dyn. 2014;243(1):59-75. Epub 2013/07/23. doi: 10.1002/dvdy.24016. PubMed PMID: 23873833; PubMed Central PMCID: PMCPMC4232920.

272. Morgan R, El-Tanani M, Hunter KD, Harrington KJ, Pandha HS. Targeting HOX/PBX dimers in cancer. Oncotarget. 2017;8(19):32322-31. Epub 2017/04/21. doi: 10.18632/oncotarget.15971. PubMed PMID: 28423659; PubMed Central PMCID: PMCPMC5458287.

273. Mortlock DP, Innis JW. Mutation of HOXA13 in hand-foot-genital syndrome. Nature genetics. 1997;15(2):179-80.

274. Shrimpton AE, Levinsohn EM, Yozawitz JM, Packard Jr DS, Cady RB, Middleton FA, et al. A HOX gene mutation in a family with isolated congenital vertical talus and Charcot-Marie-Tooth disease. The American Journal of Human Genetics. 2004;75(1):92-6.

275. Goodman F, Mundlos S, Muragaki Y, Donnai D, Giovannucci-Uzielli M, Lapi E, et al. Synpolydactyly phenotypes correlate with size of expansions in HOXD13 polyalanine tract. Proceedings of the National Academy of Sciences. 1997;94(14):7458-63.

276. Rux DR, Song JY, Swinehart IT, Pineault KM, Schlientz AJ, Trulik KG, et al. Regionally restricted Hox function in adult bone marrow multipotent mesenchymal stem/stromal cells. Developmental cell. 2016;39(6):653-66.

277. Takahashi Y, Hamada J-i, Murakawa K, Takada M, Tada M, Nogami I, et al. Expression profiles of 39 HOX genes in normal human adult organs and anaplastic thyroid cancer cell lines by quantitative real-time RT-PCR system. Experimental cell research. 2004;293(1):144-53.

278. Morgan R. Hox genes: a continuation of embryonic patterning? Trends in genetics. 2006;22(2):67-9.

279. Bhatlekar S, Fields JZ, Boman BM. Role of HOX genes in stem cell differentiation and cancer. Stem cells international. 2018;2018.

280. Kuo T-L, Cheng K-H, Chen L-T, Hung W-C. Deciphering the potential role of Hox genes in pancreatic cancer. Cancers. 2019;11(5):734.

281. Idaikkadar P, Morgan R, Michael A. HOX genes in high grade ovarian cancer. Cancers. 2019;11(8):1107.

282.   Shah N, Sukumar S. The Hox genes and their roles in oncogenesis. Nature Reviews Cancer. 2010;10(5):361-71.

283.   Abate-Shen C. Deregulated homeobox gene expression in cancer: cause or consequence? Nature Reviews Cancer. 2002;2(10):777-85.

284.   Bhatlekar S, Fields JZ, Boman BM. HOX genes and their role in the development of human cancers. J Mol Med (Berl). 2014;92(8):811-23. Epub 2014/07/06. doi: 10.1007/s00109-014-1181-y. PubMed PMID: 24996520.

285.   Taylor HS, Vanden Heuvel GB, Igarashi P. A conserved Hox axis in the mouse and human female reproductive system: late establishment and persistent adult expression of the Hoxa cluster genes. Biol Reprod. 1997;57(6):1338-45. Epub 1998/01/04. doi: 10.1095/biolreprod57.6.1338. PubMed PMID: 9408238.

286.   Cheng W, Liu J, Yoshida H, Rosen D, Naora H. Lineage infidelity of epithelial ovarian cancers is controlled by HOX genes that specify regional identity in the reproductive tract. Nat Med. 2005;11(5):531-7. Epub 2005/04/12. doi: 10.1038/nm1230. PubMed PMID: 15821746.

287.   Kelly Z, Moller-Levet C, McGrath S, Butler-Manuel S, Kavitha Madhuri T, Kierzek AM, et al. The prognostic significance of specific HOX gene expression patterns in ovarian cancer. Int J Cancer. 2016;139(7):1608-17. Epub 2016/05/27. doi: 10.1002/ijc.30204. PubMed PMID: 27225067.

288.   Naora H, Yang YQ, Montz FJ, Seidman JD, Kurman RJ, Roden RB. A serologically identified tumor antigen encoded by a homeobox gene promotes growth of ovarian epithelial cells. Proc Natl Acad Sci U S A. 2001;98(7):4060-5. Epub 2001/03/29. doi:

10.1073/pnas.071594398. PubMed PMID: 11274429; PubMed Central PMCID: PMCPMC31179.

289. Miao J, Wang Z, Provencher H, Muir B, Dahiya S, Carney E, et al. HOXB13 promotes ovarian cancer progression. Proc Natl Acad Sci U S A. 2007;104(43):17093-8. Epub 2007/10/19. doi: 10.1073/pnas.0707938104. PubMed PMID: 17942676; PubMed Central PMCID: PMCPMC2040435.

290. Ko SY, Ladanyi A, Lengyel E, Naora H. Expression of the homeobox gene HOXA9 in ovarian cancer induces peritoneal macrophages to acquire an M2 tumor-promoting phenotype. Am J Pathol. 2014;184(1):271-81. Epub 2013/12/18. doi: 10.1016/j.ajpath.2013.09.017. PubMed PMID: 24332016; PubMed Central PMCID: PMCPMC3873497.

291. Ko SY, Naora H. Adaptation of ovarian cancer cells to the peritoneal environment: Multiple mechanisms of the developmental patterning gene HOXA9. Cancer Cell Microenviron. 2014;1(6):e379. Epub 2015/05/23. PubMed PMID: 26000332; PubMed Central PMCID: PMCPMC4437227.

292. Nakayama I, Shibazaki M, Yashima-Abo A, Miura F, Sugiyama T, Masuda T, et al. Loss of HOXD10 expression induced by upregulation of miR-10b accelerates the migration and invasion activities of ovarian cancer cells. Int J Oncol. 2013;43(1):63-71. Epub 2013/05/15. doi: 10.3892/ijo.2013.1935. PubMed PMID: 23670532.

293. Zhao H, Yu H, Zheng J, Ning N, Tang F, Yang Y, et al. Lowly-expressed lncRNA GAS5 facilitates progression of ovarian cancer through targeting miR-196-5p and thereby regulating HOXA5. Gynecol Oncol. 2018;151(2):345-55. Epub 2018/09/12. doi: 10.1016/j.ygyno.2018.08.032. PubMed PMID: 30201235.

294. Odenwald WF, Taylor CF, Palmer-Hill FJ, Friedrich V, Jr., Tani M, Lazzarini RA. Expression of a homeo domain protein in noncontact-inhibited cultured cells and postmitotic neurons. Genes Dev. 1987;1(5):482-96. Epub 1987/07/01. doi: 10.1101/gad.1.5.482. PubMed PMID: 2890554.

295. Jeannotte L, Gotti F, Landry-Truchon K. Hoxa5: A Key Player in Development and Disease. J Dev Biol. 2016;4(2). Epub 2016/03/25. doi: 10.3390/jdb4020013. PubMed PMID: 29615582; PubMed Central PMCID: PMCPMC5831783.

296. Henderson GS, van Diest PJ, Burger H, Russo J, Raman V. Expression pattern of a homeotic gene, HOXA5, in normal breast and in breast tumors. Cell Oncol. 2006;28(5-6):305-13. Epub 2006/12/15. doi: 10.1155/2006/974810. PubMed PMID: 17167183; PubMed Central PMCID: PMCPMC4617796.

297. Ordóñez-Morán P, Dafflon C, Imajo M, Nishida E, Huelsken J. HOXA5 Counteracts Stem Cell Traits by Inhibiting Wnt Signaling in Colorectal Cancer. Cancer Cell. 2015;28(6):815-29. Epub 2015/12/19. doi: 10.1016/j.ccell.2015.11.001. PubMed PMID: 26678341.

298. Wang X, Zhang L, Zhang X, Xing C, Liu R, Zhang F. MiR-196a promoted cell migration, invasion and the epithelial-mesenchymal transition by targeting HOXA5 in osteosarcoma. Cancer Biomark. 2020;29(2):291-8. Epub 2020/07/18. doi: 10.3233/cbm-201674. PubMed PMID: 32675397.

299. Dziobek K, Oplawski M, Zmarzły N, Gabarek BO, Kiełbasiński R, Kiełbasiński K, et al. Assessment of Expression of Homeobox A5 in Endometrial Cancer on the mRNA and Protein Level. Curr Pharm Biotechnol. 2020;21(7):635-41. Epub 2019/12/28. doi:

10.2174/1389201021666191227121627. PubMed PMID: 31880256; PubMed Central PMCID: PMCPMC7403687.

300. Wang SL, Huang Y, Su R, Yu YY. Silencing long non-coding RNA HOTAIR exerts anti-oncogenic effect on human acute myeloid leukemia via demethylation of HOXA5 by inhibiting Dnmt3b. Cancer Cell Int. 2019;19:114. Epub 2019/06/07. doi: 10.1186/s12935-019-0808-z. PubMed PMID: 31168296; PubMed Central PMCID: PMCPMC6489230.

301. Zhang ML, Nie FQ, Sun M, Xia R, Xie M, Lu KH, et al. HOXA5 indicates poor prognosis and suppresses cell proliferation by regulating p21 expression in non small cell lung cancer. Tumour Biol. 2015;36(5):3521-31. Epub 2015/01/01. doi: 10.1007/s13277-014-2988-4. PubMed PMID: 25549794.

302. Garin E, Lemieux M, Coulombe Y, Robinson GW, Jeannotte L. Stromal Hoxa5 function controls the growth and differentiation of mammary alveolar epithelium. Dev Dyn. 2006;235(7):1858-71. Epub 2006/04/12. doi: 10.1002/dvdy.20822. PubMed PMID: 16607641.

303. Ma HM, Cui N, Zheng PS. HOXA5 inhibits the proliferation and neoplasia of cervical cancer cells via downregulating the activity of the Wnt/β-catenin pathway and transactivating TP53. Cell Death Dis. 2020;11(6):420. Epub 2020/06/06. doi: 10.1038/s41419-020-2629-3. PubMed PMID: 32499530; PubMed Central PMCID: PMCPMC7272418.

304. Chen YQ, Yang TQ, Zhou B, Yang MX, Feng HJ, Wang YL. HOXA5 overexpression promotes osteosarcoma cell apoptosis through the p53 and p38α MAPK pathway. Gene. 2019;689:18-23. Epub 2018/12/07. doi: 10.1016/j.gene.2018.11.081. PubMed PMID: 30521886.

305.	Raman V, Martensen SA, Reisman D, Evron E, Odenwald WF, Jaffee E, et al. Compromised HOXA5 function can limit p53 expression in human breast tumours. Nature. 2000;405(6789):974-8. Epub 2000/07/06. doi: 10.1038/35016125. PubMed PMID: 10879542.

306.	Stasinopoulos IA, Mironchik Y, Raman A, Wildes F, Winnard P, Jr., Raman V. HOXA5-twist interaction alters p53 homeostasis in breast cancer cells. J Biol Chem. 2005;280(3):2294-9. Epub 2004/11/17. doi: 10.1074/jbc.M411018200. PubMed PMID: 15545268.

307.	Teo WW, Merino VF, Cho S, Korangath P, Liang X, Wu RC, et al. HOXA5 determines cell fate transition and impedes tumor initiation and progression in breast cancer through regulation of E-cadherin and CD24. Oncogene. 2016;35(42):5539-51. Epub 2016/10/21. doi: 10.1038/onc.2016.95. PubMed PMID: 27157614; PubMed Central PMCID: PMCPMC5073039.

308.	Wang J, Yu XF, N OU, Luo QL, Zhao SY, Guan XF, et al. Multi-platform analysis of methylation-regulated genes in human lung adenocarcinoma. J Toxicol Environ Health A. 2019;82(1):37-45. Epub 2019/01/11. doi: 10.1080/15287394.2018.1551645. PubMed PMID: 30626254.

309.	Pineda B, Diaz-Lagares A, Pérez-Fidalgo JA, Burgués O, González-Barrallo I, Crujeiras AB, et al. A two-gene epigenetic signature for the prediction of response to neoadjuvant chemotherapy in triple-negative breast cancer patients. Clin Epigenetics. 2019;11(1):33. Epub 2019/02/23. doi: 10.1186/s13148-019-0626-0. PubMed PMID: 30786922; PubMed Central PMCID: PMCPMC6381754.

310.	Musialik E, Bujko M, Kober P, Grygorowicz MA, Libura M, Przestrzelska M, et al. Promoter DNA methylation and expression levels of HOXA4, HOXA5 and MEIS1 in acute myeloid leukemia. Mol Med Rep. 2015;11(5):3948-54. Epub 2015/01/15. doi: 10.3892/mmr.2015.3196. PubMed PMID: 25585874.

311.	Li D, Bai Y, Feng Z, Li W, Yang C, Guo Y, et al. Study of Promoter Methylation Patterns of HOXA2, HOXA5, and HOXA6 and Its Clinicopathological Characteristics in Colorectal Cancer. Front Oncol. 2019;9:394. Epub 2019/06/06. doi: 10.3389/fonc.2019.00394. PubMed PMID: 31165042; PubMed Central PMCID: PMCPMC6536611.

312.	Abba MC, Gong T, Lu Y, Lee J, Zhong Y, Lacunza E, et al. A Molecular Portrait of High-Grade Ductal Carcinoma In Situ. Cancer Res. 2015;75(18):3980-90. Epub 2015/08/08. doi: 10.1158/0008-5472.Can-15-0506. PubMed PMID: 26249178; PubMed Central PMCID: PMCPMC4768486.

313.	Kim SY, Paylor SW, Magnuson T, Schumacher A. Juxtaposed Polycomb complexes co-regulate vertebral identity. Development. 2006;133(24):4957-68. Epub 2006/11/17. doi: 10.1242/dev.02677. PubMed PMID: 17107999.

314.	Bérubé-Simard FA, Prudhomme C, Jeannotte L. YY1 acts as a transcriptional activator of Hoxa5 gene expression in mouse organogenesis. PLoS One. 2014;9(4):e93989. Epub 2014/04/08. doi: 10.1371/journal.pone.0093989. PubMed PMID: 24705708; PubMed Central PMCID: PMCPMC3976385.

315.	Fischer M. Census and evaluation of p53 target genes. Oncogene. 2017;36(28):3943-56. Epub 2017/03/14. doi: 10.1038/onc.2016.502. PubMed PMID: 28288132; PubMed Central PMCID: PMCPMC5511239.

316.   Abbas T, Dutta A. p21 in cancer: intricate networks and multiple activities. Nat Rev Cancer. 2009;9(6):400-14. Epub 2009/05/15. doi: 10.1038/nrc2657. PubMed PMID: 19440234; PubMed Central PMCID: PMCPMC2722839.

317.   Villunger A, Michalak EM, Coultas L, Müllauer F, Böck G, Ausserlechner MJ, et al. p53- and drug-induced apoptotic responses mediated by BH3-only proteins puma and noxa.   Science.   2003;302(5647):1036-8.   Epub   2003/09/23.   doi: 10.1126/science.1090072. PubMed PMID: 14500851.

318.   Pitolli C, Wang Y, Candi E, Shi Y, Melino G, Amelio I. p53-Mediated Tumor Suppression: DNA-Damage Response and Alternative Mechanisms. Cancers (Basel). 2019;11(12).   Epub   2019/12/15.   doi: 10.3390/cancers11121983.   PubMed   PMID: 31835405; PubMed Central PMCID: PMCPMC6966539.

319.   Zhang LN, Li JY, Xu W. A review of the role of Puma, Noxa and Bim in the tumorigenesis, therapy and drug resistance of chronic lymphocytic leukemia. Cancer Gene Ther. 2013;20(1):1-7. Epub 2012/11/24. doi: 10.1038/cgt.2012.84. PubMed PMID: 23175245.

320.   Chun MG, Hanahan D. Genetic deletion of the desmosomal component desmoplakin promotes tumor microinvasion in a mouse model of pancreatic neuroendocrine carcinogenesis. PLoS Genet. 2010;6(9):e1001120. Epub 2010/09/24. doi: 10.1371/journal.pgen.1001120. PubMed PMID: 20862307; PubMed Central PMCID: PMCPMC2940733.

321.   Wan H, South AP, Hart IR. Increased keratinocyte proliferation initiated through downregulation of desmoplakin by RNA interference. Exp Cell Res. 2007;313(11):2336-44. Epub 2007/05/04. doi: 10.1016/j.yexcr.2007.01.010. PubMed PMID: 17475244.

322.   Latini FR, Hemerly JP, Freitas BC, Oler G, Riggins GJ, Cerutti JM. ABI3 ectopic expression reduces in vitro and in vivo cell growth properties while inducing senescence. BMC Cancer. 2011;11:11. Epub 2011/01/13. doi: 10.1186/1471-2407-11-11. PubMed PMID: 21223585; PubMed Central PMCID: PMCPMC3032749.

323.   Latini FR, Hemerly JP, Oler G, Riggins GJ, Cerutti JM. Re-expression of ABI3-binding protein suppresses thyroid tumor growth by promoting senescence and inhibiting invasion. Endocr Relat Cancer. 2008;15(3):787-99. Epub 2008/06/19. doi: 10.1677/erc-08-0079. PubMed PMID: 18559958; PubMed Central PMCID: PMCPMC2742300.

324.   Subbarayan K, Leisz S, Wickenhauser C, Bethmann D, Massa C, Steven A, et al. Biglycan-mediated upregulation of MHC class I expression in HER-2/neu-transformed cells. Oncoimmunology. 2018;7(4):e1373233. Epub 2018/04/11. doi: 10.1080/2162402x.2017.1373233. PubMed PMID: 29632715; PubMed Central PMCID: PMCPMC5889282.

325.   Del Reino P, Alsina-Beauchamp D, Escós A, Cerezo-Guisado MI, Risco A, Aparicio N, et al. Pro-oncogenic role of alternative p38 mitogen-activated protein kinases p38γ and p38δ, linking inflammation and cancer in colitis-associated colon cancer. Cancer Res. 2014;74(21):6150-60. Epub 2014/09/14. doi: 10.1158/0008-5472.Can-14-0870. PubMed PMID: 25217523.

326.   Schindler EM, Hindes A, Gribben EL, Burns CJ, Yin Y, Lin MH, et al. p38delta Mitogen-activated protein kinase is essential for skin tumor development in mice. Cancer Res. 2009;69(11):4648-55. Epub 2009/05/22. doi: 10.1158/0008-5472.Can-08-4455. PubMed PMID: 19458068.

327. Diaz-Rodríguez E, Sotillo R, Schvartzman JM, Benezra R. Hec1 overexpression hyperactivates the mitotic checkpoint and induces tumor formation in vivo. Proc Natl Acad Sci U S A. 2008;105(43):16719-24. Epub 2008/10/23. doi: 10.1073/pnas.0803504105. PubMed PMID: 18940925; PubMed Central PMCID: PMCPMC2570608.

328. Schvartzman JM, Sotillo R, Benezra R. Mitotic chromosomal instability and cancer: mouse modelling of the human disease. Nat Rev Cancer. 2010;10(2):102-15. Epub 2010/01/23. doi: 10.1038/nrc2781. PubMed PMID: 20094045; PubMed Central PMCID: PMCPMC5526619.

329. Wang X, Zhou YX, Qiao W, Tominaga Y, Ouchi M, Ouchi T, et al. Overexpression of aurora kinase A in mouse mammary epithelium induces genetic instability preceding mammary tumor formation. Oncogene. 2006;25(54):7148-58. Epub 2006/05/23. doi: 10.1038/sj.onc.1209707. PubMed PMID: 16715125.

APPENDIX: Copyright Permission by Scientific Reports